Spectroscopic Probes of Conformational Isomerization of Biological Molecules in a Cold Ion Trap

PAR

Caroline SEAIBY

acceptée sur proposition du jury:

Prof. P. Vogel, président du jury
Prof. T. Rizzo, directeur de thèse
Prof. M. Chergui, rapporteur
Prof. M. Gerhards, rapporteur
Prof. T. Zwier, rapporteur

EPFL

ÉCOLE POLYTECHNIQUE
FÉDÉRALE DE LAUSANNE

Suisse
2011

to my father
and
to my mother

Abstract

The function of biologically active molecules depends both on their structure and on their conformational dynamics. In solution, intramolecular interaction with the solvent will influence different biological processes, i.e. protein folding. However secondary structure (helices, sheets) is heavily influenced by intramolecular forces and hence it is important to isolate biological molecules in order to study their intrinsic behavior. Moreover, gas phase studies on biomolecules provide critical information that can serve as benchmarks to test the accuracy of theoretical predictions.

The main focus of this thesis is the investigation of the potential energy surfaces of biomolecules in the gas phase. Biomolecular ions are produced in the gas phase via *nano*-electrospray, mass-selected and guided into a cold, 22-pole ion trap where they are cooled via collisions with cold helium. A variety of double-resonance techniques based on photofragmentation detection are then applied to obtain information on the molecule stable conformations, the potential barriers separating stable conformations and their connectivity. We applied these techniques on molecules of increasing size, starting with protonated phenylalanine and proceeding to the 7amino acid peptides, $Ac-Phe-(Ala)_5-LysH^+$ and the 12-residue peptide $Ac-Phe-(Ala)_3-(Gly)_4-(Ala)_3-LysH^+$.

As a first step, electronic spectra and conformation-specific IR-UV double resonance spectra are measured. These measurements, in combination with DFT calculations, allow the assignment of two stable conformers in the case of the protonated phenylalanine and four in the case of the seven residue peptide. In the second part of this work we focused on the conformational isomerization of these molecules by performing infrared and ultraviolet hole-filling spectroscopy in the ion trap. We demonstrated that we can induce isomerization between stable conformers of each molecule via vibrational excitation. After energy dissipation, the excited molecules are redistributed among the initially identified conformers, but no new minima were detected. In the last part of this thesis, the fractional populations and the isomerization quantum yields are determined through infrared induced population transfer spectroscopy. Protonated phenylalanine reveals conformational selectivity in its isomerization while the relaxation of the infrared excitation leads to the equilibrium distribution in the case

of the 12-residue glycine-containing peptide. The steps that occur during the energy dissipation are discussed in this thesis.

Résumé

La fonction particulière remplie par une molécule biologique est en grande partie liée à sa structure ainsi qu'à sa dynamique. En phase liquide, les molécules ne sont pas isolées, mais interagissent avec un solvant et d'autres macromolécules ce qui va souvent influencer les divers processus biologiques comme le pliement des protéines. Cependant la structure secondaire des protéines est stabilisée par les liaisons intramoléculaires, d'où l'importance de mener des études sur ses molécules en les isolant en phase gazeuse afin de pouvoir caractériser leurs propriétés intrinsèques. Ces études peuvent aussi fournir d'utiles informations qui peuvent servir comme points de repère et vérification de l'exactitude des prédictions théoriques.

L'objectif principal de cette thèse est d'explorer la surface d'énergie potentielle des biomolécules en phase gazeuse. Les molécules chargées sont produites en phase gazeuse par une source d'ions nano-spray et passent à travers un premier filtre de masse quadrupolaire. Les ions ainsi sélectionnés sont stockés et refroidis dans un piège à 22 pôles. Une variété de techniques spectroscopiques a été utilisée afin d'obtenir des informations sur les structures les plus basses en énergie, les états de transition qui les séparent et leur connectivité. Ces techniques ont été appliquées sur des systèmes moléculaires d'un intérêt biologique de tailles divers, allant de la phénylalanine aux peptides à 7- et 12- aminoacides, Ac-Phe-(Ala)$_5$-LysH$^+$ et Ac-Phe-(Ala)$_3$-(Gly)$_4$-(Ala)$_3$-LysH$^+$.

Dans un premier temps, les spectres électroniques et vibrationnels spécifiques à chaque conformation sont mesurés, et l'identification des structures est réalisée en comparant ces spectres avec des résultats de calculs DFT de géométries et de fréquences harmoniques. Ces comparaisons ont mis en évidence la présence de deux conformères de PheH$^+$ et quatre dans le cas de Ac-Phe-(Ala)$_5$-LysH$^+$ tout en permettant l'identification de leurs structures. Dans la deuxième partie, nous avons élaboré les techniques de spectroscopie de transfert de population induite par IR et UV dans le piège ionique afin de mener une étude sur l'isomérisation entre le différents conformères. Nous avons démontré la possibilité de transférer la population parmi les plus stables conformères détectés de chaque système moléculaire *via* l'excitation vibrationnelle. Après l'absorption d'un photon, l'énergie acquise

par la molécule va se relaxer en créant une nouvelle distribution de population entre les conformères initialement identifiés puisque aucune nouvelle conformation minimale n'est détectée. Dans la dernière partie de cette thèse, les spectres de transfert de population induit par infrarouge ont permis la détermination de l'abondance de la population relative des conformères et le rendement quantique d'isomérisation. Concernant PheH$^+$, un caractère conformationel sélectif a été relevé, en revanche la relaxation de l'excitation vibrationnelle dans le cas du peptide contenant la glycine donne une distribution similaire à l'équilibre établi lors du refroidissement des molécules à température ambiante arrivant dans le piège. Nous abordons dans cette thèse les divers processus qui ont lieu pendant la désactivation des molécules excitées.

Mots-clés: ions biologiques froids en phase gazeuse, piège ionique à 22 pôles, spectrométrie de masse en tandem, photodissociation, spectroscopie de double résonance, isomérisation, spectroscopie de transfert de population, abondance relative de population, rendement quantique d'isomérisation.

Contents

Chapter 1

Introduction

"Vital forces are molecular forces" T. H. Huxley (1860)

The study of biological molecules is largely driven by the desire to understand the phenomena that govern their behavior and activity in *vivo*, such as enzyme action, molecular transport, genetic information and processing, and protein assembly. At the same time the understanding of the complex dynamics of biological processes such as protein folding will greatly advance the treatment of human disease [1]. Large progress towards this goal has been made in the past decades with the development of numerous experimental and theoretical techniques to determine the structures of various biomolecular entities.

X-ray crystallography was the first high-resolution technique that could elucidate the three-dimensional geometries of large biomolecules as DNA and proteins on the atomic scale [2-6]. The measured structure reflects the conformational shapes in crystalline form which may differ from those in their native environment due to the influence of the packing forces. The nearest competing structural analysis method is multidimensional nuclear magnetic resonance (NMR), which can be used to determine solution structures and dynamical behavior of biomolecules, but it is restricted to molecules of no more than ~ 70 kDa [7-11]. Several

other techniques have been implemented to probe the structures of biomolecules, such as Fourier transform infrared spectroscopy (FTIR) [12], circular dichroism (CD) [13-17] and a number of fluorescence techniques [18-21]. While these techniques probe molecular structure in solution, which is considered to be the most biologically relevant environment, these structures may not be identical to those in the natural environment. For example, trans-membrane proteins are situated in the hydrophobic interior of the membrane lipid bilayer [22], which is very different than an aqueous environment. Moreover, the crowded environment in the interior of a cell is likely to be substantially different than a dilute solution.

In addition to experimental approaches, theory continues to make enormous progress in predicting the conformational structures of increasingly large biological molecules and elucidating the counterbalancing forces that control them [23-26]. Although theory is widely used, the accuracy of theoretical treatments needs to be verified by comparison with benchmark experiments. Gas phase studies on proteins and peptides, where the perturbations introduced by the local environment can be eliminated, could provide important critical information for testing the predictions of theory. Moreover, studies in the gas phase provide the possibility of modifying the molecular environment by forming clusters of biomolecules with solvent, which allows the investigation of the intermolecular interactions and the effect of the environment on the intramolecular processes. High resolution gas-phase spectroscopy of peptides will thus present the most challenging benchmarks to test and improve the theoretical methods.

Biological molecules are fluxional rather than static and thus their function depends both on their structure and their dynamics, the utility to investigate their conformational dynamics. After reviewing work on spectroscopy of gas-phase biological molecules, we turn our attention to isomerization dynamics.

1.1 Biological molecules in the gas phase

In order to study biological molecules in the gas phase one has to remove them from their natural environment. Since the standard thermal methods are limited by the decomposition of the biomolecule upon heating, several techniques have been invented to facilitate their volatilization. Among these one can mention lased desorption (LD) [27, 28], which is based on the ejection of material from a sample-covered surface using intense laser light. An improved version of this is matrix-assisted laser desorption/ionization (MALDI),

where the sample molecules are embedded in a matrix that strongly absorbs the desorbing light [29, 30]. Other techniques, such as thermospray [31, 32] and electrospray ionization [33-36], use the nebulization of a sample solution through a capillary to produce charged droplets from which ions can desorb. This latter is the method we use to produce our ions and it will be extensively described in *Chapter 2*. ESI and MALDI are the most popular production methods of gas-phase biomolecular ions present in academic research and industry. Both allow intact biomolecules of large size to be put into the gas-phase in the form of closed-shell ions.

Many techniques have been developed in order to determine the structure of biological molecules by coupling these volatilizing techniques with mass spectrometry. Mass analysis identifies the peptide fragments produced in solution by chemical or enzymatic degradation or directly in the gas phase by collision-induced or photo-induced dissociation [37-44]. The structural information that could be obtained with this approach on biological molecules was related to their primary structure. Whereas H/D exchange experiments give information on the secondary structure the molecules. The number of potentially labile hydrogen atoms replaced by deuterium when a molecule is exposed to a deuterated solvent, can provide information on the conformation of proteins [45]. The polypeptide is first volatilized then brought in contact with a deuterated solvent. Based on this method, Freitas and Marshall studied bradykinin, a nanopeptide containing two arginines, and concluded that its protonated form in the gas-phase exists as a zwitterionic structure, with both arginine side chains protonated and the terminal acidic group deprotonated [46].

In order to characterize the three dimensional shape of a biomolecule, another strategy is based on its mobility through a drift tube containing several millibars of a buffer gas under the influence of a weak electric field. The gas-phase ions enter this tube, and based on the different conformations, biomolecular ions exit the tube at different times [47-50]. After measuring drift times and converting them into cross sections, they are compared with those of model structures. Jarrold and coworkers have probed the conformations and folding properties of proteins such as cytochrome c [51, 52] and bovine pancreatic trypsin inhibitor [52] and observed the formation of a helical structure in small model peptides [53]. A similar technique based on the differential ion mobility at a high and low electric field has been developed by Guevremont and coworkers, which is called high-Field Asymmetric waveform Ion Mobility Spectrometry (FAIMS) [54, 55]. This method allows the separation of isotopes [56], stereoisomers [57], isobaric ions that in conventional ESI interfere with each other [58]

and structural isomers [59]. While FAIMS can analyze and separate different conformers, there is no simple way to extract the molecule cross section and hence shape.

Williams and coworkers developed a new technique that measures the dissociation energies of trapped protonated biomolecular ions known as blackbody infrared radiative dissociation (BIRD). It consists in measuring the kinetics dissociation of ions trapped in a Fourier transform ion cyclotron resonance mass spectrometer (FT-ICR) induced by the slow absorption of blackbody radiation from the vacuum chamber walls [60]. Temperature-dependent experiments allow the measurement of the activation energies and frequency factors for the lowest-energy dissociation pathways of mass-selected ions. Changes in the biomolecular structures affect these highly sensitive parameters that provide information on the conformational preferences of biomolecules. The Williams group has shown evidence that the most stable form of singly-protonated bradykinin is a salt-bridge structure [61] and proved that short strands of oligonucleotides forms Watson-Crick hydrogen-bonds [62].

The aforementioned methods can give valuable information on the conformational structure of gas-phase biological molecules, although not their precise geometry. Moreover, they have limitations when structural isomers or conformations do not differ by their mass, fragmentation patterns or ion mobilities.

Another approach to obtaining geometrical information on gas phase biological molecules is to use spectroscopic techniques, since the spectroscopic properties of a molecule are very sensitive to the three dimensional arrangement of its atoms, and thus small changes in it conformation can lead to detectable spectroscopic shifts. This approach can be applied to gas phase biological molecules both in their neutral and their charged forms.

1.2 Spectroscopic studies of biological molecules in the gas phase

1.2.1 Neutrals

Various optical approaches can provide an accurate value of the rotational constants of small biomolecules from which geometric information can be determined. In particular, microwave spectroscopy [63, 64], rotational coherence spectroscopy [65, 66], and fully [67, 68] or partially [69-73] rotationally-resolved electronic spectroscopy have been implemented to determine the geometries of different conformers of neutral jet-cooled analogues of the

three aromatic amino acids (tryptophan, tyrosine and phenylalanine). Electronic spectroscopy can also give structural information by detecting the influence of the environment on the chromophore photophysics [74]. On the other hand, the vibrational frequency of a given bond is highly dependent on its local environment, which makes infrared spectroscopy a powerful tool to probe biomolecular structures; several examples will be presented below.

In 1985, the Levy group reported the first electronic spectrum of neutral tryptophan in a supersonic expansion and identified the presence of several conformations using R2PI saturation and fluorescence spectroscopy [75, 76]. More recent work has confirmed their conclusion by UV-UV hole burning and IR dip spectroscopy [77-79]. The Levy group later recorded the electronic spectrum of tyrosine and phenylalanine, and demonstrated the presence of ten and five conformers respectively in the molecular beam [80]. Following this pioneering work, a number of groups extended the same methods to larger peptides and many other biomolecules, and developed innovative double resonance spectroscopic techniques (e.g., UV-UV hole-burning or IR-UV depletion spectroscopy) to acquire conformer-specific electronic and vibrational spectra [77, 81-93]. These approaches had prove extremely helpful for the study of the hydrogen bonding patterns of secondary structural elements in neutral molecules, where the size of the peptides probed increased gradually over the past decades. As consequence, it has become possible to observe some secondary structural elements of the peptide backbone, such as β- and γ- turns or 3_{10}-helices [94-98]. In the past few years, some groups have reported the application of the double-resonance IR-UV scheme to longer oligopeptides such as gramicidin, a 15-residue peptide [99-102] and to the study of the nucleotide bases [103, 104] as well base pairs [105-107]. Gerhards and coworkers identified signatures of β-sheet and γ-turn/β-turn structures [108-114] and recently extended this technique into the mid-IR region [115]. Other investigations have investigated the influence of solvation on the conformations of peptides by examining their hydrated clusters [111, 116-119]. Finally, one can mention the elaboration of an IR-IR-UV triple resonance spectroscopic hole-burning scheme proposed by Zwier and coworkers, that makes possible the measurement of conformer-specific vibrational spectra even in cases where two conformers have indistinguishable electronic spectra [120] .

1.2.2 Ions

All these spectroscopic studies were concerned with gas-phase amino acids and small peptides in their neutral form. Nonetheless, the study of charged biomolecules is of equal

importance, since in their native environment these molecules are charged. Due to the difficulty of producing sufficient gas-phase concentration of ions, the optical investigation of these species started only at the beginning of the new millennium [121, 122]. The development of MALDI and ESI, as the soft ionization techniques, allowed the volatilization of biological molecules of virtually any size in the form of closed-shell molecular ions and thus opened new avenues of investigation. However, the use of direct absorption spectroscopy or even fluorescence spectroscopy is extremely difficult because of the low density of ions. Hence, one must make use of some sort of action spectroscopy and measure a consequence of the photon absorption rather than the absorption itself to record the spectrum of gas-phase molecular ions. Action spectroscopy was first used by Andersen and coworkers to characterize closed-shell molecular ions produced by electrospray [121, 122]. They reported the electronic excitation spectra of the green fluorescent protein chromophore in its protonated and deprotonated forms in an electrostatic ion storage ring by detecting the neutral products subsequent to photofragmentation or photo-detachment respectively. Nolting *et al.*, using resonant photodissociation spectroscopy in a cold Paul trap, recorded the electronic spectrum of protonated tryptophan [123]. A room temperature spectrum of same species was reported by Dugourd and coworkers over a wider wavelength range, and the analysis of its possible structure and of its various photofragmentation channels was given [124]. Monitoring the decay of cationic and anionic mono- and di-nucleotides in an ion storage ring after absorption of a UV photon on the microsecond time scale, Nielsen and coworkers could identify both statistical and non-statistical photodissociation channels, the latter of which becomes predominant for the protonated species [125, 126]. Parks and coworkers studied the conformational dynamics of weakly bound protonated oligonucleotides duplexes in a quadrupole ion trap by fluorescence resonance energy transfer (FRET) spectroscopy, and observed an intermediate state in their dissociation [127]. Electronic spectroscopy was also used to provide information on the excited-state dynamics, which is essential to understanding the photostability of biological chromophores such as the DNA bases or the aromatic amino acids. The excited-state dynamics of positively charged chromophores have also been explored by Jouvet and coworkers on a short time scale, using a femtosecond pump-probe laser schemes [128-132] and coincidence experiments [133-135]. Using this approach, they determined the excited-state lifetimes of protonated aromatic amino acids and of di- and tri-peptides.

McLafferty and coworkers reported infrared spectra of electrosprayed peptides and proteins in a FT-ICR mass spectrometer in the light-atom stretch region by resonant infrared multiphoton dissociation (R-IRMPD), using an optical parametric oscillator (OPO) [136, 137]. Von Helden and coworkers extended IRMPD spectroscopy into the amide I and II regions of the infrared employing a free-electron laser to measure the infrared spectrum of potassiated cytochrome C formed by electrospray [138]. The analysis of the vibrational spectrum in this region suggests a large degree of α-helical content in cytochrome C. Using these methods the structures of many protonated amino acids, small peptides and other biomolecules have been elucidated [133, 138-148].

1.2.3 Low-temperature biomolecules

In order to disentangle the contributions of the intermolecular and intramolecular interactions and determine the three-dimensional structure of an isolated molecule, which provides perhaps the most stringent test of theory, biomolecules have been studied in gas phase. A direct consequence of this approach is that various types of inhomogeneous spectral broadening can be eliminated. In solution, each molecule has a slightly different environment arising from the different arrangement of solvent around it, and a spectrum represents the average of a multitude of distinct individual spectra. Examining isolated gas-phase molecules eliminates this source of heterogeneity. Secondly, inhomogeneous broadening at room temperature derives from the large number of rotational and low-energy vibrational degrees of freedom populated, and this can be greatly reduced at low temperature. Neutral molecules can be cooled in seeded supersonic expansions, attaining typical temperatures of ~ 1 K for translational degrees of freedom, a few degrees Kelvin for rotations and a few tens of degrees Kelvin for vibrations [149]. Multiple strategies have been used to cool ion-molecule complexes. Johnson and coworkers condensed solvent molecules onto argon-solvated ions formed in a supersonic expansion [150, 151]. Another method is to produce cations in a pulsed high voltage electric discharge source coupled to a pulsed nozzle supersonic expansion. Collisional cooling in the expansion leaves the cation with estimated temperatures below 100 k [152, 153].

Another approach is to confine ions in a trap maintained at low temperature, where they collide with a buffer gas for thermalization. Weinkauf and coworkers used a liquid-nitrogen cooled quadrupole ion trap that could reach a temperature of ~ 140 k to measure the electronic spectrum of protonated tryptophan [123]. Another approach consists in mounting a

linear multipole ion trap on a closed-cycle helium refrigerator, which can attain temperatures below 10 k [154]. To achieve an effective ion cooling in such traps, a large number of poles are required to avoid RF-driven heating.

Simons and coworkers developed a clever **technique** that might be applicable for the production of jet-cooled ions. In the gas phase, the molecule of interest forms a complex with a proton donor in a supersonic expansion, and a proton transfer is initiated by R2PI of the former. Detachment of the resulting radical cation leaves behind the protonated species. The jet-cooling of the warm ions generated could possibly be obtained by triggering the R2PI step early enough in the expansion [142, 147, 155, 156].

Summarizing the work that has been done to date, one can measure highly resolved conformation specific infrared spectra of neutral molecules of about a few amino acids of length [88, 108-114]. In comparison with theory this has allowed determination of reliable three-dimensional structures of these molecules. In these cases the experiments have served as important benchmarks for theoretical calculations and helped guide improving their accuracy. The situation for ions is similar although techniques for producing them are applicable for molecules of larger size. However, high resolution spectra could be obtained for peptides beyond seven amino acids only in the case where these species are cooled [157-161]. These molecules stand as critical benchmarks that should help to improve the choice and the parameterization of the force fields and DFT functionals, as well as the development of new conformational search algorithms.

1.3 Biomolecular dynamics

Knowing the structure of biological molecules is not enough to fully understand their function. It is typically the ability to change their structure under certain conditions – that is, their conformational dynamics – that allow them to carry out their tasks. Moreover, understanding the process by which biological molecules attain their structure after being synthesized *in vivo* (e.g. protein folding) is important to finding solutions to diseases based on their misfolding. A number of different approaches have been established to initiate and follow the kinetics and pathways of protein folding in condensed phases. Among these, one can mention conventional stop flow [162], and laser-induced temperature jump [163-165]

techniques. This later method, which was first used by Eigen and De Maeyer [166] involves rapidly increasing the temperature after equilibrium has been established between folded and unfolded forms, which displaces the equilibrium toward one of the two forms.

In parallel and despite the complexity of the folding process, theoretical studies made a lot of progress in understanding the general nature of the energy landscape of folding. Lee *et al.* used a thermodynamic approach to predict the native folds of proteins [167]. The Levitt group simulated protein folding using simplified representations of polypeptide chains to fold proteins by energy minimization and exhaustive enumeration [168]; they reported protein-folding pathways [169] and the folding rates [170]. An understanding of the thermodynamics and kinetics of protein folding requires knowledge of the free energy surface governing their motion and dynamics. Wales and coworkers have developed novel methods for predicting and explaining how structure, dynamics and thermodynamic properties are determined by the potential energy surface (PES) [23, 171-173]. These methods allowed the determination of the folding pathways and rate constants for peptides. The characterization of minima, transition states and pathways was accomplished by geometry optimization, and the determination of the rate constants corresponding to each transition state was done using the unimolecular rate theory [172, 174-179].

Even if condensed phase studies are closer to physiological conditions, in this media, intramolecular processes cannot be separated from the intermolecular interactions involving energy exchange between the molecular system and its environment. In particular, the investigation of the potential energy landscape of biomolecules and their conformational dynamics in the gas phase allows separating the effects due to intrinsic properties of the molecule and those induced by the external perturbation and thus better understand the energy relaxation in biomolecules.

Much work has been done investigating the dynamics of intramolecular energy flow and unimolecular reaction dynamics in isolated molecules using both time-resolved and frequency-resolved techniques [180-187], but most of this work has been focused on relatively small molecules. Zwier and coworker pioneered the extension of these ideas to small, gas-phase biomolecules by looking at the transfer of population between conformers after the deposition of energy by vibrational excitation, either directly in the infrared [188]or by stimulated emission pumping [189]. The former is a pump-recool-probe technique that consists in exciting a specific conformation with an IR laser followed by a collisional cooling

step, allowing the transfer of part of the population into the potential wells of other conformers. It was first applied on methyl-capped dipeptides and yielded values of the fractional population of the different conformers and the isomerization quantum yields [188, 190, 191]. These quantities revealed, in some cases, a slight degree of mode specificity and thus the presence of distinguishable pathways on the energy landscape of the molecules. The second approach used by this group is a pump-dump-recool-probe experiment, where in its first step a specific conformer is promoted by the pump laser to the zero-point level of an electronically excited state and then stimulated back down into a specific vibrational level in the ground state with the dump laser. This experiment enabled direct measurement of isomerization barriers and provided insight into isomerization pathways of different molecules of relatively small size [189, 192-195].

These studies have been performed on neutral gas phase molecules of relatively small size. However in their native environment, biological molecules are often charged. Molecular and spectroscopic properties of a peptide can strongly be influenced by the presence of a charge and therefore the study of charged biomolecular ions, in addition to their neutral counterparts, is of fundamental importance. The purpose of this thesis is to perform gas-phase population transfer experiments on significantly larger protonated peptides and investigate their conformational isomerization in order to further clarify the connectivity between structures and thus test the limits of theory.

1.4 Goals and outline

This introduction has provided an overview of some experimental techniques used to determine the structures and dynamics of gas-phase biomolecules. A few years ago our laboratory developed a unique machine that combines several of these approaches to perform spectroscopic investigations of cold, gas-phase biomolecular ions [196-198]. This machine employs an ESI source for ion generation and two quadrupole mass filters to select the parent ions and analyze the fragments. In between these two mass-analyzers sits a 22-pole ion trap in which the mass-selected parent ions are accumulated and cooled to ~10k. While trapped, the ions interact with laser light, and upon absorption of a resonant ultraviolet photon they can fragment. By monitoring the photofragments as a function of the laser wavenumber we measure an electronic "action" spectrum. Conformer-specific infrared spectra of cold protonated biomolecular ions in the gas-phase are measured employing a double resonance

technique. Results obtained for the three protonated aromatic amino acids in the gas-phase have proved the power of this machine [197, 199]. The low-temperature achieved by in the 22-pole ion trap makes that the spectra attained of unprecedented resolution for ions that is comparable to that achieved for neutrals in supersonic molecular beams. More recently our group has pushed these techniques to larger molecules [157, 159-161, 200]. In this thesis we report the measurements of the electronic and conformer-specific vibrational spectra of the protonated phenylalanine and two peptides, one of which has 7 amino acid residues and the other has 12.

However, the main objective of this thesis was to go beyond the structural determination and investigate the barriers separating stable conformations of biological molecules. Exploring the interconnectivity of different conformational families will provide insight into the dynamics of biomolecules and the topology of their energy landscapes. Such a fundamental understanding of the dynamics of biological process i.e., protein folding/unfolding, may shed light on the physiological activity of these molecules. As a first step we make use of electronic and conformer-specific infrared spectroscopies in order to identify the stable minima. We then use this information to develop population transfer techniques, following the example of Zwier [188, 190, 191], to exploit and investigate conformational isomerization. We extend the techniques pioneered by Zwier to large biomolecules in an attempt to clarify the connectivity between biomolecular structures and perhaps open new perspectives for the interpretation of the mechanisms that occur during biological process. In addition, this information will provide benchmark tests for the current theoretical approaches.

The outline of this thesis is as follows. In *Chapter 2* we give an overview of the machine used in this thesis, its general principles of producing, selecting, cooling and trapping the ions. Then, we will describe the UV and IR laser setups used in performing the different experimental measurements.

In *Chapter 3* we depict the timing of events in a typical pulsed experiment and explain the different types of measurements that are carried out: the recording of a photofragment mass spectrum, a standard ultraviolet photodissociation spectrum, and double resonance infrared and ultraviolet spectra. This chapter also describes the principle and the adaptation of the hole-filling and infrared population transfer techniques for studies of cold trapped ions. Some experimental results on the cooling efficiency are then presented, which allows defining

the timing diagram of these transfer experiments. In the last part of this chapter, as well as in Appendix A, we introduce the equations used to extract the fractional population and the quantum yields to isomerization.

In *Chapter 4* we report the electronic and conformer-specific vibrational spectra in the Amide A, I and II regions of the molecules studied in this thesis: protonated phenylalanine and of two peptides, Ac-Phe-(Ala)$_5$-LysH$^+$ and Ac-Phe-(Ala)$_3$-(Gly)$_4$-(Ala)$_3$-LysH$^+$. These data are combined with theoretical studies to assign two conformers for PheH+ and for the 7-residue peptide. Due to the limitation of our theoretical approach, in the case of the largest peptide the calculations did not allow the assignment of a structure to each conformer.

Chapter 5 focuses on the hole-filling experiment, investigating the changes in the conformational dynamics. In the first part we report the measured spectra on the single amino acid and the two peptides after excitation of an N-H stretch transition. We demonstrate that transfer between the identified conformations of each system is induced within the energy of the absorbed photon. We then present the IR-UV spectra of the ^{13}C-substituted 7-residue helical peptide, which allow us to selectively excite one conformer and investigate the dynamics of this molecule in the C=O stretch region. Finally, we describe the UV-UV hole filling method we applied to study and exploit the electronic excited state dynamics.

Chapter 6 reports the results of the infrared population transfer (IRPT) experiments. We first extracted the fractional population of the three molecules studied in this work. The isomerization quantum yields of different NH stretch vibrations are then obtained from the IRPT spectra in association with the IR-UV double resonance spectra. In the case of phenylalanine the results showed unexpected behavior, where after IR excitation and relaxation, the molecules primarily re-form the conformer initially pumped. In this chapter we speculate on possible explanations for this behavior.

Chapter 7 gives a summary of the main results presented in this thesis and suggests future possible research directions.

References

1.   C. M. Dobson, *Philosophical Transactions of the Royal Society of London. Series B: Biological Sciences* **356**, 133 **2001**.
2.   M. H. F. Wilkins, A. R. a. W. Stokes, H. R., *Nature* **171**, 738 **1953**.

3. R. E. Franklin, R. G. Gosling, *Nature* **171**, 740 **1953**.
4. M. F. Perutz, M. G. Rossmann, A. F. Cullis, H. Muirhead, G. Will, A. C. T. North, *Nature* **185**, 416 **1960**.
5. J. C. Kendrew, R. E. Dickerson, B. E. Strandberg, R. G. Hart, D. R. Davies, D. C. Phillips, V. C. Shore, *Nature* **185**, 422 **1960**.
6. J. D. Watson, F. H. C. Crick, *Nature* **171**, 737 **1953**.
7. K. Wuthrich, *Science* **243**, 45 **1989**.
8. K. Wuethrich, *Acc. Chem. Res.* **22**, 36 **1989**.
9. R. Riek, S. Hornemann, G. Wider, M. Billeter, R. Glockshuber, K. Wuthrich, *Nature* **382**, 180 **1996**.
10. S. Raman, O. F. Lange, P. Rossi, M. Tyka, X. Wang, J. Aramini, G. Liu, T. A. Ramelot, A. Eletsky, T. Szyperski, M. A. Kennedy, J. Prestegard, G. T. Montelione, D. Baker, *Science* **327**, 1014 **2010**.
11. A. G. Tzakos, C. R. R. Grace, P. J. Lukavsky, R. Riek, *Annu. Rev. Biophys. Biomol. Struct.* **35**, 319 **2006**.
12. M. S. Braiman, K. J. Rothschild, *Annu Rev Biophys Biophys Chem* **17**, 541 **1988**.
13. L. Velluz, M. Legrand, *Angewandte Chemie International Edition in English* **4**, 838 **1965**.
14. W. B. Gratzer, *Proceedings of the Royal Society of London. Series A. Mathematical and Physical Sciences* **297**, 163 **1967**.
15. S. Beychok, *Annu. Rev. Biochem* **37**, 437 **1968**.
16. Y.-X. Wen, E. Chen, J. W. Lewis, D. S. Kliger, *Rev. Sci. Instrum.* **67**, 3010 **1996**.
17. X. Xie, J. D. Simon, *J. Am. Chem. Soc.* **112**, 7802 **1990**.
18. L. Stryer, *Annu. Rev. Biochem* **47**, 819 **1978**.
19. S. Nie, R. N. Zare, *Annu. Rev. Biophys. Biomol. Struct.* **26**, 567 **1997**.
20. M. R. Eftink, *Biophys. J.* **66**, **1994**.
21. G. V. Semisotnov, N. A. Rodionova, O. I. Razgulyaev, V. N. Uversky, A. F. Gripas, R. I. Gilmanshin, *Biopolymers* **31**, 119 **1991**.
22. Harvey Lodish, Arnold Berk, S Lawrence Zipursky, Paul Matsudaira, David Baltimore, a. j. Darnell, *Molecular Cell Biology*. (New York: W. H. Freeman;, **2000**).
23. D. J. Wales, *Energy Landscapes, Cambridge University Press (Cambridge)* **2003**.
24. J. L. Klepeis, K. Lindorff-Larsen, R. O. Dror, D. E. Shaw, *Current Opinion in Structural Biology* **19**, 120 **2009**.
25. C. Sagui, T. A. Darden, *Annu. Rev. Biophys. Biomol. Struct.* **28**, 155 **1999**.
26. S. A.J, *The Theory of Intermolecular Forces.* . (Oxford, UK: Clarendon, **1996**).
27. M. A. Posthumus, P. G. Kistemaker, H. L. C. Meuzelaar, M. C. Ten Noever de Brauw, *Anal. Chem.* **50**, 985 **1978**.
28. R. J. Levis, *Annu. Rev. Phys. Chem.* **45**, 483 **1994**.
29. M. Karas, D. Bachmann, U. Bahr, F. Hillenkamp, *Int. J. Mass Spectrom. Ion Processes* **78**, 53 **1987**.
30. M. Karas, F. Hillenkamp, *Anal. Chem.* **60**, 2299 **1988**.
31. C. R. Blakley, J. J. Carmody, M. L. Vestal, *Anal. Chem.* **52**, 1636 **1980**.
32. C. R. Blakley, J. J. Carmody, M. L. Vestal, *J. Am. Chem. Soc.* **102**, 5931 **1980**.
33. M. Yamashita, J. B. Fenn, *J. Phys. Chem.* **88**, 4451 **1984**.
34. M. Yamashita, J. B. Fenn, *J. Phys. Chem.* **88**, 4671 **1984**.
35. J. Fenn, M. Mann, C. Meng, S. Wong, C. Whitehouse, *Science* **246**, 64 **1989**.
36. S. Nguyen, J. B. Fenn, *Proceedings of the National Academy of Sciences* **104**, 1111 **2007**.
37. D. H. Williams, C. V. Bradley, S. Santikarn, G. Bojesen, *Biochem. J.* **201**, 105 **1982**.
38. H. Y. Kim, D. Pilosof, D. F. Dyckes, M. L. Vestal, *J. Am. Chem. Soc.* **106**, 7304 **1984**.

39. D. P. Little, J. P. Speir, M. W. Senko, P. B. O'Connor, F. W. McLafferty, *Anal. Chem.* **66**, 2809 **1994**.
40. V. S. K. Kolli, R. Orlando, *J. Am. Soc. Mass. Spectrom* **6**, 234 **1995**.
41. K. Biemann, *Annu. Rev. Biochem* **61**, 977 **1992**.
42. P. Jungblut, B. Thiede, *Mass Spectrom. Rev.* **16**, 145 **1997**.
43. R. Kaufmann, D. Kirsch, B. Spengler, *Int. J. Mass Spectrom. Ion Processes* **131**, 355 **1994**.
44. J. R. Yates, *J. Mass Spectrom.* **33**, 1 **1998**.
45. B. Y, E. SW, *Proteins: Struct. Funct. Genet.* **24**, 145 **1996**.
46. M. A. Freitas, A. G. Marshall, *Int. J. Mass spectrom.* **182-183**, 221 **1999**.
47. M. T. Bowers, P. R. Kemper, G. von Helden, P. A. M. van Koppen, *Science* **260**, 1446 **1993**.
48. G. von Helden, M. T. Hsu, N. Gotts, M. T. Bowers, *J. Phys. Chem.* **97**, 8182 **1993**.
49. G. von Helden, T. Wyttenbach, M. T. Bowers, *Int. J. Mass Spectrom. Ion Processes* **146-147**, 349 **1995**.
50. T. Wyttenbach, J. E. Bushnell, M. T. Bowers, *J. Am. Chem. Soc.* **120**, 5098 **1998**.
51. D. E. Clemmer, R. R. Hudgins, M. F. Jarrold, *J. Am. Chem. Soc.* **117**, 10141 **1995**.
52. K. B. Shelimov, D. E. Clemmer, R. R. Hudgins, M. F. Jarrold, *J. Am. Chem. Soc.* **119**, 2240 **1997**.
53. M. F. Jarrold, *PCCP* **9**, 1659 **2007**.
54. R. W. Purves, R. Guevremont, *Anal. Chem.* **71**, 2346 **1999**.
55. R. W. Purves, R. Guevremont, S. Day, C. W. Pipich, M. S. Matyjaszczyk, *Rev. Sci. Instrum.* **69**, 4094 **1998**.
56. D. A. Barnett, R. W. Purves, R. Guevremont, *Nucl. Instrum. Methods Phys. Res. Sect. A-Accel. Spectrom. Dect. Assoc. Equip.* **450**, 179 **2000**.
57. M. McCooeye, L. Ding, G. J. Gardner, C. A. Fraser, J. Lam, R. E. Sturgeon, Z. Mester, *Anal. Chem.* **75**, 2538 **2003**.
58. D. A. Barnett, R. Guevremont, R. W. Purves, *Appl. Spectrosc.* **53**, 1367 **1999**.
59. D. A. Barnett, B. Ells, R. Guevremont, R. W. Purves, *Journal of the American Society for Mass Spectrometry* **10**, 1279 **1999**.
60. W. D. Price, P. D. Schnier, E. R. Williams, *Anal. Chem.* **68**, 859 **1996**.
61. P. D. Schnier, W. D. Price, R. A. Jockusch, E. R. Williams, *J. Am. Chem. Soc.* **118**, 7178 **1996**.
62. E. F. Strittmatter, P. D. Schnier, J. S. Klassen, E. R. Williams, *J. Am. Soc. Mass. Spectrom* **10**, 1095 **1999**.
63. W. Caminati, *PCCP* **6**, 2806 **2004**.
64. R. Sanchez, W. Caminati, J. C. López, J. L. Alonso, *Chem. Phys. Lett.* **414**, 226 **2005**.
65. L. L. Connell, T. C. Corcoran, P. W. Joireman, P. M. Felker, *Chem. Phys. Lett.* **166**, 510 **1990**.
66. P. M. Felker, *J. Phys. Chem.* **96**, 7844 **1992**.
67. J. T. Yi, D. W. Pratt, *PCCP* **7**, 3680 **2005**.
68. T. V. Nguyen, D. W. Pratt, *Phys. Chem. Chem. Phys.* **124**, 054317 **2006**.
69. M. R. Hockridge, S. M. Knight, E. G. Robertson, J. P. Simons, J. McCombie, M. Walker, *PCCP* **1**, 407 **1999**.
70. L. A. Philips, D. H. Levy, *Phys. Chem. Chem. Phys.* **89**, 85 **1988**.
71. M. Mons, E. G. Robertson, L. C. Snoek, J. P. Simons, *Chem. Phys. Lett.* **310**, 423 **1999**.
72. Y. Lee, J. Jung, B. Kim, P. Butz, L. C. Snoek, R. T. Kroemer, J. P. Simons, *J. Phys. Chem. A* **108**, 69 **2003**.

73. J. A. Dickinson, P. W. Joireman, R. W. Randall, E. G. Robertson, J. P. Simons, *J. Phys. Chem. A* **101**, 513 **1997**.

74. J. R. Johnson, K. D. Jordan, D. F. Plusquellic, D. W. Pratt, *Phys. Chem. Chem. Phys.* **93**, 2258 **1990**.

75. T. R. Rizzo, Y. D. Park, D. H. Levy, *J. Am. Chem. Soc.* **107**, 277 **1985**.

76. T. R. Rizzo, Y. D. Park, D. H. Levy, *Phys. Chem. Chem. Phys.* **85**, 6945 **1986**.

77. L. C. Snoek, R. T. Kroemer, M. R. Hockridge, J. P. Simons, *PCCP* **3**, 1819 **2001**.

78. F. Piuzzi, I. Dimicoli, M. Mons, B. Tardivel, Q. Zhao, *Chem. Phys. Lett.* **320**, 282 **2000**.

79. J. M. Bakker, L. M. Aleese, G. Meijer, G. von Helden, *Phys. Rev. Lett.* **91**, 203003 **2003**.

80. S. J. Martinez, J. C. Alfano, D. H. Levy, *J. Mol. Spectrosc.* **156**, 421 **1992**.

81. R. Cohen, B. Brauer, E. Nir, L. Grace, M. S. de Vries, *J. Phys. Chem. A* **104**, 6351 **2000**.

82. L. I. Grace, R. Cohen, T. M. Dunn, D. M. Lubman, M. S. de Vries, *J. Mol. Spectrosc.* **215**, 204 **2002**.

83. Y. Inokuchi, Y. Kobayashi, T. Ito, T. Ebata, *J. Phys. Chem. A* **111**, 3209 **2007**.

84. L. C. Snoek, E. G. Robertson, R. T. Kroemer, J. P. Simons, *Chem. Phys. Lett.* **321**, 49 **2000**.

85. T. Hashimoto, Y. Takasu, Y. Yamada, T. Ebata, *Chem. Phys. Lett.* **421**, 227 **2006**.

86. G. v. Helden, I. Compagnon, M. N. Blom, M. Frankowski, U. Erlekam, J. Oomens, B. Brauer, R. B. Gerber, G. Meijer, *PCCP* **10**, 1248 **2008**.

87. J. R. Cable, M. J. Tubergen, D. H. Levy, *J. Am. Chem. Soc.* **110**, 7349 **1988**.

88. J. R. Carney, T. S. Zwier, *J. Phys. Chem. A* **104**, 8677 **2000**.

89. L. C. Snoek, E. G. Robertson, R. T. Kroemer, J. P. Simons, *Chem. Phys. Lett.* **321**, 49 **2000**.

90. B. C. Dian, A. Longarte, S. Mercier, D. A. Evans, D. J. Wales, T. S. Zwier, *J. Chem. Phys.* **117**, 10688 **2002**.

91. I. Hünig, K. A. Seefeld, K. Kleinermanns, *Chem. Phys. Lett.* **369**, 173 **2003**.

92. I. Hunig, K. Kleinermanns, *PCCP* **6**, 2650 **2004**.

93. D. Řeha, H. Valdés, J. Vondrášek, P. Hobza, A. Abu-Riziq, B. Crews, M. S. de Vries, *Chemistry – A European Journal* **11**, 6803 **2005**.

94. W. Chin, J.-P. Dognon, F. Piuzzi, B. Tardivel, I. Dimicoli, M. Mons, *J. Am. Chem. Soc.* **127**, 707 **2004**.

95. W. Chin, J.-P. Dognon, F. Piuzzi, B. Tardivel, I. Dimicoli, M. Mons, *J. Am. Chem. Soc.* **127**, 707 **2004**.

96. W. Chin, I. Compagnon, J.-P. Dognon, C. Canuel, F. Piuzzi, I. Dimicoli, G. von Helden, G. Meijer, M. Mons, *J. Am. Chem. Soc.* **127**, 1388 **2005**.

97. G. A. Chass, R. S. Mirasol, D. H. Setiadi, T.-H. Tang, W. Chin, M. Mons, I. Dimicoli, J.-P. Dognon, B. Viskolcz, S. Lovas, B. Penke, I. G. Csizmadia, *J. Phys. Chem. A* **109**, 5289 **2005**.

98. Chin W. , Dognon J.P, Canuel C., Piuzzi F. , Dimicoli I, Mons M. , *Phys. Chem. Chem. Phys.* **122**, 054317 **2005**.

99. A. Abo-Riziq, B. O. Crews, M. P. Callahan, L. Grace, M. S. de Vries, *Angewandte Chemie-International Edition* **45**, 5166 **2006**.

100. J. M. Bakker, C. Plützer, I. Hünig, T. Häber, I. Compagnon, G. v. Helden, G. Meijer, K. Kleinermanns, *ChemPhysChem* **6**, 120 **2005**.

101. A. Abo-Riziq, J. E. Bushnell, B. Crews, M. Callahan, L. Grace, M. S. de Vries, *Chem. Phys. Lett.* **431**, 227 **2006**.

102. A. Abo-Riziq, B. O. Crews, M. P. Callahan, L. Grace, M. S. d. Vries, *Angew. Chem. Int. Ed.* **45**, 5166 **2006**.
103. E. Nir, L. Grace, B. Brauer, M. S. de Vries, *J. Am. Chem. Soc.* **121**, 4896 **1999**.
104. M. Mons, I. Dimicoli, F. Piuzzi, B. Tardivel, M. Elhanine, *J. Phys. Chem. A* **106**, 5088 **2002**.
105. J. M. Bakker, I. Compagnon, G. Meijer, G. von Helden, M. Kabelac, P. Hobza, M. S. de Vries, *PCCP* **6**, 2810 **2004**.
106. E. Nir, K. Kleinermanns, M. S. de Vries, *Nature* **408**, 949 **2000**.
107. E. Nir, C. Plützer, K. Kleinermanns, M. d. Vries, *Eur. Phys. J. D* **20**, 317 **2002**.
108. M. Gerhards, C. Unterberg, A. Gerlach, A. Jansen, *PCCP* **6**, 2682 **2004**.
109. M. Gerhards, C. Unterberg, A. Gerlach, A. Jansen, *Physical Chemistry Chemical Physics* **6**, 2682 **2004**.
110. H. Fricke, A. Funk, T. Schrader, M. Gerhards, *J. Am. Chem. Soc.*, **2008**.
111. H. Fricke, A. Gerlach, C. Unterberg, P. Rzepecki, T. Schrader, M. Gerhards, *PCCP* **6**, 4636 **2004**.
112. M. Gerhards, in *Principles of Mass Spectrometry Applied to Biomolecules,* C. L. Julia Laskin, Ed. (**2006**), pp. 1-61.
113. H. Fricke, A. Funk, T. Schrader, M. Gerhards, *J. Am. Chem. Soc.* **130**, 4692 **2008**.
114. H. Fricke, G. Schafer, T. Schrader, M. Gerhards, *PCCP* **9**, 4592 **2007**.
115. M. Gerhards, *Optics Communications* **241**, 493 **2004**.
116. E. G. Robertson, J. P. Simons, *PCCP* **3**, 1 **2001**.
117. T. S. Zwier, *J. Phys. Chem. A* **105**, 8827 **2001**.
118. P. Çarçabal, R. A. Jockusch, I. Hünig, L. C. Snoek, R. T. Kroemer, B. G. Davis, D. P. Gamblin, I. Compagnon, J. Oomens, J. P. Simons, *J. Am. Chem. Soc.* **127**, 11414 **2005**.
119. H. Fricke, K. Schwing, A. Gerlach, C. Unterberg, M. Gerhards, *PCCP* **12**, 3511 **2010**.
120. V. A. Shubert, T. S. Zwier, *J. Phys. Chem. A* **111**, 13283 **2007**.
121. S. B. Nielsen, A. Lapierre, J. U. Andersen, U. V. Pedersen, S. Tomita, L. H. Andersen, *Phys. Rev. Lett.* **87**, 228102 **2001**.
122. L. H. Andersen, A. Lapierre, S. B. Nielsen, I. B. Nielsen, S. U. Pedersen, U. V. Pedersen, S. Tomita, *Eur. Phys. J. D* **20**, 597 **2002**.
123. D. Nolting, C. Marian, R. Weinkauf, *PCCP* **6**, 2633 **2004**.
124. F. O. Talbot, T. Tabarin, R. Antoine, M. Broyer, P. Dugourd, *Phys. Chem. Chem. Phys.* **122**, 074310 **2005**.
125. S. B. Nielsen, oslash, ndsted, J. U. Andersen, J. S. Forster, P. Hvelplund, B. Liu, U. V. Pedersen, S. Tomita, *Phys. Rev. Lett.* **91**, 048302 **2003**.
126. E. S. Worm, I. H. Andersen, J. U. Andersen, A. I. S. Holm, P. Hvelplund, U. Kadhane, S. B. Nielsen, J.-C. Poully, K. Støchkel, *Phys. Rev. A* **75**, 042709 **2007**.
127. A. S. Danell, J. H. Parks, *Int. J. Mass spectrom.* **229**, 35 **2003**.
128. H. Kang, C. Dedonder-Lardeux, C. Jouvet, S. Martrenchard, G. Gregoire, C. Desfrancois, J. P. Schermann, M. Barat, J. A. Fayeton, *PCCP* **6**, 2628 **2004**.
129. H. Kang, C. Jouvet, C. Dedonder-Lardeux, S. Martrenchard, G. Gregoire, C. Desfrancois, J. P. Schermann, M. Barat, J. A. Fayeton, *PCCP* **7**, 394 **2005**.
130. H. Kang, C. Dedonder-Lardeux, C. Jouvet, G. Grégoire, C. Desfrançois, J. P. Schermann, M. Barat, A. Fayeton, *J. Phys. Chem. A* **109**, 2417 **2005**.
131. H. Kang, C. Jouvet, C. Dedonder-Lardeux, S. Martrenchard, C. Charriere, G. Gregoire, C. Desfrancois, J. P. Schermann, M. Barat, J. A. Fayeton, *Phys. Chem. Chem. Phys.* **122**, 084307 **2005**.
132. G. Gregoire, H. Kang, C. Dedonder-Lardeux, C. Jouvet, C. Desfrancois, D. Onidas, V. Lepere, J. A. Fayeton, *PCCP* **8**, 122 **2006**.

133. V. Lepere, B. Lucas, M. Barat, J. A. Fayeton, V. J. Picard, C. Jouvet, P. Carcabal, I. Nielsen, C. Dedonder-Lardeux, G. Gregoire, A. Fujii, *Phys. Chem. Chem. Phys.* **127**, 134313 **2007**.

134. B. Lucas, M. Barat, J. A. Fayeton, C. Jouvet, P. Çarçabal, G. Grégoire, *Chem. Phys.* **347**, 324 **2008**.

135. B. Lucas, M. Barat, J. A. Fayeton, M. Perot, C. Jouvet, G. Gregoire, S. B. Nielsen, *Phys. Chem. Chem. Phys.* **128**, 164302 **2008**.

136. H. Oh, K. Breuker, S. K. Sze, Y. Ge, B. K. Carpenter, F. W. McLafferty, *Proc. Nat. Acad. Sci. U.S.A.* **99**, 15863 **2002**.

137. H.-B. Oh, C. Lin, H. Y. Hwang, H. Zhai, K. Breuker, V. Zabrouskov, B. K. Carpenter, F. W. McLafferty, *J. Am. Chem. Soc.* **127**, 4076 **2005**.

138. J. Oomens, N. Polfer, D. T. Moore, L. van der Meer, A. G. Marshall, J. R. Eyler, G. Meijer, G. von Helden, *PCCP* **7**, 1345 **2005**.

139. B. Lucas, G. Gregoire, J. Lemaire, P. Maitre, J. M. Ortega, A. Rupenyan, B. Reimann, J. P. Schermann, C. Desfrancois, *Phys. Chem. Chem. Phys.* **6**, 2659 **2004**.

140. N. Polfer, B. Paizs, L. C. Snoek, I. Compagnon, S. Suhai, G. Meijer, G. von Helden, J. Oomens, *J. Am. Chem. Soc.* **127**, 8571 **2005**.

141. B. Lucas, G. Gregoire, J. Lemaire, P. Maitre, F. Glotin, J. P. Schermann, C. Desfrancois, *Int. J. Mass spectrom.* **243**, 97 **2005**.

142. N. A. MacLeod, J. P. Simons, *Mol. Phys.* **105**, 689 **2007**.

143. N. C. Polfer, J. Oomens, D. T. Moore, G. von Helden, G. Meijer, R. C. Dunbar, *J. Am. Chem. Soc.* **128**, 517 **2006**.

144. T. D. Vaden, T. S. J. A. de Boer, J. P. Simons, L. C. Snoek, S. n. Suhai, B. l. Paizs, *J. Phys. Chem. A* **112**, 4608 **2008**.

145. T. D. Vaden, S. A. N. Gowers, L. C. Snoek, *PCCP* **11**, 5843 **2009**.

146. A. Cimas, T. D. Vaden, T. S. J. A. de Boer, L. C. Snoek, M. P. Gaigeot, *J. Chem. Theory Comput.* **5**, 1068 **2009**.

147. T. D. Vaden, T. S. J. A. De Boer, N. A. MacLeod, E. M. Marzluff, J. P. Simons, L. C. Snoek, *Phys. Chem. Chem. Phys.* **9**, 2549 **2007**.

148. G. Gregoire, M. P. Gaigeot, D. C. Marinica, J. Lemaire, J. P. Schermann, C. Desfrancois, *Phys. Chem. Chem. Phys.* **9**, 3082 **2007**.

149. D. H. Levy, *Annu. Rev. Phys. Chem.* **31**, 197 **1980**.

150. W. H. Robertson, J. A. Kelley, M. A. Johnson, *Rev. Sci. Instrum.* **71**, 4431 **2000**.

151. E. G. Diken, N. I. Hammer, M. A. Johnson, *Phys. Chem. Chem. Phys.* **120**, 9899 **2004**.

152. G. E. Douberly, A. M. Ricks, B. W. Ticknor, M. A. Duncan, *J. Phys. Chem. A* **112**, 950 **2008**.

153. G. E. Douberly, A. M. Ricks, B. W. Ticknor, W. C. McKee, P. v. R. Schleyer, M. A. Duncan, *J. Phys. Chem. A* **112**, 1897 **2008**.

154. D. Gerlich, *J. Chem. Soc. Faraday Trans.* **89**, 2199 **1993**.

155. T. D. Vaden, T. S. J. A. de Boer, J. P. Simons, L. C. Snoek, *PCCP* **10**, 1443 **2008**.

156. N. A. Macleod, J. P. Simons, *PCCP* **6**, 2821 **2004**.

157. J. A. Stearns, O. V. Boyarkin, T. R. Rizzo, *J. Am. Chem. Soc.* **129**, 13820 **2007**.

158. J. A. Stearns, O. V. Boyarkin, T. R. Rizzo, *CHIMIA* **62**, 240 **2008**.

159. J. A. Stearns, C. Seaiby, O. V. Boyarkin, T. R. Rizzo, *PCCP* **11**, 125 **2009**.

160. T. R. Rizzo, J. A. Stearns, O. V. Boyarkin, *Int. Rev. Phys. Chem.* **28**, 481 **2009**.

161. N. S. Nagornova, T. R. Rizzo, O. V. Boyarkin, *J. Am. Chem. Soc.* **132**, 4040 **2010**.

162. H. Fabian, D. Naumann, *Methods* **34**, 28 **2004**.

163. R. B. Dyer, F. Gai, W. H. Woodruff, R. Gilmanshin, R. H. Callender, *Acc. Chem. Res.* **31**, 709 **1998**.

164. M. Gruebele, J. Sabelko, R. Ballew, J. Ervin, *Acc. Chem. Res.* **31**, 699 **1998**.

165. D. T. Leeson, F. Gai, H. M. Rodriguez, L. M. Gregoret, R. B. Dyer, *Proc. Nat. Acad. Sci. U.S.A.* **97**, 2527 **2000**.
166. M. Eigen, L. D. Maeyer, *In Technique of Organic Chemistry*. A. Weissberger, Ed.; Interscience: New York,, Ed., (**1963**), pp. p:895-1054.
167. J. Lee, A. Liwo, H. A. Scheraga, *Proc. Nat. Acad. Sci. U.S.A.* **96**, 2025 **1999**.
168. M. Levitt, A. Warshel, *Nature* **253**, 694 **1975**.
169. D. A. Hinds, M. Levitt, *Trends Biotechnol.* **13**, 23 **1995**.
170. Y. Xia, a. M. Levitt, *Proteins: Struct. Funct. Genet.* **55**, 104 **2004**.
171. D. J. Wales, H. A. Scheraga, *Science* **285**, 1368 **1999**.
172. D. J. Wales, *Mol. Phys* **102**, 891 **2004**
173. D. J. Wales, *Science* **271**, 925 **1996**.
174. D. A. Evans, D. J. Wales, B. C. Dian, T. S. Zwier, *Phys. Chem. Chem. Phys.* **120**, 148 **2004**.
175. D. A. Evans, D. J. Wales, *Phys. Chem. Chem. Phys.* **121**, 1080 **2004**.
176. S. N. Fejer, D. J. Wales, *Phys. Rev. Lett.* **99**, 086106 **2007**.
177. B. Strodel, D. J. Wales, *Chem. Phys. Lett.* **466**, 105 **2008**.
178. M. S. Bauer, B. Strodel, S. N. Fejer, E. F. Koslover, D. J. Wales, *Phys. Chem. Chem. Phys.* **132**, 054101 **2010**.
179. J. K. Agbo, D. M. Leitner, D. A. Evans, D. J. Wales, *Phys. Chem. Chem. Phys.* **123**, 124304 **2005**.
180. D. J. Nesbitt, R. W. Field, *J. Phys. Chem.* **100**, 12735 **1996**.
181. M. Gruebele, P. G. Wolynes, *Acc. Chem. Res.* **37**, 261 **2004**.
182. M. GRUEBELE, R. BIGWOOD, *Int. Rev. Phys. Chem.* **17**, 91 **1998**.
183. J. Keske, D. A. McWhorter, B. H. Pate, *Int. Rev. Phys. Chem.* **19**, 363 **2000**.
184. K. K. Lehmann, G. Scoles, B. H. Pate, *Annu. Rev. Phys. Chem.* **45**, 241 **1994**.
185. F. F. Crim, *Annu. Rev. Phys. Chem.* **35**, 657 **1984**.
186. C. G. Elles, D. Bingemann, M. M. Heckscher, F. F. Crim, *Phys. Chem. Chem. Phys.* **118**, 5587 **2003**.
187. O. V. Boyarkin, T. R. Rizzo, D. S. Perry, *Phys. Chem. Chem. Phys.* **110**, 11346 **1999**.
188. B. C. Dian, A. Longarte, T. S. Zwier, *Science* **296**, 2369 **2002**.
189. B. C. Dian, J. R. Clarkson, T. S. Zwier, *Science* **303**, 1169 **2004**.
190. B. C. Dian, A. Longarte, P. R. Winter, T. S. Zwier, *Phys. Chem. Chem. Phys.* **120**, 133 **2004**.
191. B. C. Dian, G. M. Florio, J. R. Clarkson, A. Longarte, T. S. Zwier, *Phys. Chem. Chem. Phys.* **120**, 9033 **2004**.
192. J. R. Clarkson, B. C. Dian, L. Moriggi, A. DeFusco, V. McCarthy, K. D. Jordan, T. S. Zwier, *Phys. Chem. Chem. Phys.* **122**, 214311 **2005**.
193. J. R. Clarkson, E. Baquero, T. S. Zwier, *Phys. Chem. Chem. Phys.* **122**, 214312 **2005**.
194. T. A. LeGreve, J. R. Clarkson, T. S. Zwier, *J. Phys. Chem. A* **112**, 3911 **2008**.
195. N. R. Pillsbury, C. W. Muller, T. S. Zwier, *J. Phys. Chem. A* **113**, 5013 **2009**.
196. A. Kamariotis, O. V. Boyarkin, S. R. Mercier, R. D. Beck, M. F. Bush, E. R. Williams, T. R. Rizzo, *J. Am. Chem. Soc.* **128**, 905 **2005**.
197. O. V. Boyarkin, S. R. Mercier, A. Kamariotis, T. R. Rizzo, *J. Am. Chem. Soc.* **128**, 2816 **2006**.
198. S. Mercier, **2008**.
199. J. A. Stearns, S. Mercier, C. Seaiby, M. Guidi, O. V. Boyarkin, T. R. Rizzo, *J. Am. Chem. Soc.* **129**, 11814 **2007**.
200. J. A. Stearns, M. Guidi, O. V. Boyarkin, T. R. Rizzo, *Phys. Chem. Chem. Phys.* **127**, 154322 **2007**.

Chapter 2
Experimental Setup

The experimental results in this work have been obtained with a home-built ion trap machine containing, as the central part, a cold 22-pole ion trap. The first part of this chapter gives an overview of the machine and the general principles of producing, selecting, cooling and trapping the ions. The second part gives a description of the UV and IR laser setups used in performing the different experimental measurements presented in this thesis.

2.1 Overview of our ion trap experiments

The schematic diagram of a typical trapping experiment is illustrated in Figure 2.1. It consists of an ion source, a first mass filter, an ion trap where the ion can be stored and cooled, followed by a second mass filter and an ion the detector.
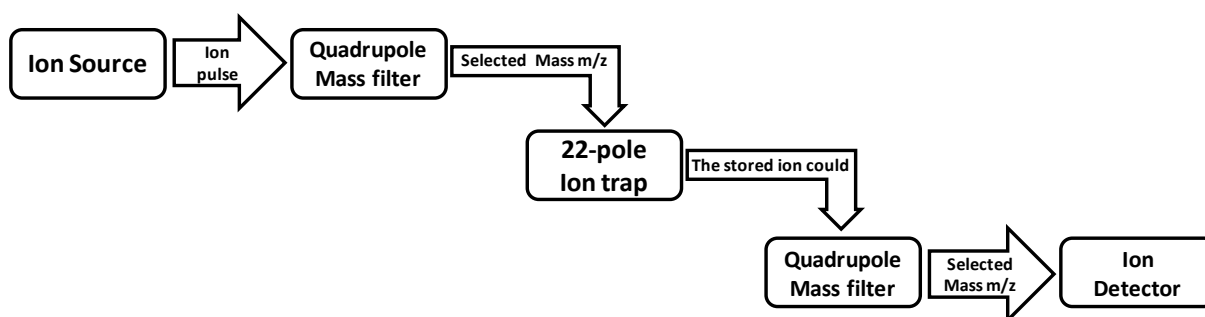
Figure 2.1 : Schematic of the sequence of events of a tandem mass spectrometric ion trap experiment

Usually, the ions are generated and stored in an external reservoir in the ion source and upon release form an ion packet. Ions of a particular mass within this packet are selected by a quadrupole mass filter and then guided into the 22-pole ion trap, where they cooled by

inelastic collisions with cold helium buffer gas. The cooled ions interact with the laser, and the resulting ions (both parent and fragments) are released from the trap and sent through a second mass filter, which analyzes their mass before they are finally detected and counted.

2.2 The home-built ion trap machine

The machine used in these studies is a home-built tandem mass spectrometer. The apparatus, as well as the operating conditions and procedures to maximize the production and the transmission of ions, have been described in great detail in the PhD thesis of Dr Anthi Kamariotis [1] and Dr Sébastien Mercier [2], and these details are not repeated here; only a general description and a summary of the important features will be given.
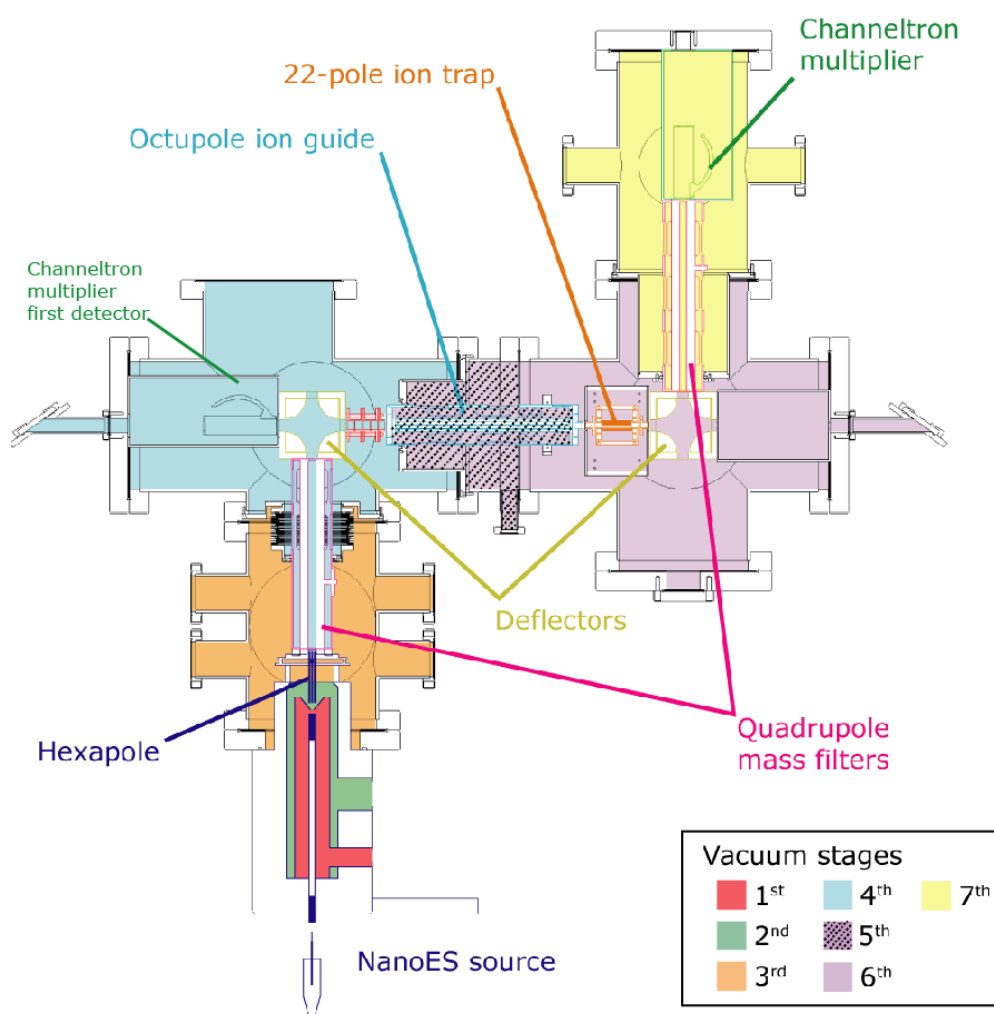
Figure 2.2: Section view of the tandem mass spectrometer

The seven differential pumping stages and the main ion optical devices needed to guide the ions through the entire machine are displayed in Figure 2.2.

The ions are produced in the gas phase *via* a commercial *nano*-electrospray device. The resulting protonated molecules are transferred from atmospheric pressure to vacuum through a glass capillary and traverse a skimmer before entering an RF-only hexapole. By raising the voltage on the exit electrode of the hexapole, one can trap the ions and allow them to equilibrate translationally. Lowering the voltage on this electrode releases the ions from the trap in a packet of approximately 0.5 ms duration. Since the electrospray process generates a variety of species in addition to the molecule of interest (such as water clusters, different charge states of the molecule and some fragmentations induced by collisions), the resulting ion packet is guided into a first quadrupole mass filter for selection of the parent ions according to their mass-charge ratio, *m/z*. Ions of the selected mass are then turned 90° by a static quadrupole deflector, either to the left towards a first ion detector or to the right to be guided to the 22-pole ion trap. The neutral molecules that enter the machine together with the ions will not be affected by the deflector's electric field and will be pumped out by the turbomolecular pump of this stage. This first ion detector helps in investigating the properties of the first part of the machine and in optimizing the voltages for the best ion transmission. After the bender, the ions travel through five decelerating cylindrical electrodes and then are guided by an RF-octupole into the 22-pole ion trap. The 22-pole is mounted on a closed cycle He refrigerator, which cools the trap and its surrounding walls to ~ 6K. Helium gas is introduced into the trap by a pulsed valve approximately 1 ms before the ion packet is released from the hexapole in order to reach the trap temperature before the arrival of the ion packet. The kinetic energy of the ions is dissipated by inelastic collisions with the helium buffer gas so that they can be trapped radially by the effective potential created by the RF electrodes and axially in the potential well created by setting the pole bias voltage of the trap lower than those of its entrance and exit electrodes. After undergoing several collisions and being thermalized to the trap environment, the ions will interact with the ultraviolet and infrared laser light that is directed down the axis of the 22-pole ion trap. Upon photon absorption the internal energy of the ions becomes sufficient to cause dissociation of one or more chemical bonds producing fragment ions. If the photodissociation is fast enough such that the fragmentation will occur in the trap, when released, the ions packet will contain both parent and daughter ions. This packet is then turned 90° by a second deflector and delivered to the final quadrupole for mass analysis before they reach the ion detector. This quadrupole

mass filter is set to detect either a specific fragment or the parent mass. In the first case, we can detect the amount of photofragments as function of the laser wavelength, generating a photofragment excitation spectrum. On alternate trapping cycles we detect the parent ions and use them to normalize the fragment signal for slow fluctuations of the ion source. Both detectors used in this machine are channeltron electron multipliers with a conversion dynode. The latter component is set at a high negative voltage (for positive ions), typically -5 kV, and emits electrons upon impact of the accelerated ions. The electrons emitted from the dynode surface are collected by the channeltron multiplier, which further amplifies the electron current. The resulting signal is sent to a fast preamplifier and then to a gated pulse counter.

The vacuum system of the machine consists of turbomolecule drag pumps backed by membrane pumps, except the first stage, which is evacuated by a mechanical pump. Typical pressures of each stage are shown in Table1. The pressure in the vacuum chambers is measured by ion gauges except for the first and second vacuum stages where Pirani gauges are used. The machine has a vacuum interlock system connected to the ion gauge of stage 4; when the pressure in this chamber exceeds 10^{-4} mbar all sensitive power supplies switch off.

Stage 1	Stage 2	Stage 3	Stage 4	Stage 5	Stage 6	Stage 7
2mbar	$2x10^{-3}$ mbar	$4x10^{-5}$mbar	$3x10^{-7}$mbar	$2x10^{-8}$mbar	$5x10^{-9}$mbar	$<2.10^{-9}$mbar

Table2.1 : Pressure (mbar) in different stage of the machine. The different stages are shown in Figure 2.2.

The following sections explain in more detail the principle of operation of the key components of the ion machine.

2.2.1 Nano electrospray

Ion generation is accomplished by the use of nano-electrospray, which is a form of electrospray that uses lower liquid flow rates and the formation of smaller droplets. The formation of a spray of small droplets by applying an intense electric field to a liquid surface was first reported in the early part of the 20th century [3, 4]. In the 1960's Dole and al. demonstrated the use of this electrospray phenomena as an ion source for mass spectrometry to ionize intact chemical species [5, 6]. Building upon the ideas of Dole, Fenn developed the electrospray as an ionization technique for high mass biologically related compounds [7-9], and since then it has become a standard technique in mass spectrometry. The processes

involved in the gas-phase ion generation by electrospray have been widely investigated and intensively debated [10-20], although its general implementation has remained basically the same. An analyte is dissolved in a polar solvent, and the solution flows through a conductive needle, which is maintained at high voltage. The electric field on the needle causes charge accumulation at the liquid surface and induces the formation of a Taylor cone [21] in which the liquid breaks up into charged droplets. When the coulombic repulsion between the charges on the droplet exceeds the surface tension (i.e. referred to as the Rayleigh limit) the drops explode in a jet-fission mode, producing a set of small progeny droplets. The droplet formation is followed by multiple uneven Rayleigh division events [22], until one of two things occur (according to different models). In one case, the field at the droplet surface is high enough that spontaneous desorption of preformed ions from the droplet can occur [12, 13]. Another model proposes that successive droplet divisions occur until there is only a single analyte molecule per droplet, from which the neutral solvent eventually evaporates[5, 11].

The development of *nano*-electrospray started in the mid 1990s [23, 24] and owes its name to the lower liquid flow rate ($\sim$1nL$\cdot$min^{-1} to 1μL$\cdot$min^{-1}) compared to conventional electrospray ($\sim$1μL$\cdot$min^{-1} to 1mL$\cdot$min^{-1}). It overcomes the propensity of large molecules to fragment when ionized, facilitates the formation of bare ions and their clusters and provides better sensitivity toward a variety of analytes, including peptides and oligosaccharides [25].

The ion source that we used is represented schematically in Figure 2.3. It is a commercial electrospray source (Analytica of Brandford, Inc., CT, USA) whose atmospheric section, which was of a regular electrospray design, has been replaced by a nano-electrospray source kit (model ES025A from Proxeon Biosystems, DK). This kit is formed from a nanospray needle consisting of a Au/Pd coated borosilicate capillary ($\sim$ 1 μm i.d. at the opening) inserted into a 1.5 mL Eppendorf vial. Both the vial and the capillary are filled with the sample solution, having a typical analyte concentration of 2×10^{-4} M in a 1:1 water/methanol mixture with 0.1% acetic acid. The assembly is connected to a high voltage power supply and mounted on an electrically isolated platform that allows adjustment of the position in the xyz-directions.
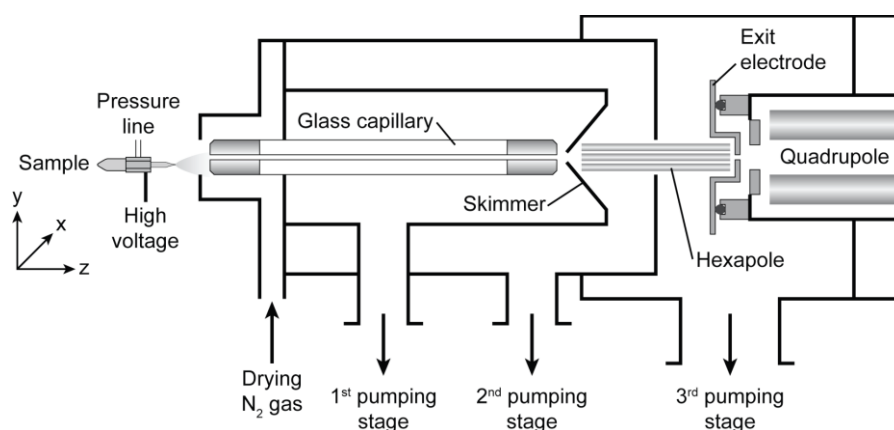
Figure 2.3 : Schematic of the nano-electrospray ion source interface.

During the spray formation a slight continuous pressure is applied to the solution, and the needle is floated ~500 V to 1 kV above ground potential. The Ni-coated entrance end of the glass capillary (24cm long), which serves as the counter-electrode, is grounded. To assist in the desolvation of the droplets, a counter-current flow of nitrogen gas can be used. Ions formed at atmospheric pressure enter the glass capillary (i.d. of 500 μm) and exit at the other end in the first vacuum stage pumped to a pressure of 2 mbar. A supersonic expansion takes place at the end of the capillary between the capillary exit and a skimmer. The metal-coated capillary exit acts itself as an electrostatic element that can accelerate ions through the skimmer, but the process may warm them through collisions with neutral background gas. These collisions should prevent condensation of the ions with solvent molecules in the carrier gas and help complete the desolvation process without disruption of the covalent bonds, although sufficiently high voltage applied to the capillary exit can cause bond breakage. Only the core of the free jet expansion passes through the skimmer orifice towards the hexapole. The latter traverses two pumping stages with significantly different average pressure. When traversing the hexapole from the high pressure side to the low side, the ions pass from a region of viscous flow where they still undergo collisions with the neutral molecules, to a region of molecular flow, where the mean free path is much larger than the instrument dimensions. The potential at which the ions are introduced into the high vacuum region is then defined by the floating potential of the hexapole rods (pole bias). By applying a voltage pulse to the exit lens of the hexapole we turn the continuous ion signal generated by the electrospray ionization source into a packet of ions, which matches the duty cycle of the ions to that of our pulsed lasers. In addition, collisions in the hexapole thermalize the ion and reduce the spread of ion kinetic energy. This will improve the transmission efficiency of the ions through the tandem mass spectrometer. However, trapping too many ions in the hexapole

can lead to RF-induced-heating effects causing fragmentation of the ions [1, 26-28]. This effect is critical when the investigated species are weakly bound complexes such as solvated ions.

2.2.2 Quadrupole mass filtering

In 1953, Paul Wolfgang developed the quadrupole mass analyzer based on a clever design where he uses alternating quadrupolar electric fields rather than magnetic fields to separate charged particles of different mass to charge ratios[29]. Later, he described the use of this same device as a means of trapping charged particles [30, 31]. Only short summary on the basics of operating rf quadrupole is given here.
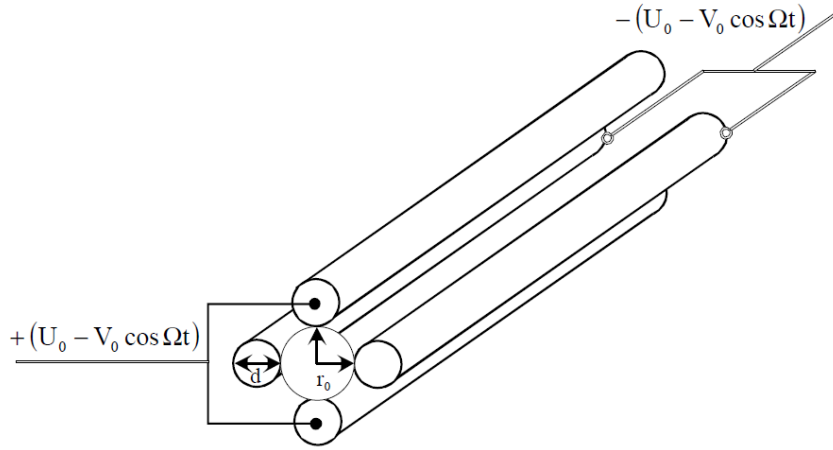
Figure 2.4: Quadrupole and supplying voltages.

A quadrupole mass analyzer consists of four parallel rods with cylindrical or hyperbolic cross section, aligned along the z-axis and equally spaced on an inscribed circle of radius r_0 (see Figure 2.4). Each pair of adjacent rods have a potential with alternate polarity, $\Phi_0 = U + V\cos\Omega t$, where U is a fixed DC and $V\cos\Omega t$ is the applied RF. The electrical potential in the region between the rods is given by

$$\Phi = \Phi_0 \frac{x^2 + y^2}{r_0^2}$$

Eq 2.1

If a charged particle is injected into the quadrupole and propelled down the z-axis, it will be subjected to forces in the *x* and *y* directions. The equations of motion of this particle

25

involve motion in 3 planes. The ion trajectory is described by the solution of a set of decoupled one-dimensional differential equations, called the Mathieu equations. Depending on their mass, the ions could follow either stable or unstable trajectories. Furthermore, the nature of the motion is a function of the two dimensionless stability parameters, *a* and *q*, independent of the initial conditions:

$$a = \frac{8eU}{mr_0^2\Omega^2} \ and \ q = \frac{4eV}{mr_0^2\Omega^2}$$ Eq 2.2

In order to understand the mass filtering ability of the quadrupole, consider the stability diagram displayed in Figure 2.5. For a fixed r_0 and Ω, particles of a specific mass follow a stable trajectory by the proper choice of *a* and *q*, or *U* and *V*, respectively, in the stability region of the diagram. Physically this means that in the stable cases, the particle oscillates in the *x* and *y* directions within the free space between the rods and eventually exits the quadrupole. In the unstable cases, the particle veers off in the *x* and/or *y* direction, hits a quadrupole rod or exits laterally and is lost.
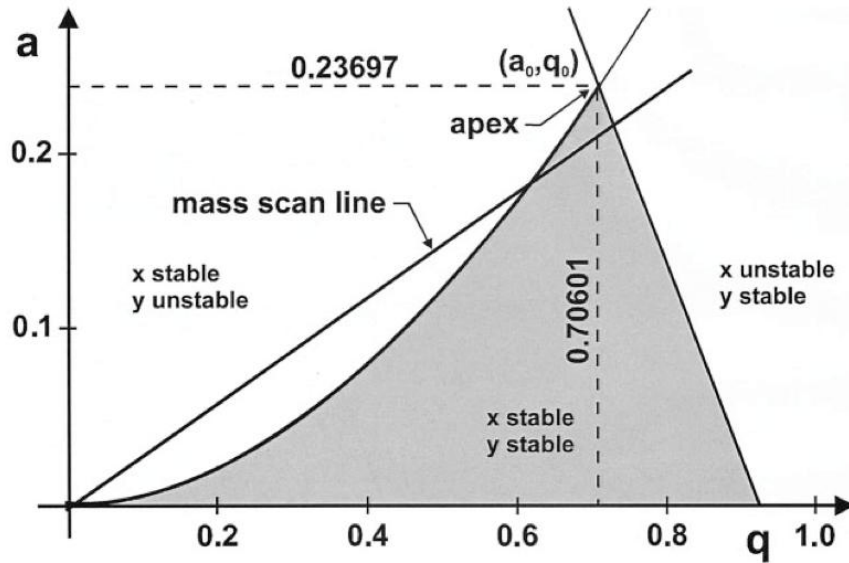
Figure 2.5: Stability diagram for a quadrupole mass filter. [32]

A mass spectrum is obtained by varying simultaneously the values of *U* and *V* along the "mass scan line" while maintaining their ratio, $U/V = a/2q$, fixed. By increasing this ratio, the quadrupole operates with a "mass scan line" of high slope that cuts across the tip of the stability region thereby allowing for high resolution of the mass spectrum. Further detail

on the basic characteristics of this device and computer simulation studies discussing the geometry and the ion motion can be found in many books, reviews and papers [32-38].

2.2.3 The 22-pole ion trap

With the objective of investigating the chemistry of ion-molecule reactions of astrochemical relevance, Gerlich and coworkers introduced the 22-pole rf ion trap[39], which allowed long trapping time and efficient buffer gas cooling. Extensive experimental and theoretical work has been devoted to characterizing this rf device [40-43].

In order to understand the principle of operation of a radio-frequency ion trap, one must treat the equation of motion within an adiabatic approximation, which leads to the introduction of the so-called effective potential V*[44]. The frequency of the inhomogeneous field applied on the rods should be high enough to stay within the range of validity of the adiabatic approximation. An adiabaticity parameter   is introduced to give a quantitative measure for the quality of such an approximation. Gerlich and Teloy proved the validity of the adiabatic approximation if, along a trajectory   always remains smaller than 0.3 [44]. Recently Wester established a new limit for   of 0.36 [45]. Under such conditions the total kinetic energy is an adiabatic constant of the motion.

The trajectory of a particle with charge *q* and mass *m*, moving in an oscillating field, can be described as the superposition of a smooth trajectory and a fast oscillatory motion. The smooth drift term can be derived from the effective potential. In the case of a linear 2n-multipole, this later is expressed by the following expression [46]:

$$V^* = \frac{1}{8}\frac{qV_0^{\ 2}}{\varepsilon}\left(\frac{r}{r_0}\right)^{2n-2}$$

Eq 2.3

where   is the characteristic energy, $\varepsilon = \left(\dfrac{1}{2n^2}\right)m\omega^2 r_0^2$

  is the inscribed radius, 2n is the number of rods,

  the amplitude and   the frequency of the rf voltage applied to the rods.

The effective potential is proportional to $r/r_0^{\ 2n-2}$, so as *n* increases the repulsive wall becomes steeper, and the field free region near the center line becomes larger. Examples

of calculated effective potentials for a quadrupole, an octupole, and a 22-pole trap are given in Figure 2.6.
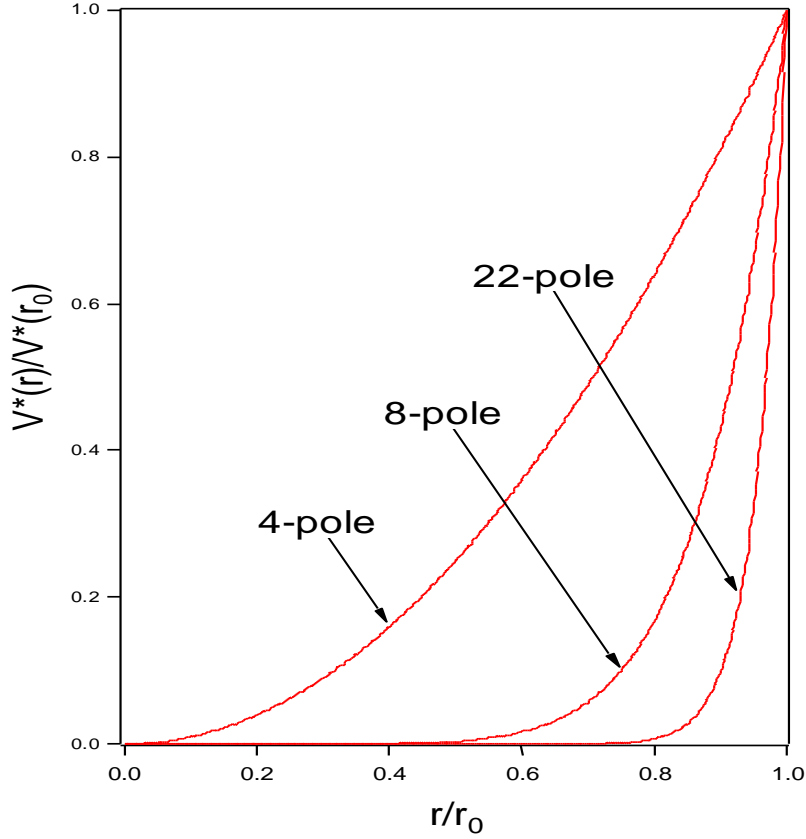
Figure 2.6: Relative effective potentials of a quadrupole, an octupole and a 22-pole.

Comparison of these curves reveals the advantage of using higher order multipoles for buffer gas cooling: they have much wider field free region which is important if one wants to minimize RF-driven heating of the stored ions. Ion trajectories for several multipoles are presented in Figure 2.7. In the trap, ions move undisturbed in the field-free region but undergo an oscillating micromotion driven by the RF when they come close to the electrodes. In the case of the 22-pole, the field-free region is wide enough such that the ions move mostly undisturbed and the wiggling motion occurs only in the close vicinity of the rods, minimizing RF heating them under the adiabatic conditions [42, 46]. In low temperature applications, a buffer gas is pulsed into the trap to cool the ions and increase the trapping efficiency. Collision between the ions and the gas occurs during both the straight and wiggling motion of the ions. In the first case, the ions are thermalized to the temperature of the buffer gas while in the second case collisions will have a heating effect.
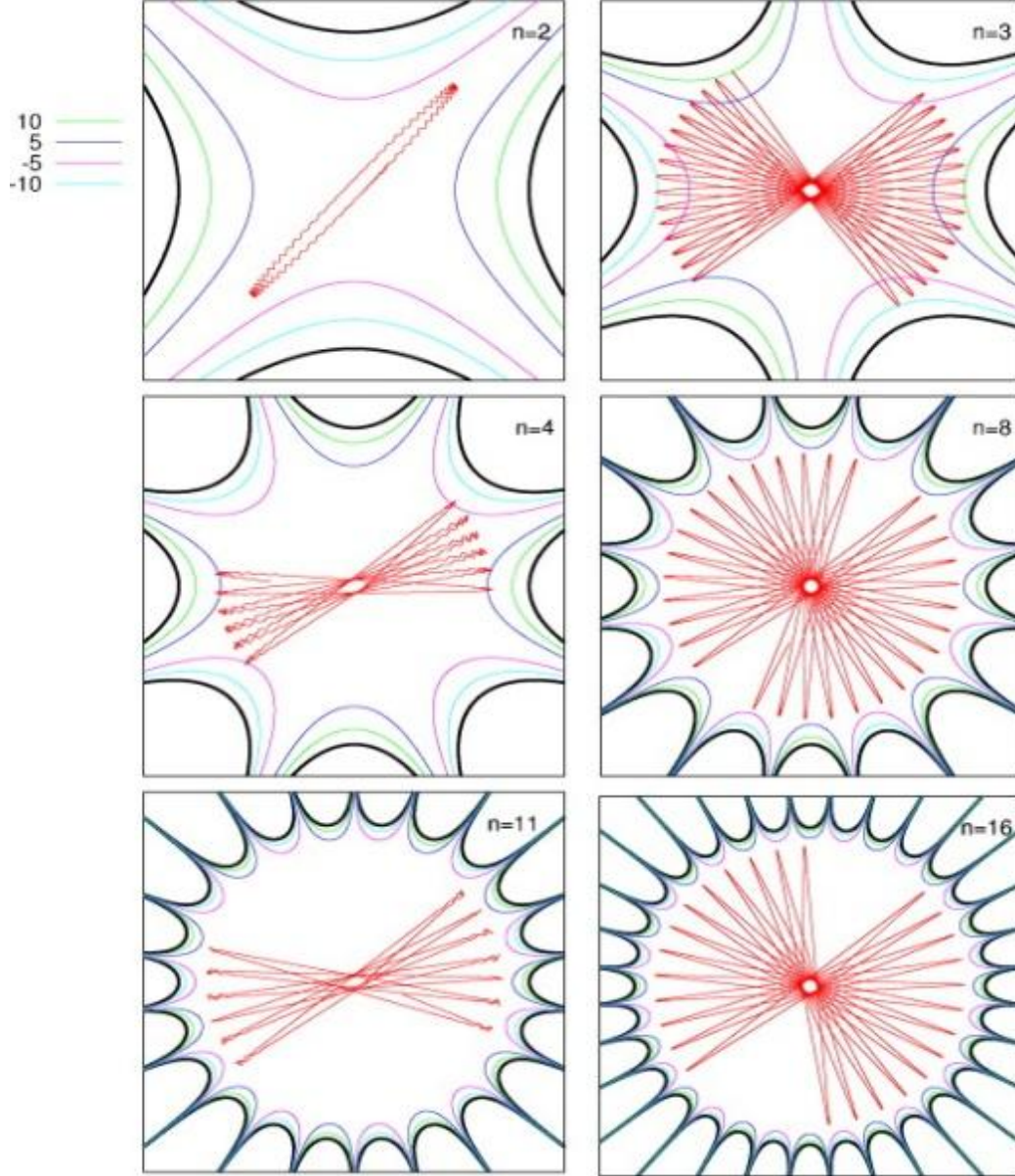
Figure 2.7: Visualization of RF fields generated by infinitely long multipoles for several values of n at a fixed time. The black lines represent the hyperbolic electrodes, the equipotential lines are shown colored coded and the red line in each figure illustrates the typical ion trajectories [42].

Different measurements and numerical simulations show that this heating behavior is almost negligible for a trap with a wide field-free region [42]. The velocity distribution of an ion in a linear multipole, in the presence of helium buffer gas at 18K, is shown in Figure 2.8. The thermal distribution approaches the Boltzmann distribution at the temperature of the buffer gas, with increasing the number of poles. For a 22-pole trap the ion temperature is only slightly higher than the buffer gas temperature.

29
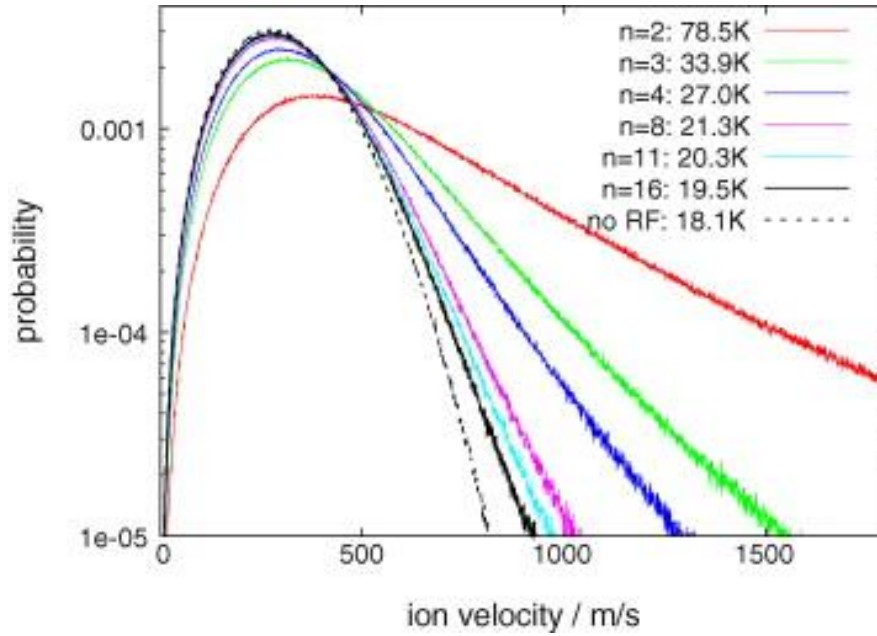
Figure 2.8: Velocity distribution of an ion stored in traps with different multipolarity n in the presence of helium buffer gas (18K) [42].

Another parameter that could lead to slight warming of the ions during the trapping process, is the potential generated by the end electrodes. It has components in the longitudinal as well as the radial direction, and the latter component can lead to a heating effect by pushing the ions towards the RF electrodes. Wester *et al.* have observed this behavior in the photodetachment of cold OH− ions in a 22-pole ion trap [41]. By performing transversal laser scans through the trap they observed a higher density of OH⁻ ions towards the RF electrodes. In a recent work, by measuring the column density distribution obtained from the position-dependent photodetachment rate, they observed ten distinct minima in the trapping potential [43]. They attributed them to a breaking of the 22-fold symmetry by a slight misalignment of some of the radiofrequency electrodes.

In addition to its excellent thermalization capability, the 22-pole enables long trapping times, which makes it an ideal device to investigate spectroscopically cold charged species. Gerlich reported a trapping time of up to minute without ion loss [39, 46].

The 22-pole trap we use in our apparatus has been designed and built by Dr. Oleg Boyarkin, based on the publications from the group of Dieter Gerlich [39, 46]. Figure 2.9 illustrates the 22-pole trap mounted on the cold head as well as a picture of the trap without its cold shields

30
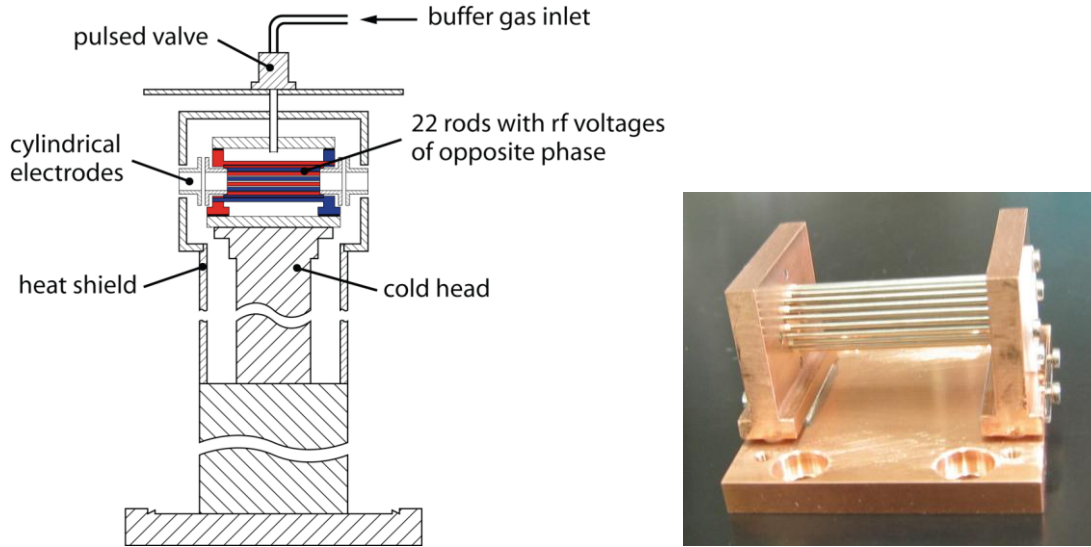
Figure 2.9: Schematic section view of the home-built 22-pole ion trap and cold head assembly, and picture of the 22 rods mounted onto their holders.

It consists of 2×11 stainless steel rods, 50 mm long and 1 mm diameter circumscribing a circle of 1 cm diameter. The rods are supported by two copper holders, each of them being electrically connected to a set of 11 alternate rods and insulated from the other 11 by ceramic sleeves. Equal RF voltage of opposite phase is applied to the holders, where thin sapphire plates insure electrical insulation, but good thermal, contact with the rest of the trap housing. In order to let the ions in, confine them and finally release them after the photodissociation, two pairs of cylindrical electrodes are placed at the entrance and exit of the trap. Suitable voltages are applied on each lens to trap or release the ions. The system is enclosed by copper walls, which are mounted onto a cold head of a cryocooler that can be cooled to 6 K. This structure is surrounded by a second thermal shield held at about 50 K. The helium buffer gas is introduced into the trap *via* a Teflon tube through a pulse valve, which is fastened into an independent plate near the heat shield. Many more details on the trap assembly, as well as its characterization and operating conditions can be found in the PhD dissertation of Dr. Sebastien Mercier [2].

2.3 Description of the laser setups

2.3.1 Generation of UV laser light

The schematic of the ultra-violet laser light generation used in this thesis is depicted in Figure 2. 10. The UV laser light is produced by frequency doubling the visible output of a dye laser pumped by third harmonic of a Nd:YAG (yttrium aluminum garnet) laser.
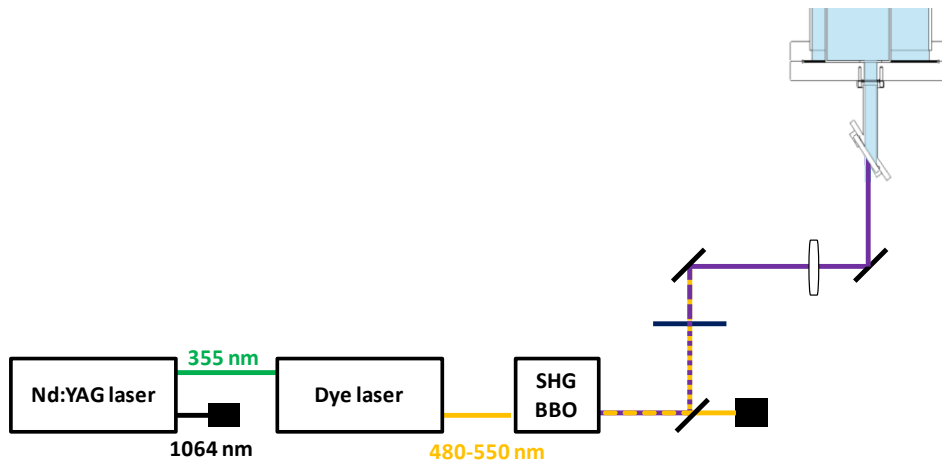
Figure 2. 10: Schematic diagram of the UV generation setup

The Nd:YAG pulse energies used to pump the dyes are on the order of 150 mJ at a repetition rate of 10 Hz or 20 Hz. We have mainly worked with Coumarin 540A and 503 Exciton dyes to cover the region from 515 to 545nm. The Nd:YAG pumping power is adjusted to obtain a maximum pulse energy of 50 mJ out of the dye lase (Lumonics model HD-500), which is limited by the damage threshold of the beta barium borate crystal (BBO) used to convert the output of the dye laser into ultraviolet light by second harmonic generation (SHG). The BBO crystal is mounted in an Autotracker III (Inrad, NJ, US) and rotated automatically, together with a fused silica compensator, to the phase-matching angle as the visible wavelength is scanned.

The resulting UV beam is separated from the remaining visible light *via* reflections on two dichroic mirrors and the use of a colored glass filter. The UV beam is then optionally focused by the use of a converging lens before being deflected by a prism through a BaF_2 window placed at Brewster's angle into the machine, on the side of the 4th vacuum stage. The

UV pulse duration is about 5-10 ns and the energy is 1.5 to 3 mJ. The typical linewidth in the UV is about 0.07 cm^{-1}.

2.3.2 Generation of IR laser light

Infrared laser light is generated by converting the horizontally polarized 1064 fundamental harmonic output of the Innolas Spitlight 600 Nd:YAG pulse laser system into tunable radiation using a multi-stage OPO/OPA system from LaserVision, shown schematically in Figure 2. 11.
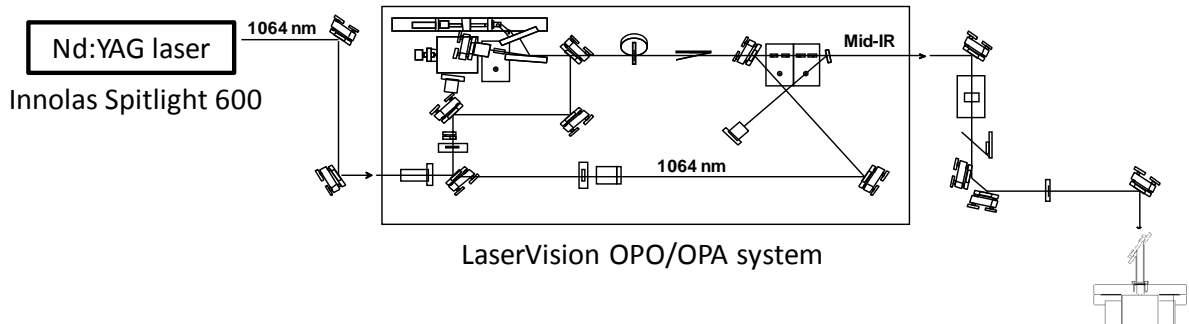
Figure 2. 11: Schematic overview of the IR laser generation setup

The output of the Nd:YAG laser pulse length is 7 ns and the line width of the unseeded beam is 0.5 cm^{-1}. The pulse energy is about 500 mJ with a repetition rate of 10 Hz. In the converter system a beam splitter divides the horizontally polarized incoming 1064 nm pump into two separate beams. One is frequency-doubled in a KTP (Potassium Titanyl Phosphate) crystal to provide the 532 nm pump light for the OPO stage, while the second beam is directed through a delay line before recombination with the vertically polarized idler output of the first stage. The idler wave of the OPO stage passes through a variable half-wave plate and two beam-steering mirrors before being combined with the delayed 1064 nm beam. The combined beams are then directed into an OPA stage for difference-frequency mixing. Four Potassium Titanyl Arsenate (KTA) crystals are used in the OPA stage. Its output consists of a horizontally polarized signal (the idler of the OPO stage) and a vertically polarized idler, which is in the mid-infrared region between 1.35 and 5 μm. A Brewster plate polarizer isolates the idler from the combined output.

To generate far-infrared radiation, a Silver Gallium Selenite (AgGaSe$_2$) crystal is added after the output of the OPA stage. A Si filter is included between the OPO and OPA stage to remove the signal wave from the beam. The pump beam is limited to a maximum energy of 30 mJ to prevent damaging the crystal. After the crystal, a ZnSe filter is used to

remove the pump light. It is mounted at an angle of 45° such that it reflects the pump light and at the same time is closer to Brewster's angle for the vertically polarized far-IR

All seven crystals are placed on motorized rotation plates. The phase matching for the desired conversion process is achieved by angle tuning via motor rotation through a Microsoft Windows based program.

The polarization of the output beam is changed using reflections off two mirrors. The horizontally polarized beam is focused by a converging lens and directed to the BaF_2 window placed at Brewster's angle on the 6th stage of the vacuum chamber. The IR pulse energy ranges from 6 to 12 mJ in the 3μm region and 0.7 to 1.4 mJ in the 6μm region. Since we are using an unseeded beam from the Innolas Nd:YAG to pump the OPO/OPA convertor, the IR linewidth is about 1 cm^{-1}. The pulse duration, after frequency mixing, is about 3 ns.

References

1. A. Kamariotis, Ph.D Thesis, EPFL **2006**.
2. S. Mercier, Ph.D Thesis, EPFL **2008**.
3. J. Zeleny, *phys. rev.* **3**, 69 **1914**.
4. J. Zeleny, *phys. rev.* **10**, 1 **1917**.
5. M. Dole, L. L. Mack, R. L. Hines, R. C. Mobley, L. D. Ferguson, M. B. Alice, *Phys. Chem. Chem. Phys.* **49**, 2240 **1968**.
6. L. L. Mack, P. Kralik, A. Rheude, M. Dole, *Phys. Chem. Chem. Phys.* **52**, 4977 **1970**.
7. M. Yamashita, J. B. Fenn, *J. Phys. Chem.* **88**, 4451 **1984**.
8. M. Yamashita, J. B. Fenn, *J. Phys. Chem.* **88**, 4671 **1984**.
9. J. Fenn, M. Mann, C. Meng, S. Wong, C. Whitehouse, *Science* **246**, 64 **1989**.
10. W. S. Law, R. Wang, B. Hu, C. Berchtold, L. Meier, H. Chen, R. Zenobi, *Analytical Chemistry*, **2010**.
11. G. Schmelzeisen-Redeker, L. Bütfering, F. W. Röllgen, *Int. J. Mass Spectrom. Ion Processes* **90**, 139 **1989**.
12. J. V. Iribarne, B. A. Thomson, *Phys. Chem. Chem. Phys.* **64**, 2287 **1976**.
13. B. A. Thomson, J. V. Iribarne, *Phys. Chem. Chem. Phys.* **71**, 4451 **1979**.
14. A. T. Iavarone, E. R. Williams, *J. Am. Chem. Soc.* **125**, 2319 **2003**.
15. D. Touboul, M. C. Jecklin, R. Zenobi, *Rapid Commun. Mass Spectrom.* **22**, 1062 **2008**.
16. D.-Y. Chang, C.-C. Lee, J. Shiea, *Anal. Chem.* **74**, 2465 **2002**.
17. P. Kebarle, M. Peschke, *Anal. Chim. Acta* **406**, 11 **2000**.
18. P. Kebarle, *J. Mass Spectrom.* **35**, 804 **2000**.
19. S. Nguyen, J. B. Fenn, *Proc. Natl. Acad. Sci.* **104**, 1111 **2007**.
20. K. McQuinn, F. Hof, J. S. McIndoe, *Chem. Commun.*, 4099 **2007**.
21. G. Taylor, *Proc. R. Soc. London, Ser. A* **280**, 383 **1964**.
22. Rayleigh, *Philosophical Magazine Series 5* **14**, 184
23. M. S. Wilm, M. Mann, *Int. J. Mass Spectrom. Ion Processes* **136**, 167 **1994**.

24. M. Wilm, M. Mann, *Anal. Chem.* **68**, 1 **1996**.

25. M. Karas, U. Bahr, T. Dülcks, *Fresenius' Journal of Analytical Chemistry* **366**, 669 **2000**.

26. K. Sannes-Lowery, R. H. Griffey, G. H. Kruppa, J. P. Speir, S. A. Hofstadler, *Rapid Commun. Mass Spectrom.* **12**, 1957 **1998**.

27. S. A. Hofstadler, K. A. Sannes-Lowery, R. H. Griffey, *Rapid Commun. Mass Spectrom.* **13**, 1971 **1999**.

28. K. A. Sannes-Lowery, S. A. Hofstadler, *J. Am. Soc. Mass. Spectrom* **11**, 1 **2000**.

29. W. Paul, H. Z. Steinwedel, *Naturforsch.* **8A**, 448 **1953**.

30. W. Paul, M. Raether, *Zeitschrift für Physik A Hadrons and Nuclei* **140**, 262 **1955**.

31. W. Paul, H. P. Reinhard, U. von Zahn, *Zeitschrift für Physik A Hadrons and Nuclei* **152**, 143 **1958**.

32. K. Blaum, C. Geppert, P. Müller, W. Nörtershäuser, E. W. Otten, A. Schmitt, N. Trautmann, K. Wendt, B. A. Bushaw, *Int. J. Mass spectrom.* **181**, 67 **1998**.

33. P. H. Dawson, *Elsevier Sceintific Pub. Co. : Amsterdam*, **1976**.

34. R. E. March, J. F. J. Todd, *Quadrupole ion trap mass spectrometry, . n. ed., Ed.,* Wiley-interscience: Hoboken, N.J (**2005**), vol. .

35. P. H. Dawson, *Mass Spectrom. Rev.* **5**, 1 **1986**.

36. W. M. Brubaker, J. Tuul, *Rev. Sci. Instrum.* **35**, 1007 **1964**.

37. R. E. March, *J. Mass Spectrom.* **32**, 351 **1997**.

38. K. Blaum, C. Geppert, P. Müller, W. Nörtershäuser, K. Wendt, B. A. Bushaw, *Int. J. Mass spectrom.* **202**, 81 **2000**.

39. D. Gerlich, S. Horning, *Chem. Rev.* **92**, 1509 **1992**.

40. G. Dieter, *Phys. Scr.* **1995**, 256 **1995**.

41. S. Trippel, J. Mikosch, R. Berhane, R. Otto, M. Weidemüller, R. Wester, *Phys. Rev. Lett.* **97**, 193003 **2006**.

42. O. Asvany, S. Schlemmer, *Int. J. Mass spectrom.* **279**, 147 **2009**.

43. R. Otto, P. Hlavenka, S. Trippel, J. Mikosch, K. Singer, M. Weidemüller, R. Wester, *J. Phys. B* **42**, 154007 **2009**.

44. E. Teloy, D. Gerlich, *Chem. Phys.* **4**, 417 **1974**.

45. J. Mikosch, U. Frühling, S. Trippel, R. Otto, P. Hlavenka, D. Schwalm, M. Weidemüller, R. Wester, *Phys. Rev. A* **78**, 023402 **2008**.

46. D. Gerlich, *Adv. Chem. Phys.* **82**, 1 **1992**.

Chapter 3

Experimental Methods

A variety of double resonance spectroscopic techniques are used in this work to provide information on isolated biological molecules in the gas phase with the goal of developing a fundamental understanding of their energy landscapes. The first part of this chapter describes briefly the technique used to measure electronic spectra of gas-phase peptides as well as the IR-UV double resonance method that provides conformer specific infrared spectra − both of these are used to determine the local minima (i.e. stable conformations) on the ground potential energy surface. The second part of this chapter describes the techniques of hole-filling spectroscopy and infrared population transfer spectroscopy, which involve the transfer of molecules from one stable conformation to another. We explain in detail how we have adapted these techniques for studies of cold, trapped ions.

3.1 Photodissociation spectroscopy

The low density of ions in the 22-pole trap compared to neutral gas samples or condensed media makes the use of the direct absorption spectroscopy impossible due to insufficient sensitivity. For this reason we must use an indirect method of measuring photon absorption by detecting one of its consequences on the molecule of interest – generating a so-called "action spectrum". In our case we measure the fragmentation of parent ions caused by photon absorption. When working with charged species this method is facilitated by the ability to collect, transmit and detect the fragment ions with high efficiency. Moreover, additional detailed information on the spectroscopy of the parent ions can be obtained by separately measuring fragments of different masses. The quantum yield of photodissociation

can be wavelength dependent, and this may lead to some drawbacks, since an action spectrum may not be identical to an absorption spectrum. Other widely used action spectroscopic techniques include, laser induced fluorescence [1-3] and resonant enhanced multiphoton ionization (REMPI) [4, 5], but these are difficult to implement in the case of cold ions in a 22-pole ion trap. In the case of fluorescence this is a result of the low ion density and the inefficiency of photon collection and detection. In the case of the REMPI, it requires high energy to remove an electron from a parent species that already has a positive charge.

Because of the low temperatures of the 22-pole trap, singly-charged parent molecular ions, AB^+, lie in their lowest vibrational state of their ground electronic state S_0 [6-8]. After the absorption of a UV laser photon of the proper resonant frequency, some of the ions reach an excited electronic state S_1, which is at an energy above their dissociation threshold. Different mechanisms represented in Figure 3.1 can lead to fragmentation.
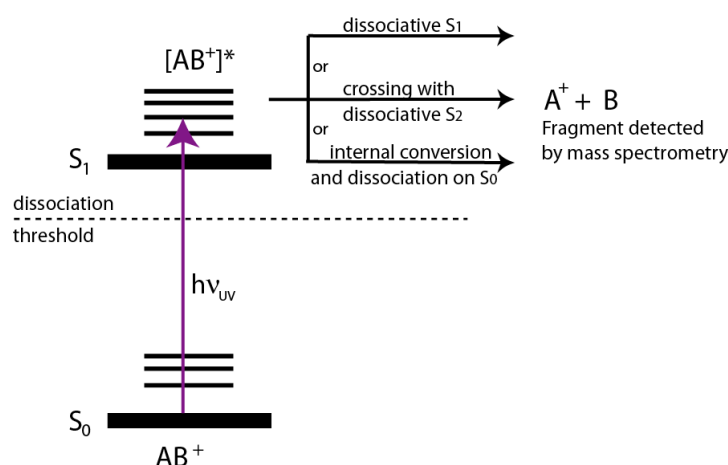
Figure 3.1: Spectroscopic scheme of photodissociation after an electronic excitation.

Direct dissociation occurs if the S_1 state is purely repulsive in the direction of a particular bond or to an indirect dissociation in case the initially excited state crosses a repulsive state S_2 though which dissociation occurs. Another possible mechanism is internal conversion from S_1 back to S_0 at an energy above the dissociation threshold such that fragmentation takes place on the ground potential energy surface. In this case the excitation energy will be redistributed among the vibrational modes of the molecules. For large molecules with many vibrational modes, intermolecular vibrational energy redistribution (IVR) will reduce the dissociation rate. Many studies have focused on the dissociation processes *via* IVR, questioning the general assumption that the excitation energy is spread out among all vibrational degrees of freedom before the dissociation occurs. Schlag and Levine

have shown that when the excess of vibrational excitation is below one quantum per mode the dissociation rate is slower than assumed by statistical theories and the energy may remain localized for a sufficiently long time to induce dissociation [9]. A fraction of the excited molecules may fragment by undergoing nonstatistical dissociation on an unexpected short time scale compared to RRKM estimations. The remaining fraction would possibly dissociate according to statistical rate constant [10, 11]. These studies were confirmed by different experimental measurements on biomolecules that reported the existence of both statistical and nonstatistical fragmentation processes [10, 12-15].

There may, in fact, be no practical upper limit to the size of molecular ions that we can photofragment in our apparatus. Our detection schemes based on photodissociation continue to be relevant for molecules that undergo fragmentation directly from the electronic excited state or nonstatistically in the ground state. However, in a recent work, Guidi *et al.* reported, a spectroscopic technique, based on IRMPE, that increases the photofragmentation yield of large molecules by more than two orders of magnitude [16, 17]. It has now become clear that the electronic spectra of large peptide ions can be recorded by selectively detecting the produced fragments (A+) as a function of the UV laser wavenumber [7, 18, 19].

3.2 Measurement of a photofragment mass spectrum

In order to record a photofragment excitation spectrum of a specific species in our apparatus, one needs to know the mass-to-charge ratio of the possible laser induced fragments. While one can find in the literature the fragmentation spectra of different molecules, the use of fragmentation techniques that are fundamentally different from ours (e.g., collision-induced, electron capture or electron impact dissociations) typically leads to different fragmentation patterns [20-25]. Moreover, in the case of the photodissociation spectra, one has to take into account that the relative fragment intensities depend on the experimental conditions (e.g., laser wavelength and ion temperature) [26-28]. For these reasons, the fragmentation mass spectrum of each parent ion must be measured with our equipment under our experimental conditions.

The fragment mass spectrum is recorded by successively dissociating several ion packets while incrementing the mass of the fragments to be detected. During the mass scan, the laser wavelength is fixed on an absorption transition of the parent ion. Because the

spectrum is not yet known for a new species, the first fragmentation mass spectrum is measured at room temperature, taking benefit of the large absorption band due to inhomogeneous broadening to fix the laser wavenumber. The resulting spectrum gives insight into the fragment ions induced by photodissociation, although their relative intensities can be different from those at low temperature. After identification of the masses of the main fragments, the low temperature optical spectra can be measured by monitoring the mass of one fragment while scanning the laser wavenumber. The transitions in the cold optical spectra are expected to be much narrower compared with those measured at room temperature. By fixing the laser wavelength on different sharp transitions, the corresponding mass fragment spectra can be recorded at low temperature. Different fragmentation patterns can be obtained from transitions that belong to distinct conformers of the same parent ions [18].

3.3 Conformer specific IR-UV double resonance spectroscopy

A unique ion species of a particular mass to charge ratio can adopt different conformations in the 22-pole ion trap corresponding to different local minima on the potential energy surface. At low temperature the optical spectrum would be a superposition of spectra of different conformers. Spectroscopic interpretation and characterization of each conformation requires disentangling the different contributions.

Various techniques have been implemented in order to distinguish different conformations and assign their individual transitions. Levy and co-workers used R2PI saturation spectroscopy and dispersed fluorescence spectroscopy to identify stable conformations of the amino acid tryptophan and some of its analogs in a supersonic molecular beam [1, 29-32]. The introduction of the double resonance hole-burning technique by the end of the 1980s was one of the most important developments in the field. Colson and coworkers reported the electronic spectrum of a single m-cresol conformer using UV-UV hole-burning spectroscopy [33]. This is a pump-probe laser technique where the pulsed probe laser is fixed on a given vibronic transition in the electronic spectrum previously measured and the second pulsed laser (the pump laser) is fired about 500 ns before the probe and is scanned across the spectrum. Each time the pump laser is in resonance with a transition of the selected conformer, a fraction of the ground state population is preexcited and does not absorb the second UV laser at the same frequency as the ground state species. This will lead to dips in the signal induced by the probe laser, producing a conformer-specific vibronic spectrum. In a

similar way, Lee and coworkers used IR-UV double resonance to study state-selective of local modes in benzene molecules and dimers [34, 35]. In this scheme an IR laser pulse is fixed on a vibrational transition specific of a particular conformer while the UV probe laser is scanned, and the difference between the UV spectra recorded with and without the IR burn laser reveals the transitions belonging to the selected conformer. The infrared spectra of conformer-selected molecules can be recorded using the same scheme but keeping the UV fixed on a specific transition while scanning the IR wavelength. These methods have been developed and applied by several groups in order to sort out the different conformers of flexible molecules or clusters in supersonic expansions [5, 36-46].

We use IR-UV double resonance techniques to record the infrared of conformer-selected molecules. The feasibility of this approach in our apparatus has been demonstrated and IR spectra of different species of increasing size have been reported [18, 19, 47, 48]. The UV absorption spectrum of the vibrationally cold ions is different from those first excited in the IR. In a recent review, Rizzo *et al.* give an overview on the possible mechanisms responsible for the shift in the UV absorption frequency of the vibrationally preexcited molecules respect to the ground state molecules [49]. Considering the time delay of 200 ns between the two laser pulses, after IR excitation the molecule will be in states of mixed vibrational character due to the energy redistribution among its vibrational modes. The UV spectrum of the preexcited species will be broadened by statistical inhomogeneous broadening [50, 51], which occurs because the different components of the mixed wave function will give rise to slightly different UV absorption frequencies.

In order to measure infrared spectra of biomolecular ions using an IR–UV double-resonance scheme, illustrated schematically in Figure 3.2a, we direct an infrared laser pulse from an OPO at 10 Hz into the ion trap 200 ns before a UV laser pulse, which comes at 20 Hz. The UV laser is fixed on a transition from the previously measured electronic spectrum while scanning the IR frequency. Each time the latter is in resonance with a vibrational transition of the selected conformer the UV photofragment signal at the probe wavelength will be depleted. An IR transition is then detected as a dip in the UV photofragmentation signal. The IR spectrum is recorded by monitoring the difference in the photofragmentation signal when the IR laser is on and off.
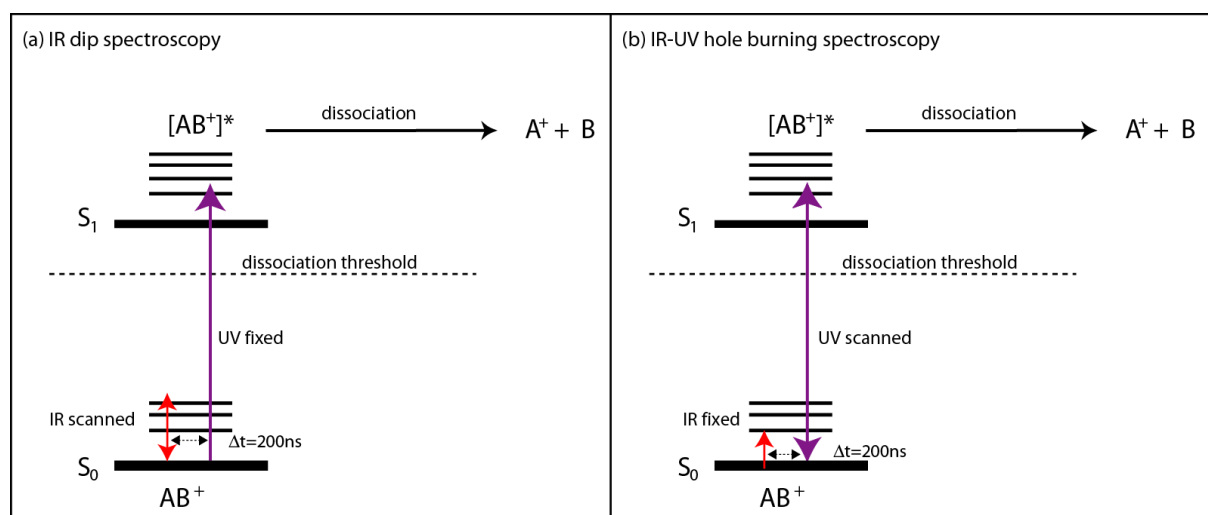
Figure 3.2: Spectroscopic schemes applied to cold biomolecular ions for measuring conformation specific infrared (a) and electronic (b) spectra via photofragment detection.

After getting the IR spectrum of a specific conformer, the IR-UV hole burning spectrum can be measured by fixing the IR wavelength on a particular transition and scanning the UV frequency, as shown in Figure 3.2b. If the chosen IR transition is unique to a specific conformer, the IR laser will deplete all vibronic transitions related to the IR tagged conformer. The subtraction of the spectrum obtained with IR on and off will generate an electronic spectrum of the selected conformer.

3.4 Population transfer spectroscopy

Many spectroscopic studies [3, 46, 49, 52-54] have been and continue to be devoted to providing information on biological molecules in gas phase giving particular attention to the minima on the potential energy surface. While local minima on the potential energy surface give essential information on the different non-covalent interactions that govern the structure of different stable conformers, the energy barriers separating them influence their dynamics, which are important to understanding their function. Zwier *et al.* performed pioneering studies looking at the transfer of population between conformers after the deposition of energy by vibrational excitation of small biological molecules cooled in a supersonic expansion [55-58]. These experiments are based on the pump-cool-probe principle, where the pump is an IR laser pulsed at the half frequency of the UV probe laser. It is a hole-filling experiment if the pump laser is fixed to a specific vibrational band of one conformer while scanning the UV after sufficient cooling collisions. The hole-filling spectra resulting from the difference of LIF signal scanned with and without the IR laser will reflect the change in population of various

conformers. The dip in the population of the selected conformer manifests itself by a depletion in the LIF signal whereas conformations gaining population cause a gain in signal. By using the exact same arrangement but keeping the UV fixed and scanning the IR wavelength Zwier and coworkers record a so-called infrared population transfer spectrum. In this case, the population change induced by infrared excitation in a selected conformer is detected. These spectra allow the extraction of fractional population if the hole-filling spectra did not result in the formation of new conformations. When associated with IR spectra taken under the same conditions one can extract the quantum yields to isomerization.

The Zwier group was also the first to describe a methodology for investigating the barrier heights separating different conformational minima [59-64] using simulated emission pumping. In this technique the IR source is replaced by two tunable ultraviolet lasers. The first laser is fixed on a vibronic band (S_0-S_1 transition) in such a way as to excite selectively one conformer. The second ultraviolet laser induces stimulated emission of a fraction of the excited state population back down to a particular vibrational level in the ground state. In this case the S_1 state must be sufficiently long-lived to allow time to drive population from the S_1 state to S_0 (v). Most of these studies have been performed on neutral molecules having the size of a single amino acid.

In this thesis work, following the example of Zwier [55], we performed population transfer experiments in order to investigate the barriers separating stable conformers of much larger protonated peptides. Although the principles remain the same (i.e., pump-cool-probe), these techniques needed to be adapted for application to ions in a cold ion trap.

3.4.1 Hole filling spectroscopy in the cold 22-pole ion trap

The hole-filling experiment, illustrated schematically in Figure 3.3, consists of selectively exciting a single conformation of a cold ion species by setting the IR laser to a unique vibrational transition. This wavelength is chosen after recording the electronic spectrum of this molecular ion and the IR spectra of its stable conformers. The selected conformer is then heated by the absorption of the IR photon. A very important element is to give enough time for the molecule to cool back down before firing the UV probe laser, which in this case will be tuned over the region of interest to monitor the changes in population of the various conformers.

The experimental procedure in our apparatus is as follows. The ions are pulsed into 22-pole trap in a package of typically 10,000 ions with a repetition rate of 20Hz. The ions are cooled to about 10K by collisions with helium, which is injected and thermalized to the temperature of the trap housing 1 ms before the arrival of the ions. An IR laser operating at 10 Hz excites a single conformation of the trapped ions, and after a time delay sufficient for the molecule to relax back the vibrational ground state excitation, the UV probe laser fires, inducing fragmentation. This is repeated at different UV wavelengths to measure a UV spectrum of the molecules after IR heating and recooling. On alternate laser shots, only the UV laser fires and we measure the difference spectrum with and without the IR excitation.
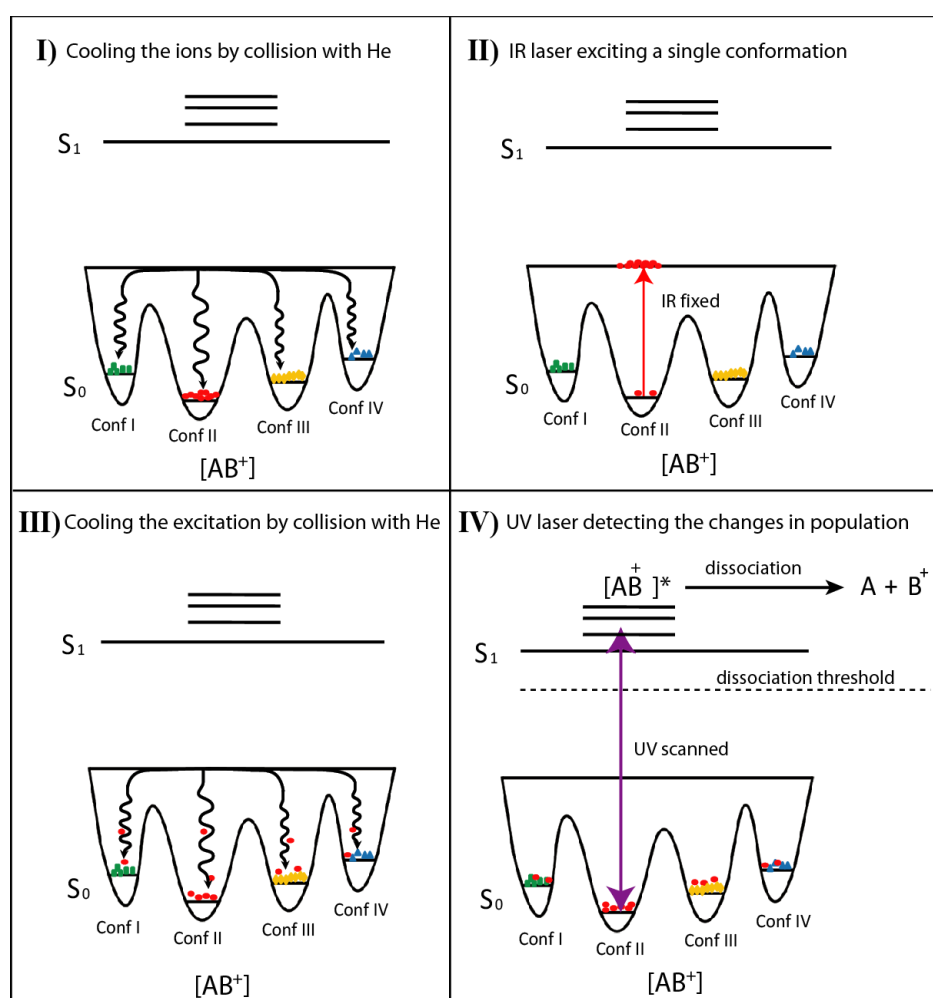
Figure 3.3: Spectroscopic scheme of the Hole-filling experiment in a cold 22-pole ion trap. I) the ions are cooling by collision with He, II) infrared burn laser excites a single conformation of the cold ion species, III) the excited conformer is cooled back by collision with the remaining He, IV) the UV probe laser scanned detects the changes in population.

This difference spectrum will reveal whether the photon energy was high enough in energy to bring the molecule above the barrier to isomerization and cause the changes in

population of different conformations. The depletions and gains in the photofragmentation signal will reflect the loss and gain in the population.

3.4.2 IR-population transfer spectroscopy in the cold 22-pole ion trap

In the IR-population transfer experiment, the basic scheme of cool-excite-recool-probe is maintained, but in this case the UV laser fixed on a transition of a particular conformer and the IR laser tuned. This is shown schematically in Figure 3.4.
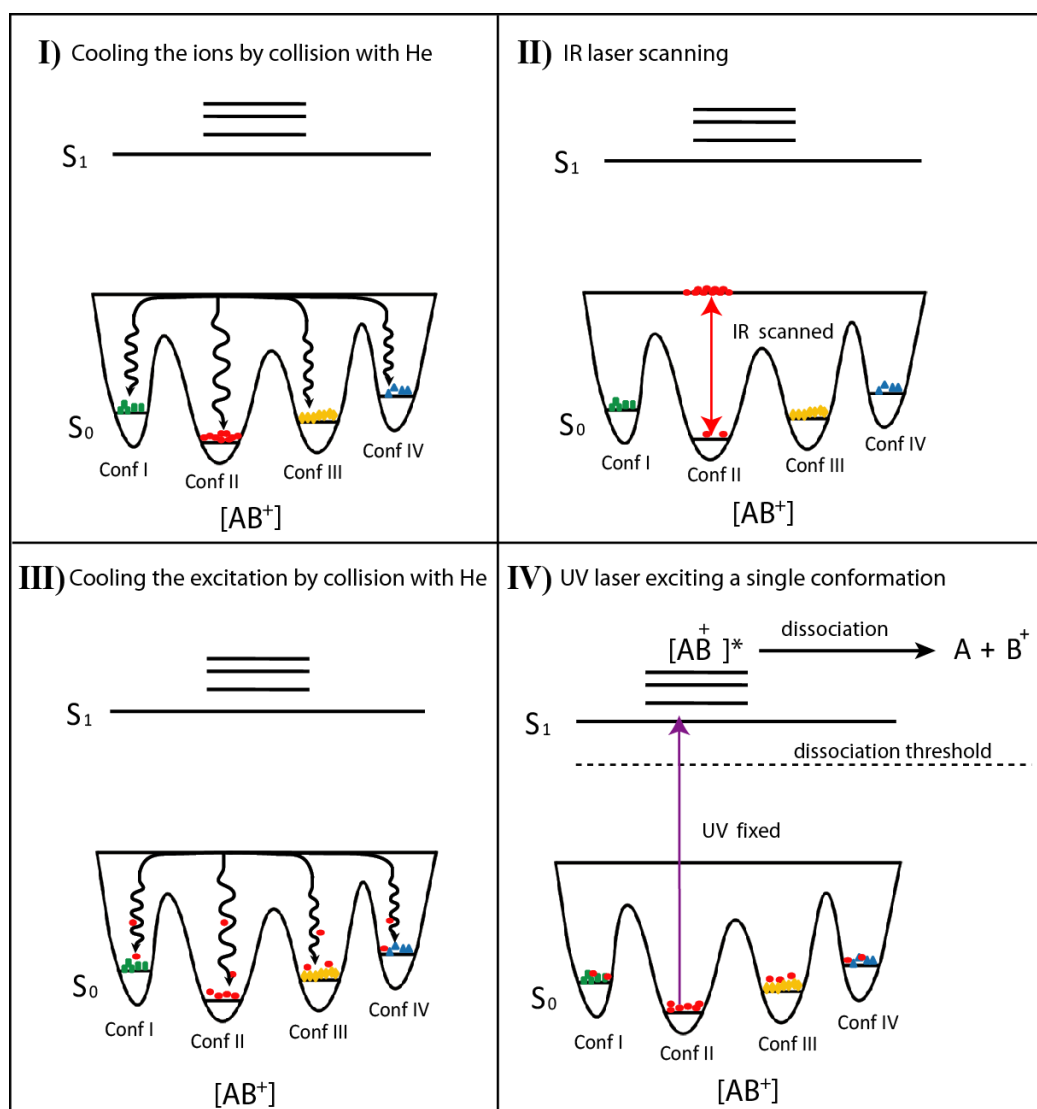
Figure 3.4: Spectroscopic scheme of the IR-population transfer experiment in a cold 22-pole ion trap. I) the ions are cooling by collision with He, II) infrared burn laser scanned, III) the excited conformer is cooled back by collision with the remaining He, IV) the UV probe laser fixed, detecting the changes in population of the selected conformer.

The resulting spectra obtained from the difference of the photofragmentation signal after IR excitation and recooling and in the absence of this IR excitation reflect the population

changes induced by IR laser on the population of the selected conformer. The infrared transitions due to the probed conformer will be recognized as depletions in the fragmentation signal, while gains occur from the transitions where other conformers absorb and transfer population into the selected one. Together with conformer-specific IR-UV spectra taken under the same conditions, these spectra allow the extraction of quantitative data on the fractional population and the quantum yields to isomerization. The equations that allow us to extract these quantitative data will be developed in *Section 3.5*.

3.4.3 Adaptation to the condition of the cold tapped ions

The first step in our experiment is to vibrationally excite cold molecules, and for this we need a diagnostic of the temperature of the molecules so that we can determine the time required to cool them. As shown in Figure 3.5, in the usual spectroscopic experiment we fire the laser at the end of our trapping cycle, however in this case the same He pulse should be used to cool the molecules initially and later recool them after the burn excitation.
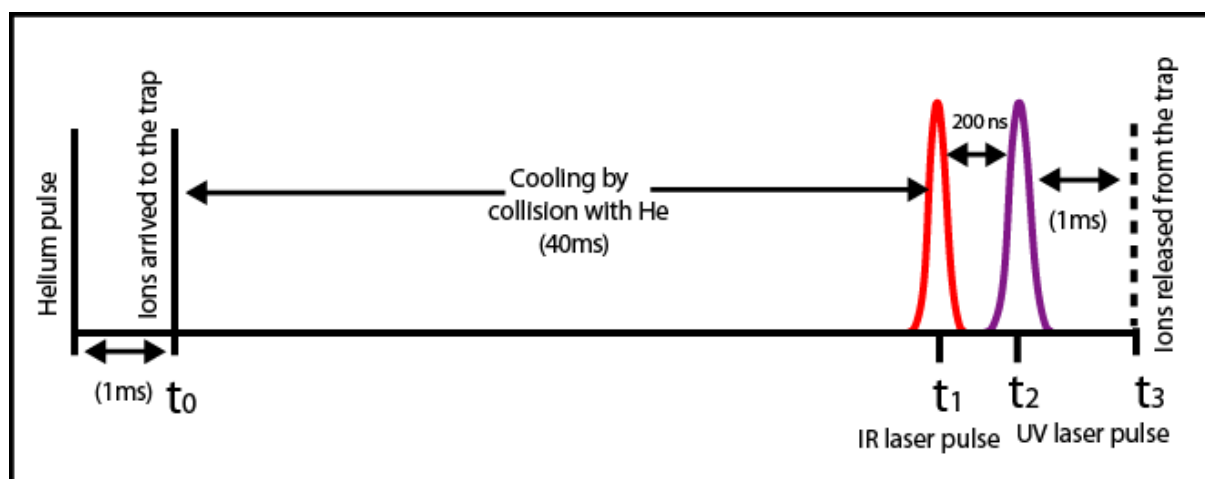
Figure 3.5: Timing diagram of the IR-UV double resonance experiment in 22-pole ion trap.

The temperature verification is done by recording ultraviolet photofragment spectra at different residence times of the ions in the trap. If the molecule is sufficiently cold, excited rotational and vibrational levels can be very effectively depopulated, and the spectrum will be greatly simplified. Assuming a Boltzmann distribution at thermal equilibrium of the ion packet, one can get an estimation of the vibrational temperature of the molecule from the intensity of the hot bands. Assuming that the intensity of a hot-band $S_{0 \leftarrow 1}$ and the corresponding vibronic band $S_{1 \leftarrow 0}$, will have similar Franck-Condon factors, the populations

46

of the respective initial states will be proportional to their measured intensities. Thus, the temperature is obtained from the following expression:

$$\frac{I_{1\leftarrow 0}}{I_{0\leftarrow 1}} = e^{\frac{\Delta E}{k_B T}} \Rightarrow T = \frac{\Delta E}{k_B \ln\left(\dfrac{I_{1\leftarrow 0}}{I_{0\leftarrow 1}}\right)} \qquad\qquad Eq\ 3.1$$

where ΔE is the energy difference between the band origin and the hot band. (i.e., the energy of the vibrational mode giving raise to the hot band)
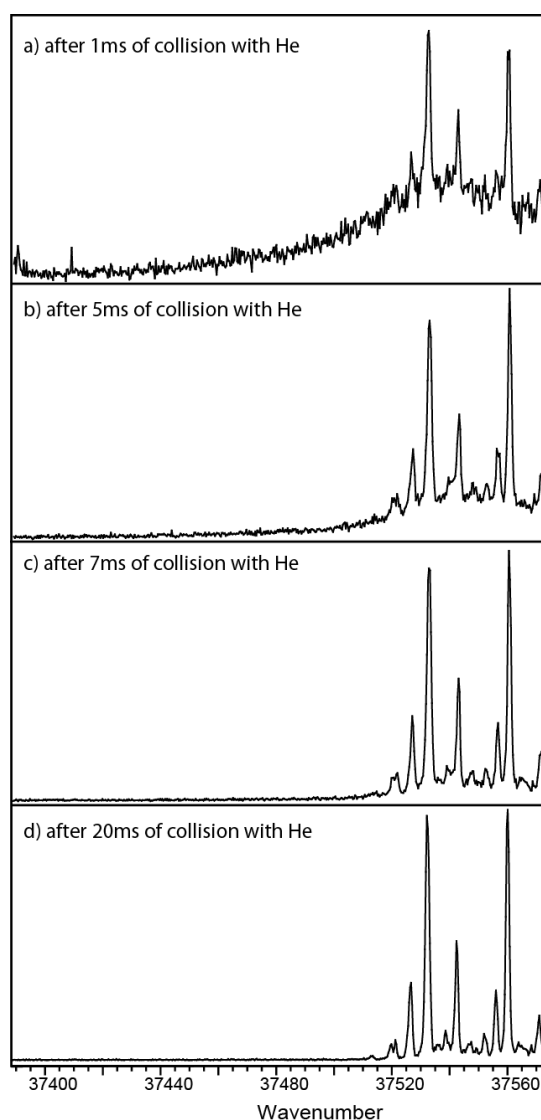
Figure 3.6: Electronic spectra of the seven amino acid peptide (Ac-Phe-(Ala)5-Lys) [48] recorded at different trapping times.

The data of Figure 3.6 shows that the longer the delay between the arrival of the ions to the trap and the laser excitation, the more resolved the spectrum is. The first spectrum

recorded after 1ms of collisions with helium shows a background with unresolved bands due to incomplete cooling. In Figure 3.6 b and c the spectra become more resolved, but the bands are still broad and the estimated temperature indicates that the ions are still slightly warm. After an additional 20 ms for cooling, the vibrational temperature is estimated between 10 and 15K.

Having defined the delay time need for the ions to cool before we fire the IR burn laser, we need to determine the time that the ions need to dissipate the absorbed IR photon energy before firing the UV probe laser pulse. This is simply done by scanning the time delay between the two laser pulses – the first which is from an IR source fixed at a frequency in resonance with a vibrational transition specific to a particular conformer and the second from a UV laser tuned to a given vibronic transition of a different conformer than the one selected by the IR laser. We scan the time delay between the two lasers, monitoring the difference in signal between IR laser on and off. Figure 3.7 illustrates the gain in the photofragment signal of conformer B of a seven amino acid peptide having population in four different conformations [48, 65], while the IR laser is fixed at a transition belongs to conformer A. The curve shows an increase in the signal during the first microseconds, after which it reaches a maximum and stays stable for 10ms. In view of this, a delay in time of 7 ms was chosen to ensure that the excited molecules have enough time to relax back to their ground vibrational level and redistribute across the trap.
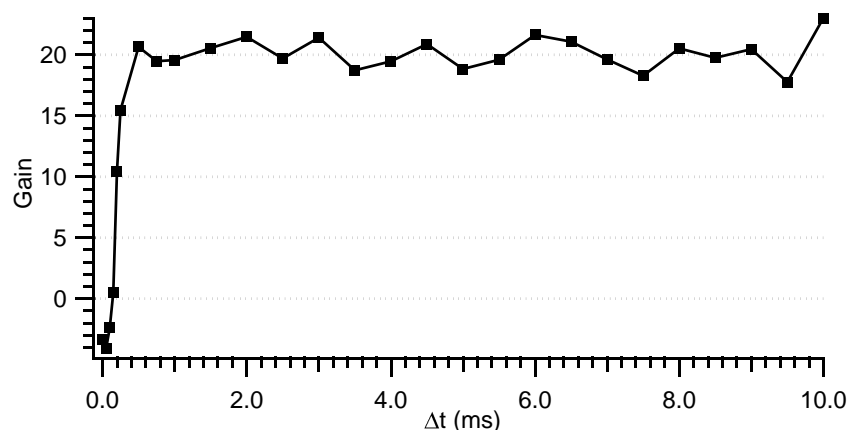
Figure 3.7: The gain in the photofragment signal, of Ac-Phe-(Ala)5-Lys conformer B, detected as a function of time delay between the IR and UV lasers, fixed in wavenumber. The IR laser is set to a vibrational transition of conformer A at 3347 cm^{-1} while the UV laser probes conformer B at 37'577.83 cm^{-1}.

Since the ion temperature in the 22-pole trap depends on several parameters [66-68], the timing diagram presented in Figure 3.8 is verified before each set of population transfer experiments for the molecules studied in this work.
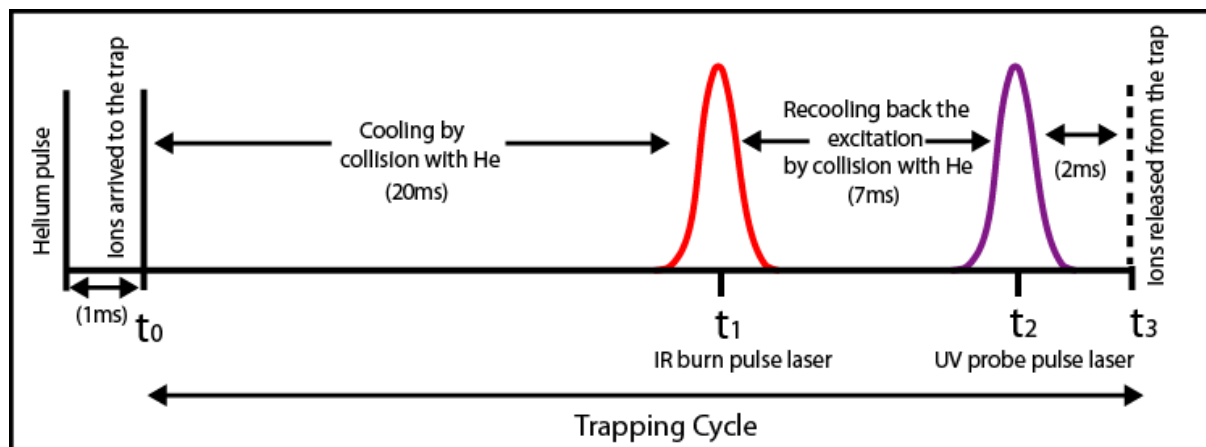
Figure 3.8: Timing diagram of the population transfer experiments in 22-pole ion trap.

The successful implementation of the population transfer experiments in the ion trap requires a good overlap in space between the lasers and the ion packet. The IR beam has slightly large diameter than the UV beam. The latter is first aligned with the ions by maximizing the photofragment signal. Once this is done, the IR beam is positioned by optimizing the depletion in the UV signal.

3.4.4 Timing of the events

All the population transfer experiments on a single ion packet reported in this work, from the electrospray ion generation to the detection of the products, lasts typically 50 ms. The repetition rate of these experiments is 20 Hz, and a single point of a spectrum is obtained by averaging the signals of certain number of cycles (between 50 and 100). After recording the first point, the laser wavelength is then changed by a small increment, and a new point is acquired. This procedure is repeated until a complete spectrum is measured.

The timing diagram of Figure 3.9 shows the sequence of events taking place during a population transfer experiment presented in the next chapters. The continuous nano-electrospray ion signal is collected in the hexapole for 40 ms and transformed into an ion packet, which is pulsed out of this ion reservoir by lowering the exit lens potential for 9 ms. The parent ions, mass-selected in the first quadrupole Q1, enter the 22-pole trap where they will be stored for 29 ms and cooled by collisions with helium buffer gas which is pulsed ~1ms

prior to their arrival. In this case, the IR laser repetition rate is set to 10 Hz and the UV laser to 20 Hz, which make it possible to acquire one data point with IR laser on and one with IR laser off and subtract the two in order to obtain the population transfer spectrum. As discussed above, an IR laser pulse is fired through the 22-pole trap after 20 ms of trapping time and followed 7 ms later by a UV laser pulse that excites the parent ions to an excited electronic state from which some fraction of them dissociate. The excited parent ions are given 2 ms to fragment before the potential on the exit lens of the 22-pole is lowered and the parent and daughter ions are released and directed towards the second quadrupole mass filter, Q3. This latter transmits a fragment of a given mass-to-charge ration (*m/z*) for detection. The number of daughter ions after IR induced population transfer, is recorded on channel A of the pulse counter. During the following trapping cycle, channel B of the counter measures the number of fragment ions without the IR laser firing. During the IR-UV spectroscopic studies without population transfer, this process is the same but with a delay of 200 ns between the two lasers fired 1 ms before the trap opens.
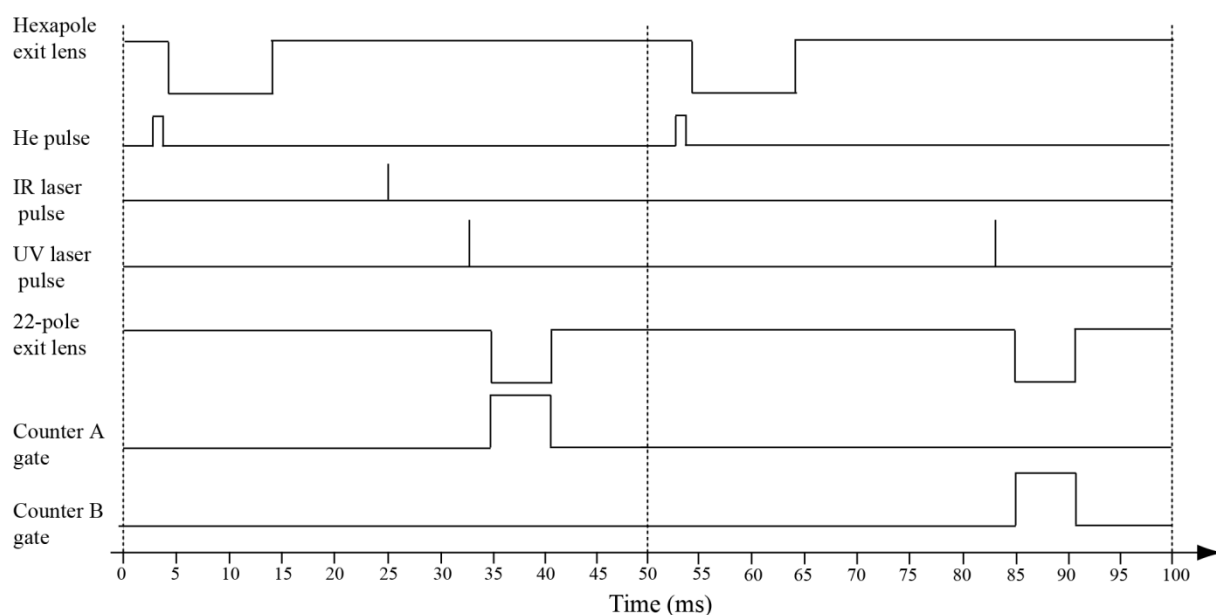
Figure 3.9: Timing diagram of the events taking place in a single population transfer experiment.

3.5 Extracting the fractional population and the isomerization quantum yields

3.5.1 Extracting the fractional population

The IR-population transfer spectrum detects the population changes induced in a single conformation by the absorption of an IR photon. Consider the case of a molecule with population in three stable conformations (A, B and C) in the ion trap. If the hole filling spectra of all the stable conformers of a given molecule do not show evidence of any new minima, this will mean that there is no change in the total ion population and the following equation will be satisfied [55]:

$$\Phi_{XA} + \Phi_{XB} + \Phi_{XC} = 1 \qquad\qquad Eq\ 3.2$$

where Φ_{XY} is the isomerization quantum yield going from conformer X to conformer Y.

The peak intensity of an IR-population transfer spectrum is given by subtracting the IR laser-on signal and IR laser-off signal and dividing it by the IR off signal acquired almost simultaneously. If the IR pulse is fixed at a wavenumber at which all three conformers absorb, the UV pulse is tuned to conformer A, and there is enough time for the absorbed IR energy to be completely dissipated and the ions to be redistributed in the trap, the IR-population transfer peak intensity will be given by:

$$IRPTS_A = \frac{F_{A:UV,IR} - F_{A:UV}}{F_{A:UV}} \qquad\qquad Eq\ 3.3$$

where, $F_{A:UV}$ is the total number of fragment ions from conformer A; and $F_{A:UV,IR}$ is the total number of fragment ions from conformer A after cooling the IR excitation.

Equation 3.3 is developed in detail in the appendix A; here we will give the final expression of the peak intensity of an IR-population transfer spectrum:

$$IRPTS_A = \frac{\left[\sum_{X\neq A} p_X \cdot \sigma_{X,IR} \cdot \Phi_{XA} - p_A \cdot \sigma_{A,IR} \cdot (1-\Phi_{AA})\right] \cdot E_{IR}}{p_A \cdot A_{ion} \cdot \hbar\omega_{IR}} \qquad\qquad Eq\ 3.4$$

where p_A and p_X the fractional population of ions in conformation A and X. σ is the absorption cross section at the utilized laser wavelength. E_{IR} is the pulse energy and ω_{IR} is the frequency of the IR laser pulse.

The weighted sum of the population transfer spectra for the three conformation at all infrared wavelengths is given by:

$$p_A.IRPTS_A + p_B.IRPTS_B + p_C.IRPTS_C =$$

$$\left(\sum_{X \neq A} p_X \cdot \sigma_{X,IR,} \cdot \Phi_{XA} - p_A.\sigma_{A,IR} \cdot (1-\Phi_{AA}) \right) \cdot \frac{E_{IR}}{A_{ion}.\hbar\omega_{IR}}$$

$$+\left(\sum_{X \neq B} p_X \cdot \sigma_{X,IR,} \cdot \Phi_{XB} - p_B.\sigma_{B,IR} \cdot (1-\Phi_{BB}) \right) \cdot \frac{E_{IR}}{A_{ion}.\hbar\omega_{IR}}$$

$$+\left(\sum_{X \neq C} p_X \cdot \sigma_{X,IR,} \cdot \Phi_{XC} - p_C.\sigma_{C,IR} \cdot (1-\Phi_{CC}) \right) \cdot \frac{E_{IR}}{A_{ion}.\hbar\omega_{IR}}$$

$$= \frac{E_{IR}}{A_{ion}.\hbar\omega_{IR}} \cdot \left(\begin{array}{l} p_A.\sigma_{A,IR} \cdot (\Phi_{AB} + \Phi_{AC} - (1-\Phi_{AA})) \\ + p_B.\sigma_{B,IR} \cdot (\Phi_{BA} + \Phi_{BC} - (1-\Phi_{BB})) \\ + p_C.\sigma_{C,IR} \cdot (\Phi_{CA} + \Phi_{CB} - (1-\Phi_{CC})) \end{array} \right)$$

Since equation *3.2* holds for all conformers, then:

$$\Phi_{AB} + \Phi_{AC} - (1-\Phi_{AA}) =$$
$$\Phi_{BA} + \Phi_{BC} - (1-\Phi_{BB}) =$$
$$\Phi_{CA} + \Phi_{CB} - (1-\Phi_{CC}) = 1-1 = 0$$

and therefore,

$$p_A.IRPTS_A + p_B.IRPTS_B + p_C.IRPTS_C = 0 \qquad \text{*Eq 3.5*}$$

This equation demonstrates that all the infrared excited population is redistributed among the existing conformers. In the meantime the fractional population of the molecule sum to 1:

$$\sum p_X = p_A + p_B + p_C = 1 \qquad \text{*Eq 3.6*}$$

The *IRPTS$_X$* are obtained experimentally and thus from the weighted-sum of the infrared population transfer spectra and Equation 3.6 we can extract the fractional populations of the conformation of the molecule under the trap conditions.

3.5.2 Extracting the quantum yields to isomerization

To extract the quantum yield to isomerization from the IRPT spectra, we need information about the number of molecules that are excited by the infrared laser pulse. This piece of information could be extracted from an IR dip spectrum taken under the same conditions of the IR population transfer spectrum. This is done by moving the UV laser pulse in time so it will fire early in the trapping cycle, 200ns after the IR laser. The IR spectrum peak intensity is given by:

$$IR_A = \frac{F_{A:UV,IR} - F_{A:UV}}{F_{A:UV}} = -\sigma_{A,IR} \cdot \frac{E_{IR}}{\max(A_{UV}, A_{IR}).\hbar\omega_{IR}} \qquad Eq\ 3.7$$

where, $F_{A:UV}$ is the total number of fragment ions from conformer A; and $F_{A:UV,IR}$ is the total number of fragment ions from conformer A after the IR excitation. A_{UV} and A_{IR} are the area of the UV and IR laser beam. This equation is developed in detail in the appendix A.

Substituting $\sigma_{A,IR}$ into the IRPTS expression, Equation 3.4:

$$IRPTS_A = \frac{-\max(A_{UV}, A_{IR})}{p_A.A_{ion}} \cdot \left(\sum_{X \neq A} p_X.\ IR_X.\Phi_{XA} - p_A.IR_A.(1-\Phi_{AA}) \right)$$

If we consider $\gamma = \dfrac{\max(A_{UV}, A_{IR})}{A_{ion}}$

This will lead to a final set of IRPTS equations for the three conformers A, B and C:

$$IRPTS_A = \left(-\frac{p_B}{p_A}.\ IR_B.\Phi_{BA} - \frac{p_C}{p_A}.\ IR_C.\Phi_{CA} + IR_A.(1-\Phi_{AA}) \right).\gamma \qquad Eq\ 3.8$$

$$IRPTS_B = \left(-\frac{p_A}{p_B}.\ IR_A.\Phi_{AB} - \frac{p_C}{p_B}.\ IR_C.\Phi_{CB} + IR_B.(1-\Phi_{BB}) \right).\gamma \qquad Eq\ 3.9$$

53

$$IRPTS_C = \left(-\frac{p_A}{p_C} \cdot IR_A \cdot \Phi_{AC} - \frac{p_B}{p_C} \cdot IR_B \cdot \Phi_{BC} + IR_C \cdot (1-\Phi_{CC}) \right) \cdot \gamma \qquad Eq\ 3.10$$

However if the quantum yields are extracted at transition where just conformer A absorbs, this set of equation will give:

$$IRPTS_A = IR_A \cdot (1-\Phi_{AA}) \cdot \gamma$$

$$IRPTS_B = -\frac{p_A}{p_B} IR_A \cdot \Phi_{AB} \cdot \gamma$$

$$IRPTS_C = -\frac{p_A}{p_C} IR_C \cdot \Phi_{AC} \cdot \gamma$$

In the case of the unique absorption band of conformer B:

$$IRPTS_B = IR_B \cdot (1-\Phi_{BB}) \cdot \gamma$$

$$IRPTS_A = -\frac{p_B}{p_A} IR_B \cdot \Phi_{BA} \cdot \gamma$$

$$IRPTS_C = -\frac{p_B}{p_C} IR_C \cdot \Phi_{BC} \cdot \gamma$$

In the case of the unique vibration band of conformer C, give

$$IRPTS_C = IR_C \cdot (1-\Phi_{CC}) \cdot \gamma$$

$$IRPTS_A = -\frac{p_C}{p_A} IR_C \cdot \Phi_{CA} \cdot \gamma$$

$$IRPTS_B = -\frac{p_C}{p_B} IR_B \cdot \Phi_{CB} \cdot \gamma$$

The only unknown quantities in these equations are the quantum yields since the peak intensities of the infrared population transfer and infrared spectra are measured experimentally and the fractional population could be extracted from the weighted sums of the population transfer spectra us demonstrated in the previous paragraph. We assume to be working under optimized conditions for a maximum of overlapping between the lasers and the ions and thus γ is assumed to be close to 1.

References

1.   Y. D. Park, T. R. Rizzo, L. A. Peteanu, D. H. Levy, *Phys. Chem. Chem. Phys.* **84**, 6539 **1986**.
2.   J. R. Lakowzic, n. Ed., Ed. (New York : Kluwer Academic/plenum Publisher, **1999**).

3.   T. S. Zwier, *J. Phys. Chem. A* **105**, 8827 **2001**.
4.   R. Cohen, B. Brauer, E. Nir, L. Grace, M. S. de Vries, *J. Phys. Chem. A* **104**, 6351 **2000**.
5.   I. Hünig, K. A. Seefeld, K. Kleinermanns, *Chem. Phys. Lett.* **369**, 173 **2003**.
6.   S. R. Mercier, O. V. Boyarkin, A. Kamariotis, M. Guglielmi, I. Tavernelli, M. Cascella, U. Rothlisberger, T. R. Rizzo, *J. Am. Chem. Soc.* **128**, 16938 **2006**.
7.   O. V. Boyarkin, S. R. Mercier, A. Kamariotis, T. R. Rizzo, *J. Am. Chem. Soc.* **128**, 2816 **2006**.
8.   S. Mercier, Ph.D Thesis, EPFL **2008**.
9.   E. W. Schlag, R. D. Levine, *Chem. Phys. Lett.* **163**, 523 **1989**.
10.   Y. Hu, B. Hadas, M. Davidovitz, B. Balta, C. Lifshitz, *J. Phys. Chem. A* **107**, 6507 **2003**.
11.   E. W. Schlag, H. L. Selzle, P. Schanen, R. Weinkauf, R. D. Levine, *J. Phys. Chem. A* **110**, 8497 **2006**.
12.   R. Weinkauf, P. Schanen, A. Metsala, E. W. Schlag, M. Burgle, H. Kessler, *J. Phys. Chem.* **100**, 18567 **1996**.
13.   M. S. Thompson, W. Cui, J. P. Reilly, *Angew. Chem. Int. Ed.* **43**, 4791 **2004**.
14.   W. Cui, M. S. Thompson, J. P. Reilly, *J. Am. Soc. Mass. Spectrom* **16**, 1384 **2005**.
15.   G. Gregoire, H. Kang, C. Dedonder-Lardeux, C. Jouvet, C. Desfrancois, D. Onidas, V. Lepere, J. A. Fayeton, *PCCP* **8**, 122 **2006**.
16.   M. Guidi, U. J. Lorenz, G. Papadopoulos, O. V. Boyarkin, T. R. Rizzo, *J. Phys. Chem. A* **113**, 797 **2009**.
17.   M. Guidi, Ph.D Thesis, EPFL **2010**.
18.   J. A. Stearns, S. Mercier, C. Seaiby, M. Guidi, O. V. Boyarkin, T. R. Rizzo, *J. Am. Chem. Soc.* **129**, 11814 **2007**.
19.   N. S. Nagornova, T. R. Rizzo, O. V. Boyarkin, *J. Am. Chem. Soc.* **132**, 4040 **2010**.
20.   W. D. Bowers, S. S. Delbert, R. T. McIver, *Anal. Chem.* **58**, 969 **1986**.
21.   W. Gabryelski, L. Li, *Rev. Sci. Instrum.* **70**, 4192 **1999**.
22.   E. R. Williams, J. J. P. Furlong, F. W. McLafferty, *J. Am. Soc. Mass. Spectrom* **1**, 288 **1990**.
23.   A. G. Harrison, *J. Am. Soc. Mass. Spectrom* **12**, 1 **2001**.
24.   D. M. Horn, K. Breuker, A. J. Frank, F. W. McLafferty, *J. Am. Chem. Soc.* **123**, 9792 **2001**.
25.   H. El Aribi, G. Orlova, A. C. Hopkinson, K. W. M. Siu, *J. Phys. Chem. A* **108**, 3844 **2004**.
26.   R. E. Tecklenburg, M. N. Miller, D. H. Russell, *J. Am. Chem. Soc.* **111**, 1161 **1989**.
27.   W. Gabryelski, L. Li, *Rapid Commun. Mass Spectrom.* **16**, 1805 **2002**.
28.   T. Tabarin, R. Antoine, M. Broyer, P. Dugourd, *Rapid Commun. Mass Spectrom.* **19**, 2883 **2005**.
29.   T. R. Rizzo, Y. D. Park, L. A. Peteanu, D. H. Levy, *J. Chem. Phys.* **84**, 2534 **1986**.
30.   T. R. Rizzo, Y. D. Park, D. H. Levy, *Phys. Chem. Chem. Phys.* **85**, 6945 **1986**.
31.   L. A. Philips, D. H. Levy, *Phys. Chem. Chem. Phys.* **89**, 85 **1988**.
32.   T. R. Rizzo, Y. D. Park, D. H. Levy, *J. Am. Chem. Soc.* **107**, 277 **1985**.
33.   R. J. Lipert, S. D. Colson, *J. Phys. Chem.* **93**, 3894 **1989**.
34.   R. H. Page, Y. R. Shen, Y. T. Lee, *J. Chem. Phys.* **88**, 5362 **1988**.
35.   R. H. Page, Y. R. Shen, Y. T. Lee, *J. Chem. Phys.* **88**, 4621 **1988**.
36.   C. Riehn, C. Lahmann, B. Wassermann, B. Brutschy, *Chem. Phys. Lett.* **197**, 443 **1992**.
37.   R. N. Pribble, T. S. Zwier, *Science* **265**, 75 **1994**.

38. R. K. Frost, F. C. Hagemeister, C. A. Arrington, T. S. Zwier, K. D. Jordan, *Phys. Chem. Chem. Phys.* **105**, 2595 **1996**.

39. J. R. Carney, T. S. Zwier, *J. Phys. Chem. A* **104**, 8677 **2000**.

40. W. H. James, E. E. Baquero, V. A. Shubert, S. H. Choi, S. H. Gellman, T. S. Zwier, *J. Am. Chem. Soc.* **131**, 6574 **2009**.

41. L. C. Snoek, E. G. Robertson, R. T. Kroemer, J. P. Simons, *Chem. Phys. Lett.* **321**, 49 **2000**.

42. L. C. Snoek, R. T. Kroemer, M. R. Hockridge, J. P. Simons, *PCCP* **3**, 1819 **2001**.

43. I. Hunig, K. Kleinermanns, *PCCP* **6**, 2650 **2004**.

44. H. Fricke, A. Gerlach, C. Unterberg, P. Rzepecki, T. Schrader, M. Gerhards, *PCCP* **6**, 4636 **2004**.

45. B. Crews, A. Abo-Riziq, L. Grace, M. Callahan, M. Kabelac, P. Hobza, M. S. d. Vries, *PCCP* **7**, 3015 **2005**.

46. P. Çarçabal, R. A. Jockusch, I. Hünig, L. C. Snoek, R. T. Kroemer, B. G. Davis, D. P. Gamblin, I. Compagnon, J. Oomens, J. P. Simons, *J. Am. Chem. Soc.* **127**, 11414 **2005**.

47. J. A. Stearns, M. Guidi, O. V. Boyarkin, T. R. Rizzo, *Phys. Chem. Chem. Phys.* **127**, 154322 **2007**.

48. J. A. Stearns, O. V. Boyarkin, T. R. Rizzo, *J. Am. Chem. Soc.* **129**, 13820 **2007**.

49. T. R. Rizzo, J. A. Stearns, O. V. Boyarkin, *Int. Rev. Phys. Chem.* **28**, 481 **2009**.

50. A. A. Stuchebrukhov, S. I. Ionov, V. S. Letokhov, *J. Phys. Chem.* **93**, 5357 **1989**.

51. A. A. Makarov, I. Y. Petrova, E. A. Ryabov, V. S. Letokhov, *J. Phys. Chem. A* **102**, 1438 **1998**.

52. W. Chin, F. Piuzzi, I. Dimicoli, M. Mons, *PCCP* **8**, 1033 **2006**.

53. R. Brause, H. Fricke, M. Gerhards, R. Weinkauf, K. Kleinermanns, *Chem. Phys.* **327**, 43 **2006**.

54. L. Biemann, M. Braun, K. Kleinermanns, *J. Mol. Spectrosc.* **259**, 11 **2010**.

55. B. C. Dian, A. Longarte, T. S. Zwier, *Science* **296**, 2369 **2002**.

56. B. C. Dian, G. M. Florio, J. R. Clarkson, A. Longarte, T. S. Zwier, *Phys. Chem. Chem. Phys.* **120**, 9033 **2004**.

57. B. C. Dian, A. Longarte, P. R. Winter, T. S. Zwier, *Phys. Chem. Chem. Phys.* **120**, 133 **2004**.

58. D. A. Evans, D. J. Wales, B. C. Dian, T. S. Zwier, *Phys. Chem. Chem. Phys.* **120**, 148 **2004**.

59. B. C. Dian, J. R. Clarkson, T. S. Zwier, *Science* **303**, 1169 **2004**.

60. J. R. Clarkson, B. C. Dian, L. Moriggi, A. DeFusco, V. McCarthy, K. D. Jordan, T. S. Zwier, *Phys. Chem. Chem. Phys.* **122**, 214311 **2005**.

61. J. R. Clarkson, E. Baquero, T. S. Zwier, *Phys. Chem. Chem. Phys.* **122**, 214312 **2005**.

62. T. S. Zwier, *J. Phys. Chem. A* **110**, 4133 **2006**.

63. T. A. LeGreve, J. R. Clarkson, T. S. Zwier, *J. Phys. Chem. A* **112**, 3911 **2008**.

64. N. R. Pillsbury, C. W. Muller, T. S. Zwier, *J. Phys. Chem. A* **113**, 5013 **2009**.

65. J. A. Stearns, C. Seaiby, O. V. Boyarkin, T. R. Rizzo, *PCCP* **11**, 125 **2009**.

66. O. Asvany, S. Schlemmer, *Int. J. Mass spectrom.* **279**, 147 **2009**.

67. S. Trippel, J. Mikosch, R. Berhane, R. Otto, M. Weidemüller, R. Wester, *Phys. Rev. Lett.* **97**, 193003 **2006**.

68. R. Otto, P. Hlavenka, S. Trippel, J. Mikosch, K. Singer, M. Weidemüller, R. Wester, *J. Phys. B* **42**, 154007 **2009**.

Chapter 4

Conformer-specific spectroscopy by IR-UV double resonance

The objective of this thesis is to investigate conformational dynamics by exploring the energy landscapes of biological molecules and transitions between them. It is primordial that our attention focuses first on the number of conformers that a given molecule could adopt, their structures as well as their spectroscopic signatures. In this chapter, we present spectroscopic studies that provide information about the local minima on the potential energy surface. We first discuss the spectroscopy of the amino acid phenylalanine which serves as chromophores in the peptides used in this thesis work. In the second part, we describe our spectroscopic studies of two small peptides, Ac-Phe-(Ala)$_5$-LysH$^+$ a 7 amino acid helical peptide and Ac-Phe-(Ala)$_3$-(Gly)$_4$-(Ala)$_3$-LysH$^+$ a twelve amino acid peptide, in the Amide A, I and II regions of the infrared spectrum.

4.1 Spectroscopy of the amino acid phenylalanine

4.1.1 Introduction

Many gas phase studies have focused on understanding the intrinsic properties of the aromatic amino acids for the simple reason that they are responsible for photochemistry and photophysics of proteins in the UV region. In 1985, the Levy group reported the first electronic spectrum of tryptophan in a supersonic expansion and identified six different conformations using R2PI saturation and fluorescence spectroscopy [1, 2]. The desire to understand more completely the relationships among conformation, chromophore environment, and photophysics has led to numerous gas phase spectroscopic studies of the

amino acids and their derivatives in which the complicating effects of solvent have been removed [3-9]. The spectrum of the neutral aromatic amino acid, phenylalanine, first recorded by Martinez *et al.*, about 20 years ago in a supersonic jet using laser-induced fluorescence spectroscopy, revealed the presence of five stable conformers [6]. Other groups applied a combination of spectroscopic techniques, coupled with high-level ab initio calculations, and demonstrated the presence of six conformations and predicted their assignments [10-13].

All these spectroscopic studies were concerned with the gas-phase amino acids in their neutral form. The study of charged biomolecules is of at least equal importance since in their native environment these molecules are charged. Several groups have put a considerable effort in order to understand the spectroscopy, structure, various photofragmentation channels and the excited-state dynamics of the aromatic amino acids and their derivatives [14-24].

Stearns *et al.* reported the ultraviolet photofragmentation spectra of protonated tyrosine and phenylalanine [19]. The electronic spectrum of TyrH$^+$ was measured by monitoring the fragment *m/z* 107 amu which corresponds to the tyrosine side chain radical cation and exhibits sharps features, making possible the use of the IR-UV double resonance techniques. The IR spectra combined with the DFT calculations at the B3LYP/6-31G** revealed the presence of four stable conformations sorted in two classes depending on the orientation of the backbone, *anti* and *gauche*, which exhibit different fragmentation patterns. The following section will represent the spectroscopic studies of the protonated phenylalanine, in which I contributed.

4.1.2 Results on the spectroscopy of protonated phenylalanine

Phenylalanine ions are produced by electrospray, pre-trapped in the hexapole for ion packet formation, mass-selected and injected into a cold ion trap, where they are cooled by collisions with helium. We then irradiate these cold ions with different combinations of UV and IR laser pulses and measure spectra by detecting fragments that are produced after photon absorption as a function of the laser frequency.

The vibrationally resolved ultraviolet photofragmentation spectrum of PheH$^+$ is presented in Figure 4.1. The signal was recorded by monitoring the fragment at *m/z* 74 as a function of wavenumber of the UV dissociation laser. This fragment corresponds to NH$_2$-CH-COOH, the radical cation left upon loss of a hydrogen atom and breakage of the C$_\alpha$-C$_\beta$ bond. It is not observed in collision-induced dissociation (CID) [25] and must result from a direct

dissociation from an excited electronic state. Assuming that phenylalanine behaves like tyrosine, this bond cleavage mechanism, according to Lucas *et al.*, is based on light-induced electron transfer from the aromatic ring to the carboxylic acid, followed by a fast internal proton transfer from the ammonium group to the carboxylic group [26].
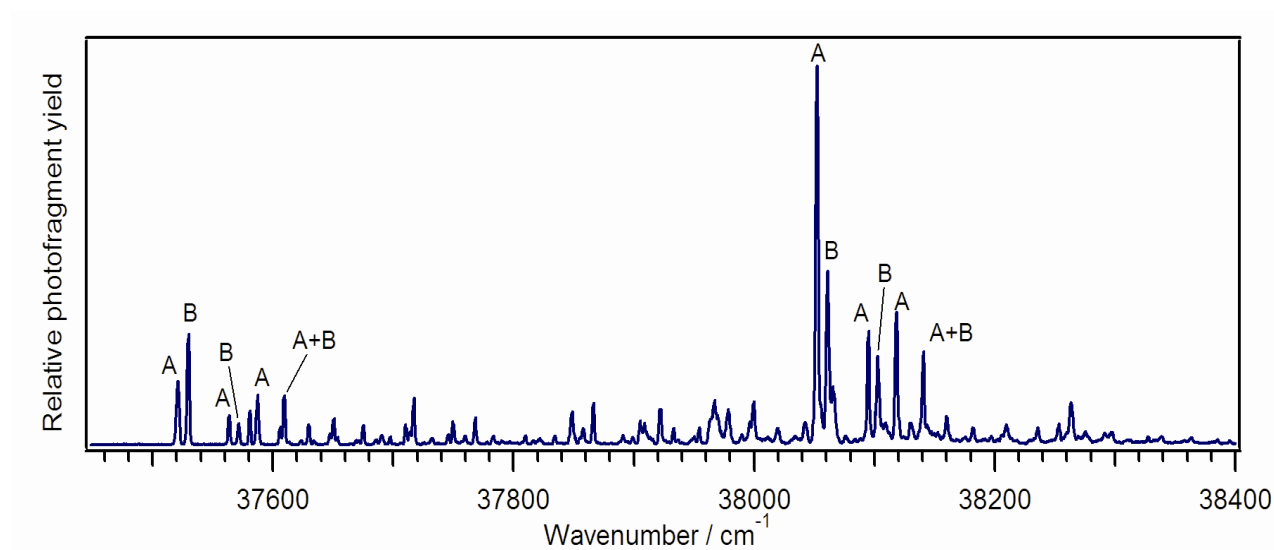
Figure 4.1: Ultraviolet photofragment excitation spectrum of PheH[+] recorded by detecting the m/z 74 fragment. The conformational assignments are based on the infrared and IR-UV hole burning spectra.

Excitation of the first two UV transitions of PheH[+] (37 520.9 cm^{-1} and 37 529.6 cm^{-1}) induces the same fragmentation mass spectrum, shown in Figure 4.2. The fragment *m/z* 74 has the most intense signal, and another major fragment is detected over the mass channels 91-93. Mass 93 is observed in CID and attributed to the loss of (H_2O + CO + HCN) [25]. Mass 91 corresponds to the side chain radical cation [21], but it is not clearly distinguishable from *m/z* 93, since we run our analyzing quadrupole at relatively low resolution in order to maximize ion transmission.
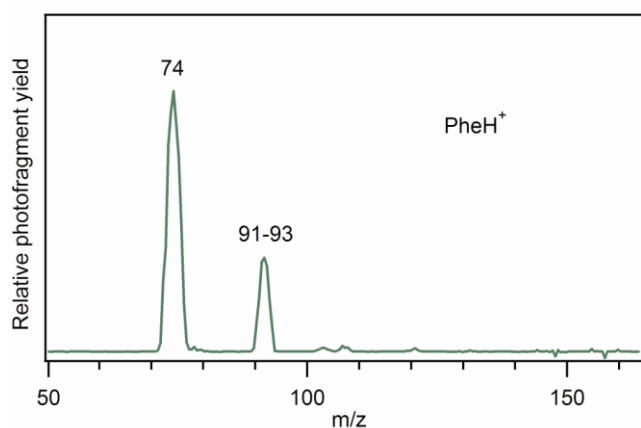
Figure 4.2: Photofragment mass spectrum of protonated phenylalanine.

The UV spectra record monitoring the fragment *m/z* 91-93 or *m/z* 74 are identical. The first origin transition occurs at 37 520.9 cm^{-1} and is shifted to the red of that of the neutral species by only 17 cm^{-1}. The second peak in the UV spectrum of PheH$^+$ is larger than the first and spaced from the latter by 10.5 cm^{-1}. This small energy difference between the first two peaks and the absence of a further progression of peaks suggests that these two features are not a part of a Franck-Condon progression but the origin transitions of different conformers.

Figure 4.3 shows the IR spectrum recorded with the UV laser set to the first transition of PheH$^+$ at 37 520.9 cm^{-1}, fired 200 ns after the scanned IR laser. The different calculated spectra are presented below the experimental spectrum, each representing a family of structures sorted according to the NH$_3$ and COOH orientations. Figure 4.3a displays the global minimum which contains two stabilizing hydrogen-bond interactions of the charged NH$_3$ group, one with the π-cloud of the ring and one with the carbonyl oxygen. Figure 4.3b presents the calculated spectrum for a conformer in which the rotation of the carboxylic acid group results in an NH-OH interaction that is considerably weaker than the NH-O=C interaction shown in Figure 4.3a, increasing the energy by 16.0 kJ/mol and shifting the NH stretching frequency up from 3188 cm^{-1} to 3283 cm^{-1}. The loss of the NH-π interaction in the conformers shown in Figure 4.3c and d also results in a higher frequency NH stretch and considerably higher energies. Only the lowest energy structure is consistent with the experimental spectrum. There are two structures with NH$_3$ and COOH orientations like that of Figure 4.3a that differ in the orientation of the backbone with respect to the ring by a rotation of the angle χ_1. The structure with $\chi_1 = 72°$ (*gauche*) is 3.2 kJ/mol higher in energy than the global minimum structure, which has $\chi_1 = 169°$ (*anti*).

Assuming that phenylalanine is protonated on the N-terminus, initial conformational searches on the protonated amino acids using the AMBER force field [27] within the MacroModel [28] program were performed. Re-optimization of the lowest energy structures and calculation of harmonic and anharmonic vibrational frequencies were carried out using B3LYP/6-31++G** in Gaussian03 [29]. Harmonic hydride stretch frequencies were scaled by 0.954 for comparison to the infrared spectra, but all frequencies were left unscaled in the zero-point energy calculations. Anharmonic frequency calculations were left unscaled.[1]

---

[1] The DFT/B3LYP/6-31++G** calculations were performed in our laboratory by Dr Jaime A. Stearns.
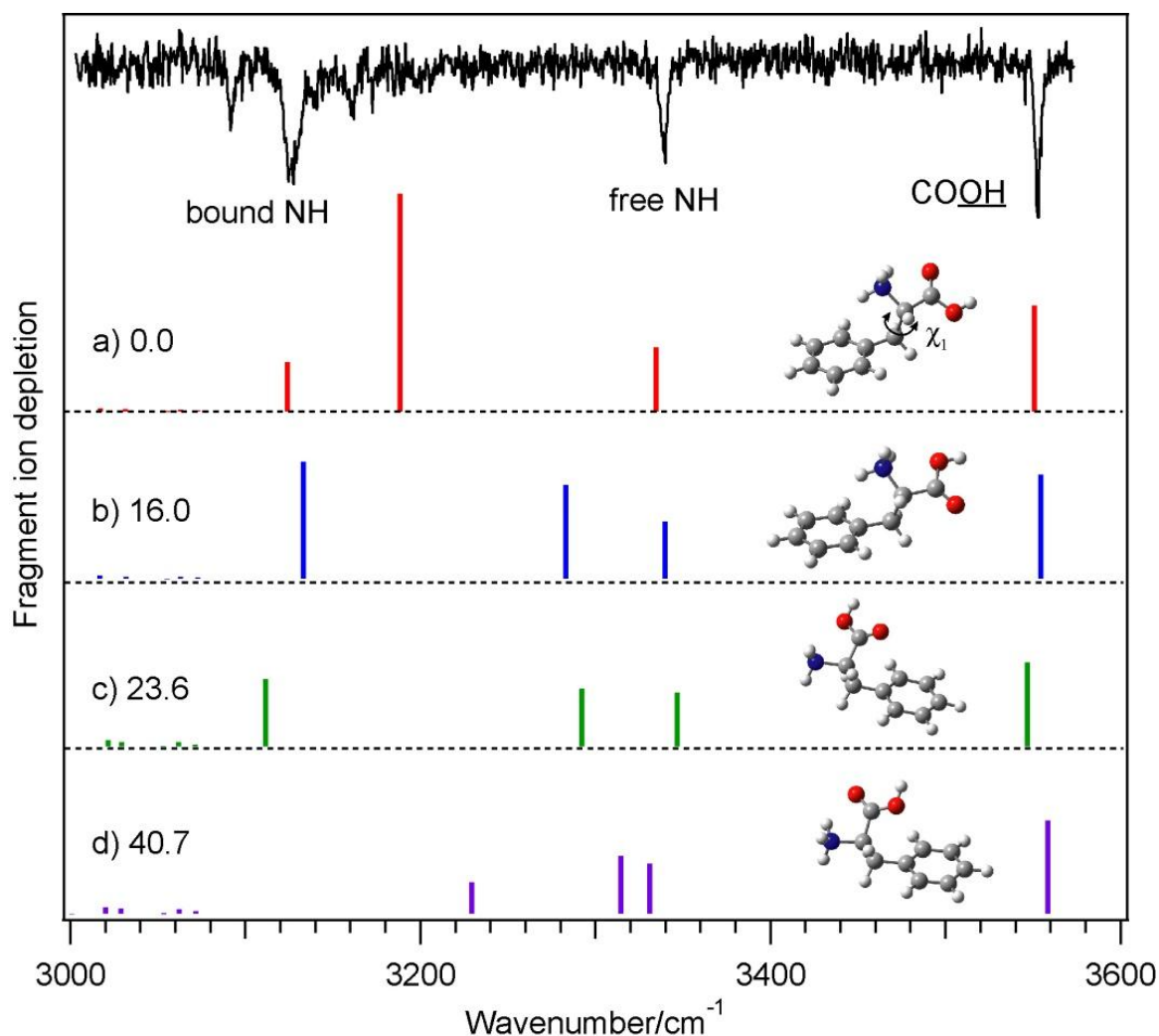
Figure 4.3: Experimental infrared spectrum of conformer A and the calculated spectra at the B3LYP/6-31++G** level of theory (a)-(d) for four families of conformers, with the zero-point corrected energy of each structure in kJ/mol.

The infrared spectra associated with the first two transitions in the UV spectrum are presented in Figure 4.4. While the peak corresponding to the carboxylic acid OH stretch is the same for the two, the vibrational frequency of the non-interacting ammonium NH stretch differs by 15 cm^{-1}, supporting the conclusion that the peaks in the UV spectrum belong to different conformers. Further differences occur in the lower frequency region between 3000-3150 cm^{-1} where the vibrational bands of the NH groups interacting with the π cloud and the carboxyl group appear. Comparison with the anharmonic and scaled harmonic calculated frequencies for PheH$^+$ suggests assigning the spectrum of Figure 4.4a to conformer A, which corresponds to the global minimum *anti* structure, and that of Figure 4.4b to conformer B, the *gauche* structure. This assignment is made based upon the good agreement between the calculated and observed free NH stretch frequencies as well as the prediction that the hydrogen bonded NH stretches are further shifted to the red in conformer B.
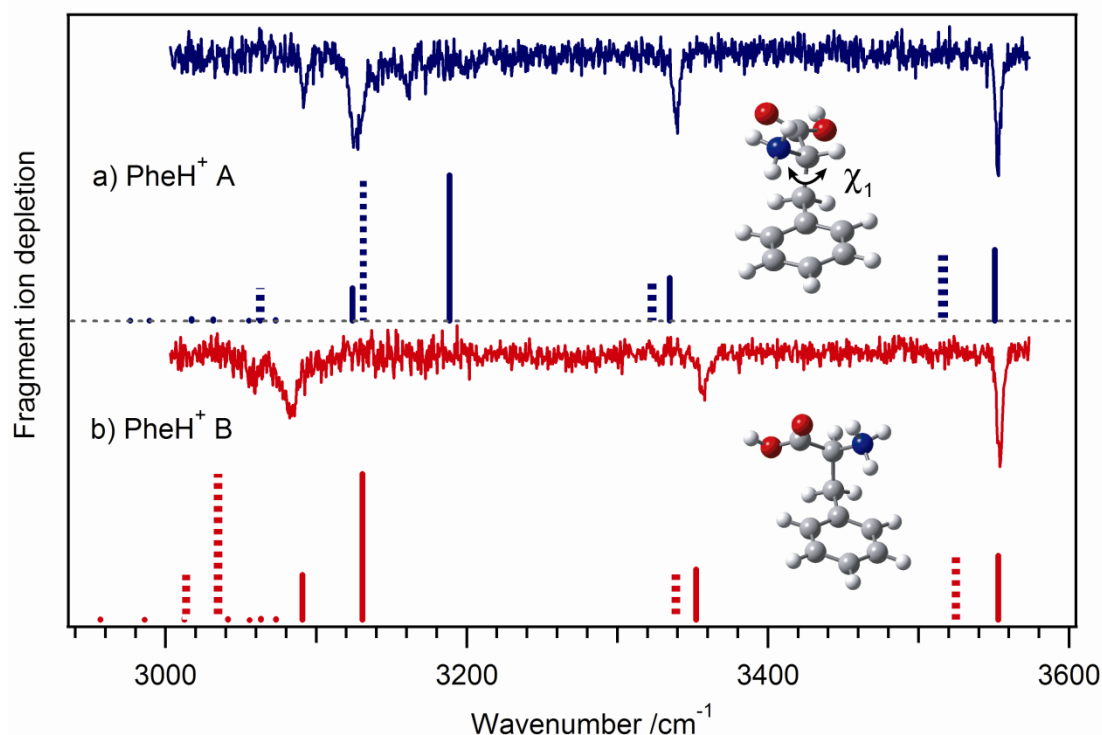
Figure 4.4: Infrared spectra of conformers (a) A and (b) B of PheH$^+$. Calculated spectra (B3LYP/6-31++G**) and structures are shown below the experimental spectra. The solid line spectra represent scaled harmonic frequencies, and the dashed line spectra are unscaled anharmonic frequencies.

This assignment is further supported by the correct prediction of the greater splitting between the bound NH stretches in conformer A compared to those of conformer B. To help assign the conformers associated with many of the transitions in the UV spectrum of Figure 4.1, similar infrared spectra were obtained. Moreover, IR-UV hole burning electronic spectra have been recorded for both conformers A and B, as shown in Figure 4.5.

The red traces in Figure 4.5 show the first 260 cm^{-1} of the IR-UV hole burning spectra of PheH$^+$ measured by fixing the IR laser on the N-H transition, in the low frequency region, at 3122 cm^{-1} and 3079 cm^{-1} for conformers A (a) and B (b) respectively. The black traces correspond to the signal recorded while the IR laser pulse is off. The depletion in the signal of the hole-burning spectra and the comparison between them illustrate that each vibronic transition observed could be attributed to conformer A or conformer B.

The electronic spectra of both conformers exhibit a hot band (at -43.6 cm^{-1} for A and -42.9 cm^{-1} for B), which is too small to be observed on the scale of Figure 4.1. Using the intensity of this hot band, we estimate a vibrational temperature of PheH$^+$ of ~12 K, which is similar to that determined for protonated tyrosine. A vibrational mode of similar frequency in

the excited state (43.6 cm^{-1} for A and 42.0 cm^{-1} for B) seems to be built off of the origin for each conformer.
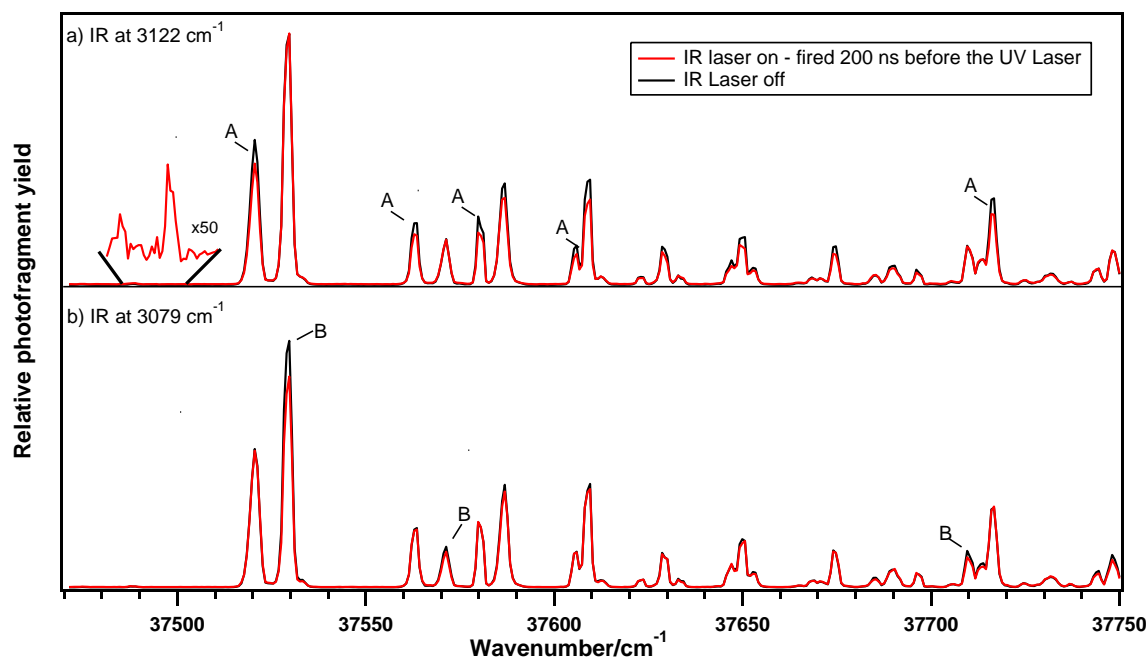
Figure 4.5: IR-UV hole burning spectra (in red) recorded by fixing the IR the transition of (a) conformer A at 3122cm^{-1} and (b)conformer B at 3079cm^{-1} of PheH$^+$. The black traces are recorded with the IR laser off.

The lowest frequency vibration predicted by the calculations is a torsion of the phenyl ring with respect to the backbone that has a ground state harmonic frequency of 45 cm^{-1} for conformer A and 43 cm^{-1} for conformer B. Conformer A shows considerably more vibronic activity than conformer B, indicating a larger geometry change upon excitation. The low-frequency vibrations are also built off of the intense vibronic bands at 38054.2 cm^{-1} and 38061.1 cm^{-1}, which are 531 cm^{-1} above the band origins of conformers A and B, respectively. This vibrational mode corresponds well to the *6b* vibration of benzene and its derivatives, which appears at 530 cm^{-1} in the excited state of toluene [30]. The intensity of this transition in toluene and other substituted benzenes derives from vibronic coupling between the L$_b$ and L$_a$ $\pi\pi^*$ excited states, and this is likely also the case for PheH$^+$. Since we had clearly identified different peaks with conformer A and B, the inversion of the relative intensities between the origins and *6b* bands suggests that the intensities are not simply related to the relative population. This subject will be addressed further in *Chapter 6.*

We had recently extended the IR region to cover the 6 μm by generating laser light by an IR OPO together with difference-frequency mixing in a AgGaSe$_2$ crystal. The IR spectra of

the first two transitions in the UV spectrum of protonated phenylalanine are presented in Figure 4.6.
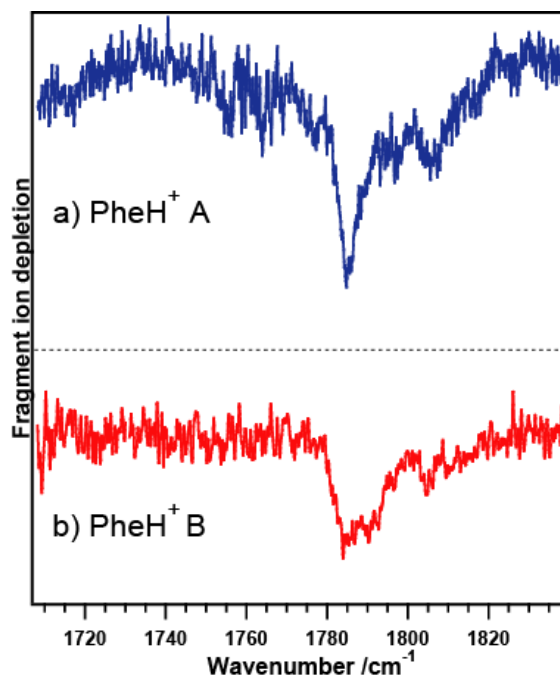
Figure 4.6: Infrared spectra of conformers (a) A and (b) B of PheH$^+$ in the amide I region.

The peak around 1785 cm^{-1} is assigned to the excitation of the C=O stretching mode while the small peak appearing to the blue of these transitions could be an overtone of lower frequency vibrations. The C=O transition has a width of about 5.1 cm^{-1} and 11cm^{-1} in the case of conformers A and B, the factors leading to this difference are likely a combination of the hydrogen bonding and interaction with the π cloud of the phenyl ring although it could be some mixing with the overtone.

This band appears close in frequency to the C=O group of neutral phenylalanine with the carbonyl oxygen hydrogen bonded [10, 13, 31]. This observation confirms our previous structural assignment based on the association with the spectra in the NH stretch region, where both conformers A and B have the C=O hydrogen bonded.

4.1.3 Conclusion

The protonated aromatic amino acids are closed shell species with ultraviolet chromophores and $\pi\pi^*$ excitation energies similar to those of the neutrals. Protonation results in a red shift of the S_0-S_1 transition energies of only about 50 cm^{-1} for phenylalanine, indicating the $\pi\pi^*$ state does not depend strongly on protonation state for these species. Only

the lowest energy calculated structures give infrared spectra that are consistent with those measured here, suggesting the cooling process does not trap molecules in higher energy potential minima. The conformations observed for PheH[+] belong to the same familie, each having two backbone orientations, with dihedral angle $\chi_1 = \sim170°$ (*anti*) and $\sim70°$ (*gauche*). These two conformers are analogous to conformers II and VII calculated for the neutral, although VII was not observed in a gas phase experiment [10].

4.2 Spectroscopy of seven and twelve residue peptides

4.2.1 Introduction

The secondary structure of a peptide corresponds to local three-dimensional structural elements, while the tertiary structure is the molecule's overall shape. These three-dimensional arrangements are governed by weak non-covalent interactions between the amino acids, i.e. hydrogen bonds. One of the most common secondary structural elements in proteins is the helix. There are different types of helices, which differ in their hydrogen-bonding patterns. The most common and prevalent type of secondary structure and which plays important role in the protein folding is the α-helix [32]. Based on the Pauling and Corey nomenclature, it is a 3.6_{13}-helix that represents a repeating pattern of hydrogen bonds between the amide carbonyl oxygen on the ith residue and the amide NH of the $i+4$[th] residue, forming hydrogen-bonded rings of 13 atoms, denoted C_{13} [33]. The 3_{10} helix is a tighter, less common structure formed by 10-membered rings (C_{10}) of an $i, i+3$ bonding pattern.

The gas phase provides a medium for studying the intrinsic conformational preferences of peptides that is not dissimilar to the low dielectric constant environment of biological membranes. In the absence of solvent a peptide can adopt conformations driven by only intramolecular forces, providing the opportunity to study these interactions in detail using high-resolution spectroscopic techniques. At the same time, gas phase studies provide benchmarks to test and improve theoretical predictions of the conformational structure and the counterbalancing forces that control them. Several IR spectroscopic studies have identified helical structures in gas phase peptides. Oomens and coworkers measured IR spectra for several charge states of cytochrome c by multiple-photon dissociation spectroscopy in an FT-ICR mass spectrometer [34]. They assigned their spectrum mostly to features indicative of α-helices, in keeping with its known solution structure. Mons and coworkers, using IR-UV dip

spectroscopy in the NH stretch region, identified 3_{10} helical motifs for Ac-Ala-Phe-Ala-NH$_2$ and Ac-Aib-Phe-Aib-NH$_2$ [35]. They studied many other small peptides with the aim of characterizing the interactions responsible for the formation of the secondary structures in proteins and understanding the competition between the several of these secondary structures, namely β-turns, β-strands, or 3_{10} and α-helices [36-40]. De Vries and coworkers reported the infrared spectra of the pentapeptide FDASV and several 15-residue gramicidin peptides in the hydride stretch region and suggested the presence of gas-phase helical structures, the former containing a single C_{13} α-turn, and the latter each showing a large, unresolved band in the NH-stretch region attributed to hydrogen bonds involved in a helix [41, 42].

In parallel to the spectroscopic studies, ion mobility has been applied to assigning the geometries and the factors that stabilize the secondary structure of peptides and proteins [43-47]. Jarrold and coworkers established that peptides consisting of seven or more alanines with a lysine at the C-terminus form extremely stable gas-phase helices, while those without the lysine or with the lysine at the N-terminus are globular [45, 46]. Recently using IRMPD spectroscopy in the high-frequency stretch region, Vaden *et al.* confirmed the globular nature of small alanine peptides lacking the C-terminal lysine [48]. The protonated lysine side-chain plays an important role in helix formation, by providing hydrogen-bonding sites for three carbonyls at the C-terminus and by stabilizing the macro-dipole of the helix.

Recently Stearns *et al.* reported first results of the spectroscopic studies of cold, protonated, lysine-capped polyalanine helices Ac-Phe-(Ala)$_5$-Lys-H$^+$ and Ac-Phe-(Ala)$_{10}$-Lys-H$^+$. They assigned the spectroscopic features associated with the conformers of the smaller peptide and speculated as to the corresponding conformers observed in the larger [49, 50]. The presence of the phenylalanine was essential, since a chromophore is needed for these spectroscopic experiments and is not expected to change significantly the helical shape predicted by the ion mobility studies. The IR spectra in the NH stretch region of the small peptide exhibits seven well resolved bands, which were assigned by comparison with calculations together with nitrogen-15 isotopic substitution studies. The helical geometries found spectroscopically seem to be in agreement with the ion mobility studies of Jarrold and coworkers [43-47]. Stearns *et al.* also reported the effects of N-terminus substitution on the structure and spectroscopy of gas-phase helices [51]. It was found that the acetylation of the N-terminus has a very little effect on the spectroscopy and structure, however protonation of

the N-terminus changes the infrared spectrum to the point that it may also change the structure of the peptide.

The Ac-Phe-(Ala)$_5$-Lys-H$^+$ peptide is one of the systems that we choose to explore its conformational isomerization by population transfer experiments. First it is important to identify the number of conformers and their structure. The following section will report the spectroscopic studies on this small peptide. In order to present the entire picture it is necessary to reported some of the data Dr. Stearns obtained, but this will be specified.

4.2.2 Results of spectroscopic studies of Ac-Phe-(Ala)$_5$-Lys-H$^+$

The UV photofragment spectra of the Ac-Phe-(Ala)$_5$-Lys-H$^+$ peptide, shown in the Figure 4.7, was recorded monitoring the fragment m/z=474 corresponding to the b$_5$ fragment [49]. Despite the large size of the molecule, the UV spectrum shows sharp features without significant congestion from Franck-Condon activity, a large number of conformers or hot bands.
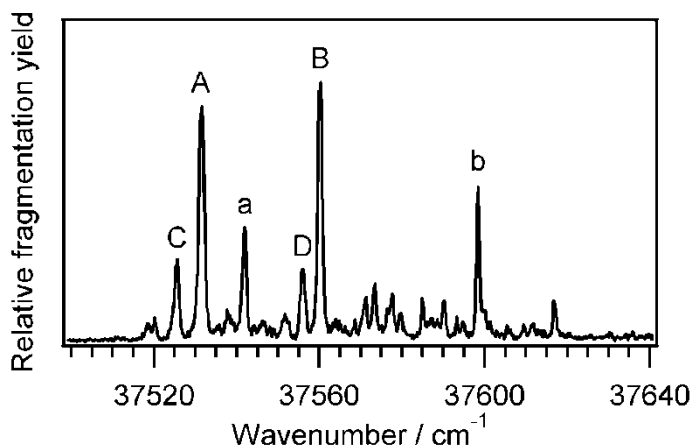
Figure 4.7: Ultraviolet photofragment spectrum of Ac-Phe-(Ala)$_5$-Lys-H$^+$, recorded by detecting the m/z 474 fragment. The conformational assignments are based on the infrared IR-UV spectra.

By fixing the UV laser on different transitions in the photofragment spectrum while scanning the IR laser 200 ns earlier, we recorded the IR spectrum associated with each of these transitions. The largest peaks have different IR spectra and are labeled A and B. The next most intense peaks, 10 cm^{-1} and 38 cm^{-1} to the blue of peaks A and B, have the same IR spectra as A and B, so we assign them as vibronic bands of the same conformers, and label them with the corresponding lower-case letter. The two transitions to the red of A and B have different infrared spectra, and therefore represent the third and fourth conformers, C and D.

Figure 4.8 presents four IR spectra in the NH stretch region associated with conformers A-D as identified by their respective transitions in the UV spectrum. We noticed some gains in the infrared spectra of conformers C and D (dashed-line), which arise because of statistical broadening [52] in the UV spectrum of conformers A and B following IR excitation. This spreads a small amount of absorption intensity to the UV wavelengths at which conformers C and D are probed. Because the fragmentation signals from conformers A and B are significantly more intense than those of C and D, this gain on the fragmentation signal is on the same scale as the IR-induced depletion of C and D. The populations of C and D are sufficiently small that the inverse is not perceptible [53]. The spectra represented with a solid line in the case of C and D are the same as those dashed, but the gains have been removed by subtracting the contributions from conformers A and B.
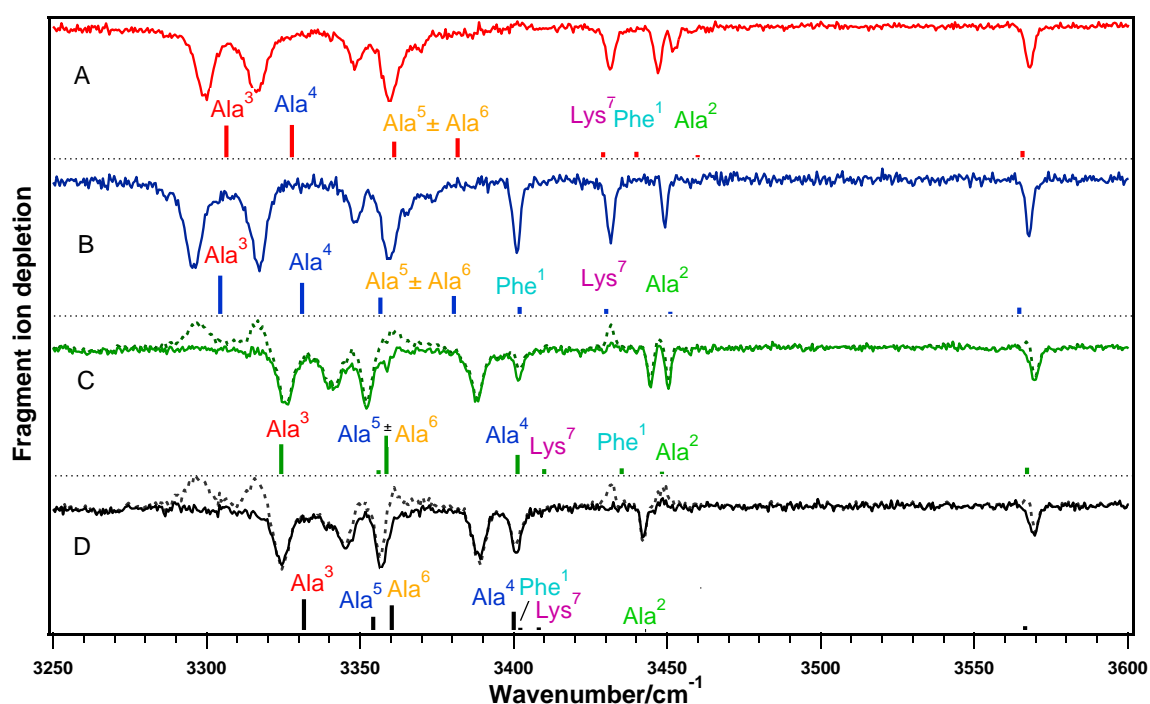
Figure 4.8: IR-UV double resonance spectra of Ac-Phe-(Ala)$_5$-Lys-H$^+$ recorded at the labeled transitions in the UV spectrum. The positive-going signals in the spectra of C and D (the dashed-line) are gains due to conformers A and B. The best matching calculated spectra are presented directly under each experimental spectrum together with the assignments of each peak to a specific amino acid residue.

The four infrared spectra exhibit a C-terminal carboxylic acid OH stretch band at 3572 cm^{-1} and show seven resolved amide NH stretches except in D, where two of the peaks may overlap. In general, the amide NH stretch bands below 3400 cm^{-1} belong to the NH groups involved in stronger hydrogen bonds, whereas the higher-frequency NH stretch bands arise from those in weaker interactions. The significant differences in the low-frequency region

between the two pairs of conformers A/B and C/D suggest different hydrogen-bonding patterns for each pair (see discussion below). We also observed several broad transitions between 2900-3100 cm^{-1} (not shown), which we assign to the NH stretches of the ammonium group of the lysine side chain. In protonated amino acids, ammonium NH stretches appear around 3350 cm^{-1} in the absence of hydrogen bonding, and around 3000 cm^{-1} when hydrogen-bonded [19], implying that the ammonium NH groups in Ac-Phe-(Ala)$_5$-Lys-H$^+$ are involved in hydrogen bonds.

To help assign the amide NH bands, Dr. Stearns carried out calculations at the B3LYP/6-31G** level of theory and recorded infrared spectra of three isotopologues of Ac-Phe-(Ala)$_5$-Lys-H$^+$, each with an alanine amide nitrogen replaced by N-15: ^{15}N-Ala^2, ^{15}N-Ala^4, and ^{15}N-Ala^6, (the right superscript index of the residue indicates its position from the N-terminus). These studies allow the identification of four helical conformers that can be sorted in two families according to their hydrogen-bonding scheme of the peptide backbone, as shown schematically in Figure 4.9 (A-B backbone II and C-D backbone I). The global minimum is a helix with two C$_{10}$ and two C$_{13}$ rings, as shown schematically in Figure 4.9a, and denoted backbone I. The hydrogen-bonded rings involve the amide NH groups of Ala^3, Ala^4, Ala^5, and Ala^6 in such a way that the middle two share a carbonyl while the amide NH groups at the ends of the molecule do not participate in C$_{10}$ or C$_{13}$ NH···C=O hydrogen bonds. The lysine amide NH is in a C$_5$ arrangement with the C-terminal carbonyl, and the phenylalanine NH can be in a π-hydrogen bond with the aromatic ring, depending on the orientation of the phenylalanine side chain. The second-lowest-energy hydrogen-bonding pattern, II, has three C$_{10}$ rings and one C$_{13}$ ring, with the Ala^5 and Ala^6 NH groups hydrogen-bonded to the same carbonyl (Figure 4.9b). The hydrogen bonding schemes for the end residues are the same as backbone I.
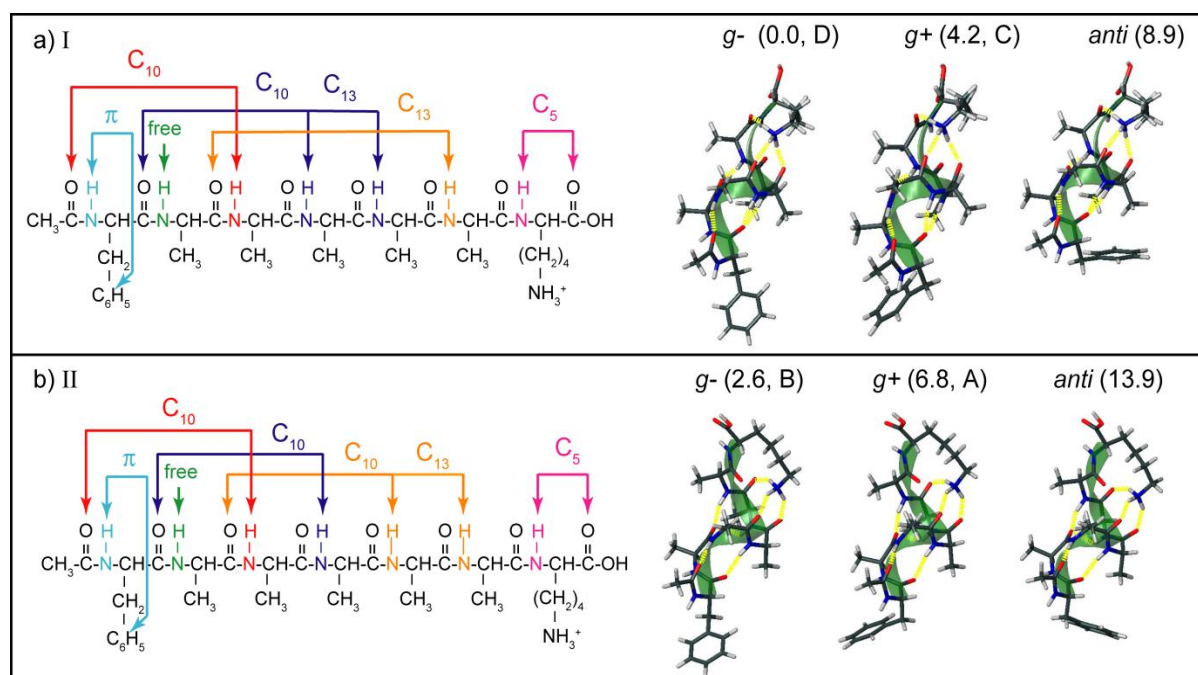
Figure 4.9: Schematic depictions of the structures of the lowest-energy conformers of Ac-Phe-(Ala)$_5$-Lys-H$^+$, with the hydrogen-bonding schemes of the helices on the left and calculated structures on the right. The calculated structures have the helix axes aligned to better show the orientation of the phenylalanine ring: g+, g-, or anti. The conformers are also labeled with their zero-point-corrected energy in kJ/mol and their assignment (A, B, C, or D).

In each conformational family the orientation of the phenylalanine side chain changes by rotation around the C_α-C_β bond, such that the Phe^1 χ_1 angle, measured along the N-C_α-C_β-C_γ atoms, can take values of approximately 180°, +60°, or -60°, corresponding to labels of *anti*, *gauche + (g+)*, and *gauche – (g-)*. In all the structures, the *gauche* structures were lower in energy because they allowed the Phe^1 amide NH to form a favorable π-hydrogen bond with the aromatic ring, which, based on the vibrational frequencies, seems to be especially strong in the *g-* structures (Figure 4.9). The best matches to A and B are shown directly under the experimental spectra, and they both have the C_{10}-C_{10}-C_{10}-C_{13} hydrogen-bonding pattern (backbone II) and respectively the *g+* and *g-* orientations of the Phe^1 side chain. The *g-* structure proposed for conformer B has the Phe^1 NH group in a stronger π-hydrogen bond than does conformer A, giving the NH stretch a lower frequency in conformer B, which is the only significant difference between the two spectra. The calculated spectra that give the best match to the experimental spectra of C and D correspond to conformers with backbone I, C_{10}-C_{10}-C_{13}-C_{13} hydrogen-bonding pattern. The assignment of the Phe ring orientation was made on the basis of the Phe^1 NH stretch, which is present above 3430 cm^{-1} in conformer C and the *g+* structure. In conformer D, the Phe^1 NH stretch is apparently shifted from that of Ala^2 (which was assigned by isotopic substitution), and the calculated spectrum for the *g-*

structure suggests that it may be buried underneath that of Ala[4] or Lys[7]. In the spectrum of ^{15}N-Ala[4] conformer D, the Ala[4] transition shifts to the red but reveals no underlying Phe[1] NH stretch, so perhaps it lies underneath that of the Lys[7] amide NH transition at 3404 cm^{-1}, which appears broader in conformer D than in conformer C.

While the level of theory used here was sufficient to help assign the infrared spectra, it was not particularly accurate for predicting precise vibrational frequencies or the relative energies of the various conformers as determined from the observed relative intensities of the band origins in the UV spectra (C and D are calculated to be lower in energy but they have smaller intensities in the UV spectrum). Although the DFT methods and modest basis set used here performed surprisingly well, Hobza and coworkers had previously noted unsatisfactory results in other peptides because of the lack of inclusion of dispersive interactions [54]. Dispersion may also be the reason that Phe[1] NH frequencies are predicted rather poorly in the *g+* conformers A and C.

In order to understand more fully the spectroscopic signature of helices and to complement our current data in the NH stretch region, we extended our conformer-specific IR spectra of these helical molecules into the amide I and amide II regions, shown in Figure 4.10 for conformers A-D together with calculated spectra. The laser light was generated by an IR OPO together with difference-frequency mixing in a $AgGaSe_2$ crystal. The four spectra exhibit peaks around 1630-1800 cm^{-1} that correspond to bands with mainly C=O stretch character while the lower intensity peaks at lower wavenumber arise from the NH bending vibrations (amide II), although there is some degree of mixing between these modes in both regions. The calculated spectra of the four conformers assigned by comparison with our measured spectra in the NH stretch regions, reveal an acceptable match with the new data in the amide I and II regions although a different scale factor (0.973) has been used here. That a different scale factor should be necessary for these different spectral regions is entirely expected, since the anharmonicity of CO vibrations will be quite different from light atom stretch vibrations.
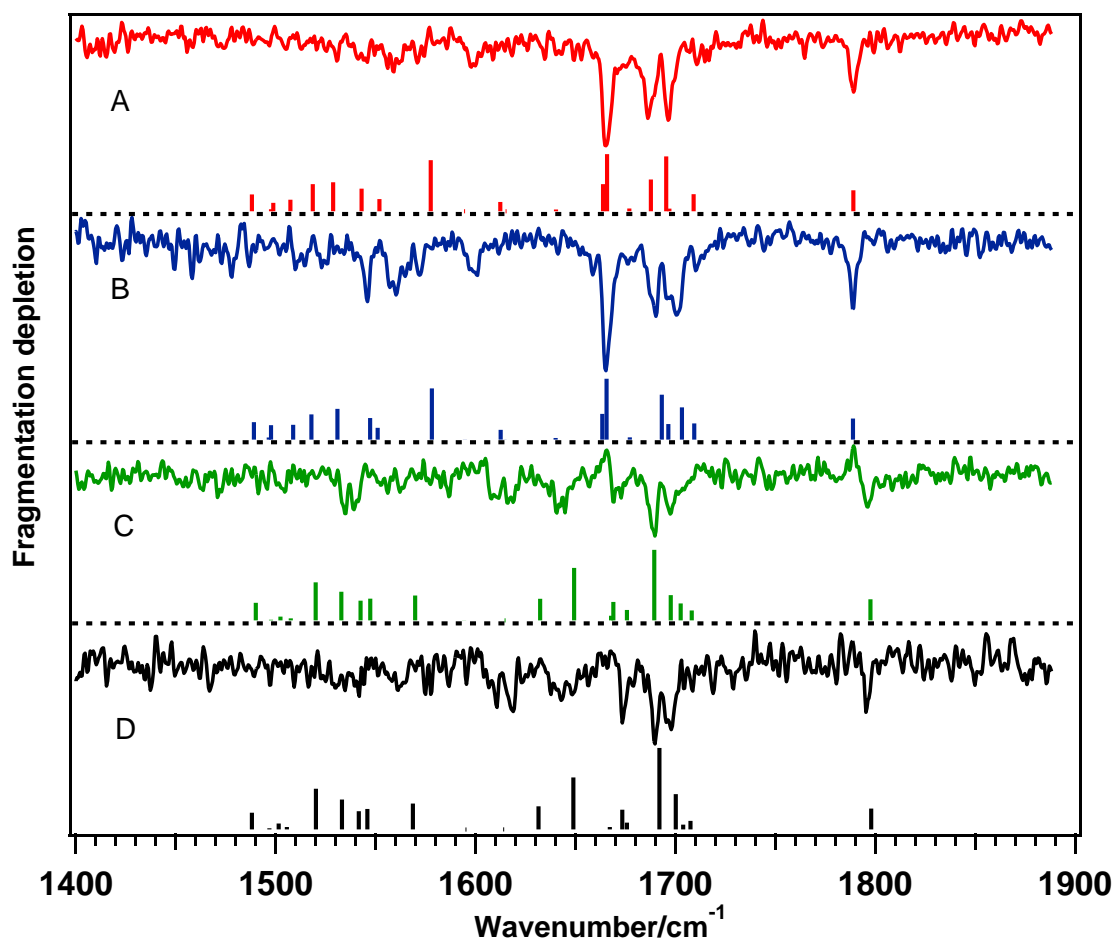
Figure 4.10: IR-UV double resonance spectra of Ac-Phe-(Ala)$_5$-Lys-H$^+$ recorded in the amide I and II region, at the labeled transitions in the UV spectrum. The best matching calculated spectra are presented directly under each experimental spectrum.

The four spectra show a transition around 1792 cm^{-1} which can be assigned to the CO stretch of the C-terminal carboxylic group. The C-terminal C=O band is slightly red shifted upon hydrogen bonding with the N-H group [55], which is consistent with the conclusion drawn earlier in the region of the NH and OH stretches where the lysine amide NH in all conformations is in a C$_5$ arrangement with the C-terminus. If a lone pair of the oxygen atom is involved in a hydrogen bond the CO distance will increase and the vibrational frequency will red-shift by about 50 cm^{-1}. Based on the work of Bakker *et al.* [55], the transitions between 1660 and 1710 cm^{-1} are assigned to weakly hydrogen-bond C=O stretching vibrations, and the bands below 1660 cm^{-1} to a stronger hydrogen-bond C=O stretching vibrations. The absence of a significant difference between the two spectra of A and B reflects the similarity in the helical structure attributed previously for these conformations (A and B). The spectra of conformers C and D also have transitions between 1685-1700 cm^{-1} that can be ascribed to free or weakly hydrogen-bonded C=O stretches. In this same region and below 1685 cm^{-1}, the

spectra of C and D differ from A and B in the position of these lowest frequency transitions that are red-shifted due to the C=O hydrogen bonding. These reflect the difference in the backbone hydrogen-bonding schemes between the two groups of conformations mentioned above. The transitions of the amide II are concentrated around 1500-1600 cm^{-1} in all spectra, the blue shifted transitions reflect clearly that the NH are bonded, while the lower frequency bands belong to the free or weakly bounded [55]. The distribution of these transitions is different between the two conformational families. The frequencies in A and B are comparable in position although those of B are more intense, but they differ completely of the transition in C and D.

In addition to the complementary information that these spectra bring for the structural assignment, they are useful for the population transfer experiments allowing us to try IR-induced conformational isomerization at lower energies and thus bracket better the energy threshold to isomerization.

4.2.3 Results of spectroscopic studies of Ac-Phe-(Ala)$_3$-(Gly)$_4$-(Ala)$_3$-Lys-H$^+$

We modified the 12-residue peptide, Ac-Phe-(Ala)$_{10}$-Lys-H$^+$, already reported to have a helical shape [49, 50, 56], by substituting four alanines by four glycines, an amino acid that has a low helix-forming propensity [47, 56] in order to tune the stability of helical structure to the point where helical and non-helical conformers might have similar stability. Our goal in doing this was to find cases in which we could cause unfolding transitions subsequent to IR excitation. The initial conformational searches on this molecule using the AMBER force field [27] within the MacroModel [28] program gives an initial collection of both folded and unfolded conformers with similar energies under 50 kJ/mol.

Figure 4.11 depicts the electronic spectrum of this molecule recorded by monitoring the fragment *m/z* 858 as a function of wavenumber in the region between 37450 and 37700 cm^{-1}. The UV spectrum shows well resolved bands with major peaks at 37536 cm^{-1} and 37574 cm^{-1}. There also seems to be a Franck–Condon progression in a 9.5 cm^{-1} vibrational mode built upon the first major peak.
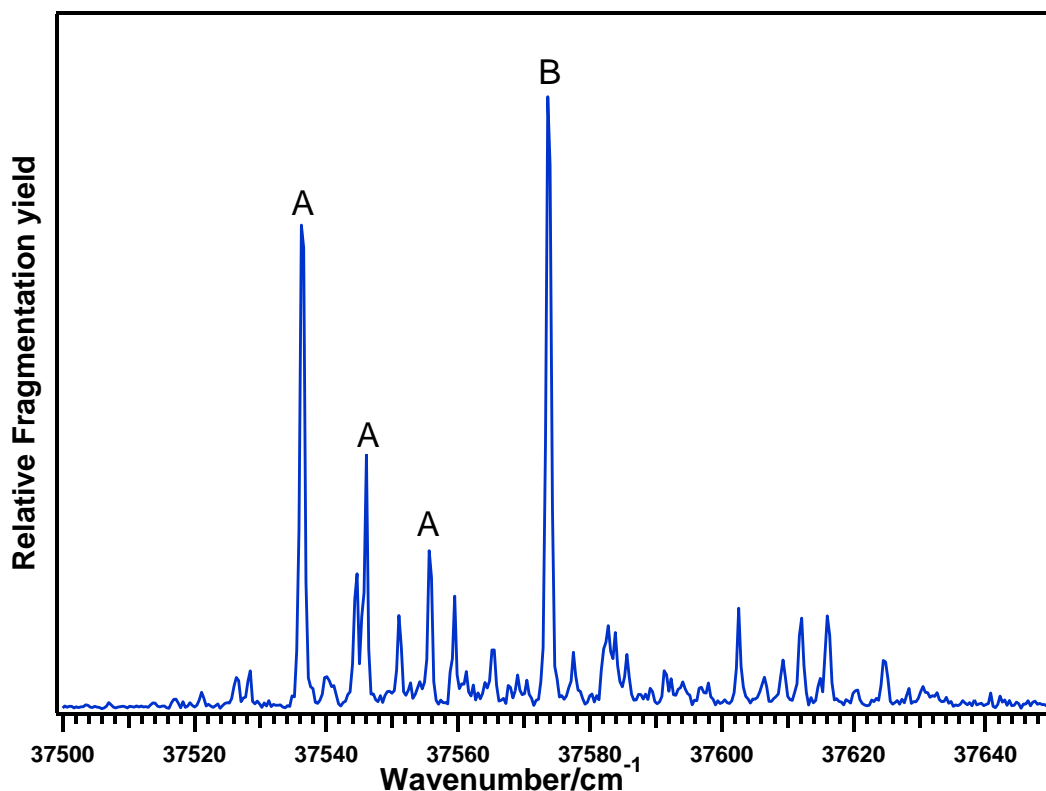
Figure 4.11: Electronic spectrum of Ac-Phe-$(Ala)_3$-$(Gly)_4$-$(Ala)_3$-Lys-H^+ recorded monitoring the photofragment m/z 858. The transitions are labeled by conformation, as determined by IR-UV double-resonance spectroscopy.

By setting the UV laser on different transitions we get the same photofragment mass spectrum shown, in Figure 4.12. The transitions in the UV spectrum were labeled based on the IR-UV double resonance spectroscopy recorded using each band. Only two different vibrational spectra were observed, suggesting the existence of two distinct conformers, labeled A and B.
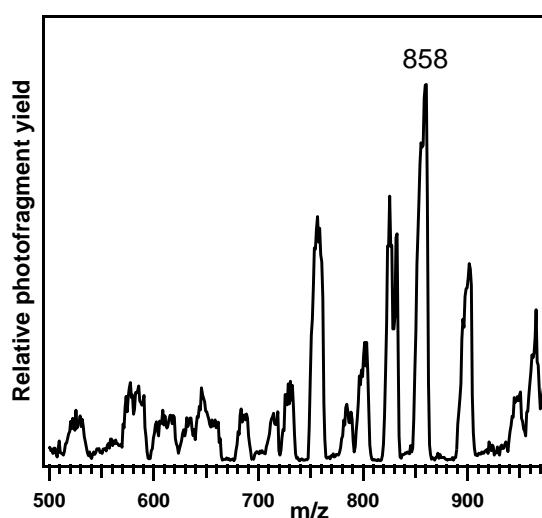
Figure 4.12: Photofragment mass spectrum of Ac-Phe-$(Ala)_3$-$(Gly)_4$-$(Ala)_3$-Lys-H^+.

Figure 4.13 shows two infrared spectra of Ac-Phe-(Ala)$_3$-(Gly)$_4$-(Ala)$_3$-Lys-H$^+$ measured in the NH and OH stretch region. The red trace is associated with the UV transition labeled A and the blue with B. The spectra show at least 9 of the 12 amide N-H that are sufficiently resolved. Most of the activity in these spectra is concentrated in the region below 3380 cm^{-1}, where vibrations are associated N-H groups in strong hydrogen bonds. The transitions above 3380 cm^{-1} are narrower and characteristic of free or weakly interacting N-H bonds. In these two spectra the carboxylic acid OH stretch occurs as a sharp peak around 3575 cm^{-1}, its position is similar to the free OH stretch observed in conformers of protonated peptides previously reported [49, 50, 57]. The fact that the OH group is not hydrogen-bonded is already evidence that the two conformations of this molecule may be helical, because the rigid structure of the helix would prevent the C-terminus from wrapping around to form any hydrogen bonds. One would expect that in a globular structure, the carboxylic OH may be hydrogen-bonded, which would shift the corresponding band to lower wavenumber. The observation of the free OH transition in both conformations suggests that both of the observed conformers may be helical.
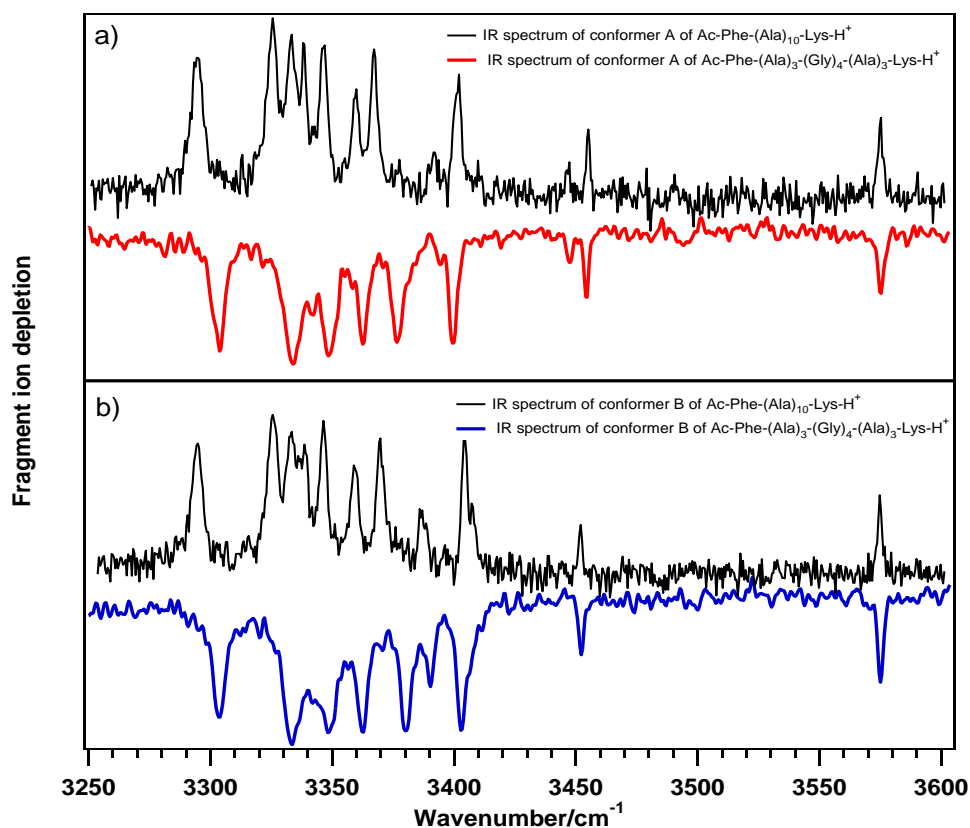
Figure 4.13: IR-UV double resonance spectra of Ac-Phe-(Ala)$_3$-(Gly)$_4$-(Ala)$_3$-Lys-H$^+$ recorded at the labeled UV transitions A (red trace) and B (blue trace) in the UV spectrum. The black traces correspond to the IR spectra of conformer B (a) and A (b), respectively, of Ac-Phe-(Ala)10-Lys-H$^+$ [49, 50].

Since our computational capabilities are limited for large molecules, we based our structural identification for this molecule on the comparison with the infrared spectra of the 12 residue peptide Ac-Phe-(Ala)$_{10}$-Lys-H$^+$, which is almost certainly helical. In

Figure 4.13, above the IR spectra of Ac-Phe-(Ala)$_3$-(Gly)$_4$-(Ala)$_3$-Lys-H$^+$, the black traces in a and b, correspond to the IR-dip spectra of conformer A and B, respectively, of Ac-Phe-(Ala)$_{10}$-Lys-H$^+$ reported by Stearns *et al.* [49, 50]. As with Ac-Phe-(Ala)$_{10}$-Lys-H$^+$ and conformers C and D of Ac-Phe-(Ala)$_5$-Lys-H$^+$, the intense transitions that appear between 3320 and 3350 cm^{-1} could be assigned to the internal N-H groups of an α-helix, and they are in very similar environments with C$_{13}$ hydrogen-bonded rings. The intense N-H stretch near 3300 cm^{-1} may well be attributed to the second alanine in a C$_{10}$ arrangement. The similarity between the spectra of the two molecules as shown in Figure 4.13, lead us to suggest a helical shape for the glycine containing peptide.

Some other structural clues may also be inferred from the position of the C=O stretches vibrations of this molecule. The IR spectra of conformers A and B of Ac-Phe-(Ala)$_3$-(Gly)$_4$-(Ala)$_3$-Lys-H$^+$ in the amide I and II region are illustrated in Figure 4.14.
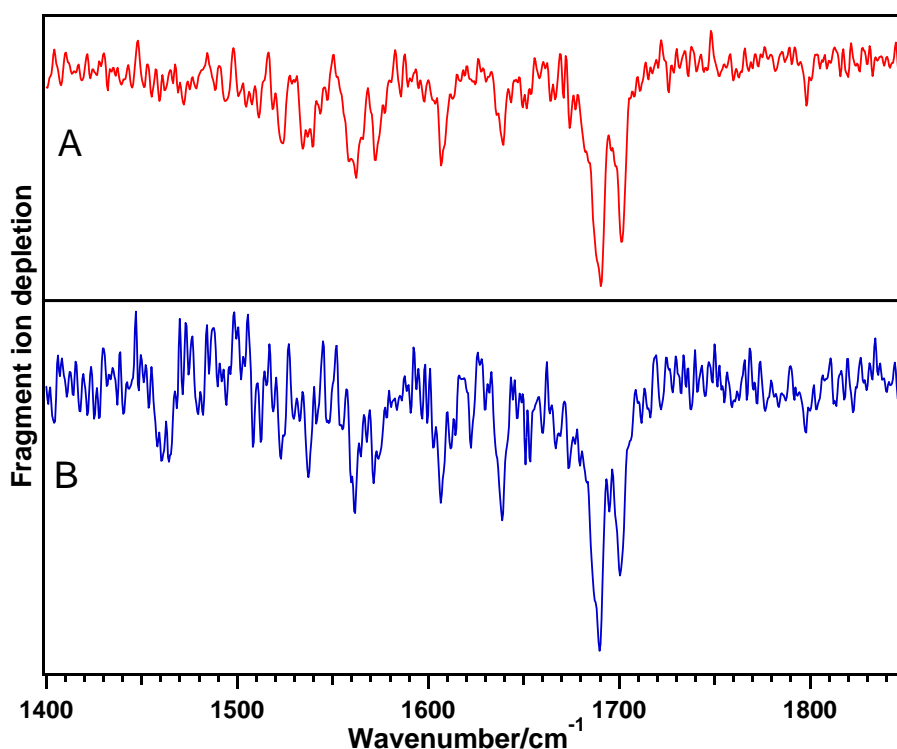
Figure 4.14: IR-UV double resonance spectra of Ac-Phe-(Ala)$_3$-(Gly)$_4$-(Ala)$_3$-Lys-H$^+$, in the amide I and II region, recorded at the labeled UV transitions A (red trace) and B (blue trace) in the UV spectrum.

In the amide I region, the resonances that appear at 1690 and 1700cm^{-1} in both spectra, are assigned to weakly hydrogen-bond C=O stretching vibrations, and the band below

1655 cm^{-1} to a strong hydrogen-bond shifted C=O stretching vibration. The C=O stretch of the carboxylic group appears as a small band at 1798 cm^{-1}. The position of these transitions is close to what we observed previously in the case of conformer C and D of the Ac-Phe-(Ala)$_5$-Lys-H$^+$. Moreover the common bands at 1608 and 1639 cm^{-1} are almost inexistent in the spectra of conformation A and B of Ac-Phe-(Ala)$_5$-Lys-H$^+$ which has a C$_{10}$-C$_{10}$-C$_{10}$-C$_{13}$ hydrogen-bonding pattern. The similarity between the two spectra of Ac-Phe-(Ala)$_3$-(Gly)$_4$-(Ala)$_3$-Lys-H$^+$ and the spectra of conformer C and D of the Ac-Phe-(Ala)$_5$-Lys-H$^+$ in the amide I region suggests similar hydrogen-boding pattern. In the case of A and B (Figure 4.14), the N-H bending vibrations appear in the interval between 1500 and 1570 cm^{-1} where the lowest bands reveal the existence of free N-H and the blue shifted the bound N-H [55]. This confirms the existence of free and bound NH depicted in the amide A region. Unfortunately in the case of the 7-residue peptide, the amide II bands are not well resolved and thus exclude any possible comparison.

No significant differences were observed between the IR spectra depicted in Figure 4.14, implying that the lowest energy structures in the glycine-containing peptide adopt similar conformational shapes. The substitution of four alanines with four glycines does not seem to be enough to destabilize the helical structure. From the comparison with the spectra of some previously assigned helical peptides, we can exclude a globular conformation. The IR spectra in the amide II and amide A regions show some common transitions in the spectra of conformers C and D of Ac-Phe-(Ala)$_5$-Lys-H$^+$ suggesting a helical shape to this molecule.

4.2.4 Conclusion

We have presented conformer specific IR spectra of 7- and 12-residue peptides, which demonstrate the power of our IR-UV double resonance technique to investigate large molecules. The reported spectra cover the spectral region of the N-H and O-H stretches as well as the amide I and II bands, both of which help to define the structural assignments for these molecules. The IR spectra of the seven amino acid peptides reveal the existence of two conformational families that differ from each other by the hydrogen-bonding pattern of the backbone. Within the same family, the conformations have a different orientation of the phenylalanine side chain. The conformational structures were predicted by comparison with DFT calculations with the help of isotopic substitution studies. However our computational power was insufficient to do calculations on the larger peptide. Assignments were thus

suggested by the comparison with previously reported spectra of helical peptides [49, 50]. Based on the common transitions in the C=O, N-H and O-H stretches regions that were observed in the spectra of the minor conformation of Ac-Phe-(Ala)$_5$-Lys-H$^+$ and the spectra of the large peptide we could suggest that both conformations of the glycine containing peptide adopt a helical shape where the N-H groups in the center of the helix are involved in C$_{13}$ interactions. These data provide a benchmark for improving the computations of peptide structure and protein folding. Moreover, they provide the spectroscopic assignments needed for population transfer experiments to be presented in *Chapter 5* of this thesis.

References

1.   T. R. Rizzo, Y. D. Park, D. H. Levy, *J. Am. Chem. Soc.* **107**, 277 **1985**.
2.   T. R. Rizzo, Y. D. Park, D. H. Levy, *Phys. Chem. Chem. Phys.* **85**, 6945 **1986**.
3.   L. C. Snoek, R. T. Kroemer, M. R. Hockridge, J. P. Simons, *PCCP* **3**, 1819 **2001**.
4.   F. Piuzzi, I. Dimicoli, M. Mons, B. Tardivel, Q. Zhao, *Chem. Phys. Lett.* **320**, 282 **2000**.
5.   J. M. Bakker, L. M. Aleese, G. Meijer, G. von Helden, *Phys. Rev. Lett.* **91**, 203003 **2003**.
6.   S. J. Martinez, J. C. Alfano, D. H. Levy, *J. Mol. Spectrosc.* **156**, 421 **1992**.
7.   R. Cohen, B. Brauer, E. Nir, L. Grace, M. S. de Vries, *J. Phys. Chem. A* **104**, 6351 **2000**.
8.   L. I. Grace, R. Cohen, T. M. Dunn, D. M. Lubman, M. S. de Vries, *J. Mol. Spectrosc.* **215**, 204 **2002**.
9.   Y. Inokuchi, Y. Kobayashi, T. Ito, T. Ebata, *J. Phys. Chem. A* **111**, 3209 **2007**.
10.   L. C. Snoek, E. G. Robertson, R. T. Kroemer, J. P. Simons, *Chem. Phys. Lett.* **321**, 49 **2000**.
11.   Y. Lee, J. Jung, B. Kim, P. Butz, L. C. Snoek, R. T. Kroemer, J. P. Simons, *J. Phys. Chem. A* **108**, 69 **2003**.
12.   T. Hashimoto, Y. Takasu, Y. Yamada, T. Ebata, *Chem. Phys. Lett.* **421**, 227 **2006**.
13.   G. v. Helden, I. Compagnon, M. N. Blom, M. Frankowski, U. Erlekam, J. Oomens, B. Brauer, R. B. Gerber, G. Meijer, *PCCP* **10**, 1248 **2008**.
14.   F. O. Talbot, T. Tabarin, R. Antoine, M. Broyer, P. Dugourd, *Phys. Chem. Chem. Phys.* **122**, 074310 **2005**.
15.   O. V. Boyarkin, S. R. Mercier, A. Kamariotis, T. R. Rizzo, *J. Am. Chem. Soc.* **128**, 2816 **2006**.
16.   S. Mercier, Ph.D Thesis, EPFL **2008**.
17.   D. Nolting, C. Marian, R. Weinkauf, *PCCP* **6**, 2633 **2004**.
18.   T. R. Rizzo, Y. D. Park, L. Peteanu, D. H. Levy, *Phys. Chem. Chem. Phys.* **83**, 4819 **1985**.
19.   J. A. Stearns, S. Mercier, C. Seaiby, M. Guidi, O. V. Boyarkin, T. R. Rizzo, *J. Am. Chem. Soc.* **129**, 11814 **2007**.

20. H. Kang, C. Dedonder-Lardeux, C. Jouvet, S. Martrenchard, G. Gregoire, C. Desfrancois, J. P. Schermann, M. Barat, J. A. Fayeton, *PCCP* **6**, 2628 **2004**.

21. H. Kang, C. Jouvet, C. Dedonder-Lardeux, S. Martrenchard, G. Gregoire, C. Desfrancois, J. P. Schermann, M. Barat, J. A. Fayeton, *PCCP* **7**, 394 **2005**.

22. H. Kang, C. Jouvet, C. Dedonder-Lardeux, S. Martrenchard, C. Charriere, G. Gregoire, C. Desfrancois, J. P. Schermann, M. Barat, J. A. Fayeton, *Phys. Chem. Chem. Phys.* **122**, 084307 **2005**.

23. G. Grégoire, C. Jouvet, C. Dedonder, A. L. Sobolewski, *J. Am. Chem. Soc.* **129**, 6223 **2007**.

24. S. R. Mercier, O. V. Boyarkin, A. Kamariotis, M. Guglielmi, I. Tavernelli, M. Cascella, U. Rothlisberger, T. R. Rizzo, *J. Am. Chem. Soc.* **128**, 16938 **2006**.

25. H. El Aribi, G. Orlova, A. C. Hopkinson, K. W. M. Siu, *J. Phys. Chem. A* **108**, 3844 **2004**.

26. B. Lucas, M. Barat, J. A. Fayeton, M. Perot, C. Jouvet, G. Gregoire, S. B. Nielsen, *Phys. Chem. Chem. Phys.* **128**, 164302 **2008**.

27. W. D. Cornell, P. Cieplak, C. I. Bayly, I. R. Gould, n. Jr, D. M. Ferguson, D. C. Spellmeyer, T. Fox, J. W. Caldwell, P. A. Kollman, *J. Am. Chem. Soc.* **117**, 5179 **1995**.

28. . (vesion 9.1; Schrödinger LLC:New York 2005).

29. G. W. T. M. J. Frisch, H. B. Schlegel, G. E. Scuseria, M. A. Robb, J. R. Cheeseman, J. J. A. Montgomery, T. Vreven, K. N. Kudin, J. C. Burant, J. M. Millam, S. S. Iyengar, J. Tomasi, V. Barone, B. Mennucci, M. Cossi, G. Scalmani, N. Rega, G. A. Petersson, H. Nakatsuji, M. Hada, M. Ehara, K. Toyota, R. Fukuda, J. Hasegawa, M. Ishida, T. Nakajima, Y. Honda, O. Kitao, H. Nakai, M. Klene, X. Li, J. E. Knox, H. P. Hratchian, J. B. Cross, V. Bakken, C. Adamo, J. Jaramillo, R. Gomperts, R. E. Stratmann, O. Yazyev, A. J. Austin, R. Cammi, C. Pomelli, J. W. Ochterski, P. Y. Ayala, K. Morokuma, G. A. Voth, P. Salvador, J. J. Dannenberg, V. G. Zakrzewski, S. Dapprich, A. D. Daniels, M. C. Strain, O. Farkas, D. K. Malick, A. D. Rabuck, K. Raghavachari, J. B. Foresman, J. V. Ortiz, Q. Cui, A. G. Baboul, S. Clifford, J. Cioslowski, B. B. Stefanov, G. Liu, A. Liashenko, P. Piskorz, I. Komaromi, R. L. Martin, D. J. Fox, T. Keith, M. A. Al-Laham, C. Y. Peng, A. Nanayakkara, M. Challacombe, P. M. W. Gill, B. Johnson, W. Chen, M. W. Wong, C. Gonzalez, and J. A. Pople,. (Gaussian, Inc.: Pittsburgh, PA, 2003).

30. J. B. Hopkins, D. E. Powers, R. E. Smalley, *J. Chem. Phys.* **72**, 5039 **1980**.

31. Y. Lee, J. Jung, B. Kim, P. Butz, L. C. Snoek, R. T. Kroemer, J. P. Simons, *J. Phys. Chem. A* **108**, 69 **2004**.

32. D. F. Sticke, L. G. Presta, K. A. Dill, G. D. Rose, *J. Mol. Biol.* **226**, 1143 **1992**.

33. L. Pauling, R. B. Corey, H. R. Branson, *Proc. Nat. Acad. Sci. U.S.A.* **37**, 205 **1951**.

34. J. Oomens, N. Polfer, D. T. Moore, L. van der Meer, A. G. Marshall, J. R. Eyler, G. Meijer, G. von Helden, *PCCP* **7**, 1345 **2005**.

35. W. Chin, F. Piuzzi, J.-P. Dognon, I. Dimicoli, B. Tardivel, M. Mons, *J. Am. Chem. Soc.* **127**, 11900 **2005**.

36. W. Chin, I. Compagnon, J.-P. Dognon, C. Canuel, F. Piuzzi, I. Dimicoli, G. von Helden, G. Meijer, M. Mons, *J. Am. Chem. Soc.* **127**, 1388 **2005**.

37. W. Chin, J.-P. Dognon, F. Piuzzi, B. Tardivel, I. Dimicoli, M. Mons, *J. Am. Chem. Soc.* **127**, 707 **2004**.

38. W. Chin, F. Piuzzi, I. Dimicoli, M. Mons, *PCCP* **8**, 1033 **2006**.

39. V. Brenner, F. Piuzzi, I. Dimicoli, B. Tardivel, M. Mons, *J. Phys. Chem. A* **111**, 7347 **2007**.

40. E. Gloaguen, R. Pollet, F. Piuzzi, B. Tardivel, M. Mons, *PCCP* **11**, 11385 **2009**.

41.   A. Abo-Riziq, J. E. Bushnell, B. Crews, M. Callahan, L. Grace, M. S. de Vries, *Chem. Phys. Lett.* **431**, 227 **2006**.
42.   A. Abo-Riziq, B. O. Crews, M. P. Callahan, L. Grace, M. S. d. Vries, *Angew. Chem. Int. Ed.* **45**, 5166 **2006**.
43.   E. S. Baker, M. T. Bowers, *J. Am. Soc. Mass. Spectrom* **18**, 1188 **2007**.
44.   S. L. Bernstein, N. F. Dupuis, N. D. Lazo, T. Wyttenbach, M. M. Condron, G. Bitan, D. B. Teplow, J.-E. Shea, B. T. Ruotolo, C. V. Robinson, M. T. Bowers, *Nat Chem* **1**, 326 **2009**.
45.   R. R. Hudgins, M. F. Jarrold, *J. Am. Chem. Soc.* **121**, 3494 **1999**.
46.   M. Kohtani, T. C. Jones, J. E. Schneider, M. F. Jarrold, *J. Am. Chem. Soc.* **126**, 7420 **2004**.
47.   M. F. Jarrold, *PCCP* **9**, 1659 **2007**.
48.   T. D. Vaden, T. S. J. A. de Boer, J. P. Simons, L. C. Snoek, S. n. Suhai, B. l. Paizs, *J. Phys. Chem. A* **112**, 4608 **2008**.
49.   J. A. Stearns, O. V. Boyarkin, T. R. Rizzo, *J. Am. Chem. Soc.* **129**, 13820 **2007**.
50.   J. A. Stearns, C. Seaiby, O. V. Boyarkin, T. R. Rizzo, *PCCP* **11**, 125 **2009**.
51.   J. A. Stearns, O. V. Boyarkin, T. R. Rizzo, *CHIMIA* **62**, 240 **2008**.
52.   R. Bossart, O. V. Boyarkin, A. A. Makarov, T. R. Rizzo, *Phys. Chem. Chem. Phys.* **126**, 054302 **2007**.
53.   C. Seaiby, A. Svendsen, O. V. Boyarkin, T. R. Rizzo, *in preparation*
54.   D. Řeha, H. Valdés, J. Vondrášek, P. Hobza, A. Abu-Riziq, B. Crews, M. S. de Vries, *Chemistry – A European Journal* **11**, 6803 **2005**.
55.   J. M. Bakker, C. Plützer, I. Hünig, T. Häber, I. Compagnon, G. v. Helden, G. Meijer, K. Kleinermanns, *ChemPhysChem* **6**, 120 **2005**.
56.   C. Nick Pace, J. Martin Scholtz, *Biophys. J.* **75**, 422 **1998**.
57.   M. Guidi, Ph.D Thesis, EPFL **2010**.

Chapter 5

Hole-filling spectroscopy

5.1 Introduction

One of the goals of this thesis work is to investigate the barriers separating stable conformations of biological molecules using population transfer experiments in which one selectively excites a single conformation of a cold ion species in a 22-pole ion trap. Exploring the interconnectivity of different conformational families will provide insight into the dynamics of biomolecules and the topology of their energy landscapes. Such a fundamental understanding of the dynamics of biological process such as protein folding/unfolding may shed light on the physiological activity of these molecules, which in turn may advance the treatment of human diseases [1].

Different condensed phase experimental studies have made great advances toward this goal. Numerous techniques had been implemented to probe the progress of the folding process by monitoring the evolution of secondary and tertiary structure. X-ray crystallography was the first and perhaps most powerful technique elucidate the geometries of large biomolecular at an atomic scale [2-6]. Multidimensional nuclear magnetic resonance (NMR) has also proven to be a powerful approach in the detection of the solution structures of large proteins and in probing their dynamical behavior [7-12]. Incorporating NMR-derived data into protein structure prediction serves to guide conformational searches toward the lowest-energy conformations in the folding landscape. In addition to the above-mentioned techniques, several other experimental strategies can provide structural information on biomolecules such as Fourier transform infrared spectroscopy (FTIR) [13], circular dichroism (CD) [14-18] a number of fluorescence techniques [19-22] and the multidimensional IR spectroscopy [23-27]. Different approaches have been established to initiate folding in order

to follow the kinetics of the folding pathways, including the conventional stopped flow [28], and laser-induced temperature jump [29-31]. This later method, which was first used by Eigen and De Maeyer [32] involves rapidly increasing the temperature after equilibrium has been established between folded and unfolded forms, which displaces the equilibrium toward one of the two forms.

While condensed phase studies are closer to physiological conditions, isolating the molecules in the gas phase and cooling them to low temperature allows the spectroscopic study of peptide structures without any effects due to the solvent and hence the investigation of their intrinsic properties: in particular their potential energy landscape and their conformational dynamics. Zwier and coworker pioneered this approach by looking at the transfer of population between conformers of small biomolecules in the gas phase after the deposition of energy by vibrational excitation, either directly in the infrared [33-35] or by stimulated emission pumping [36-40].

Following this pioneering work, we have performed gas-phase population transfer experiments on significantly larger protonated peptides. Before investigating the dynamics of conformational isomerization one must first identify the different accessible conformational minima. Toward this aim, we have measured UV and conformer specific IR-UV double resonance spectra for the three systems that form the core of this thesis work. *Chapter 4* presented the IR spectra the in regions between 3000–3600 cm^{-1} and 1400-2000 cm^{-1}. This wide range of energy that covers OH and NH stretch vibrations as well as the Amide I and II bands allow multiple choices for infrared-induced conformational isomerization. On the basis of the infrared spectra and density functional theory calculations, we determined there are two conformations of protonated phenylalanine present in our experiment, which are stabilized by hydrogen bonding between the charged NH_3 group and the aromatic ring and carbonyl oxygen [41]. Conformation-specific IR-UV double resonance spectroscopy, together with nitrogen-15 isotopic substitution, allow us to identify four conformers of the peptide Ac-Phe-$(Ala)_5$-Lys-H^+, which were classified into two families based on their helical geometries [42]. The infrared spectra of the twelve amino acid peptide Ac-Phe-$(Ala)_3$-$(Gly)_4$-$(Ala)_3$-Lys-H^+ reveal the existence of two stable conformations in the cold ion trap.

Having identified different conformers, we then performed population transfer experiments using IR excitation of the amide A (NH stretch) and the Amide I (CO stretch) vibrations. In the first part of this chapter, we present results on the isomerization of the

amino acid phenylalanine. This is followed by the first hole-filling spectroscopic studies reported on gas-phase protonated peptides, where we investigate the 7-residue helical peptide Ac-Phe-(Ala)$_5$-Lys-H$^+$ after IR excitation of the N-H and C=O stretch vibrations. We then present hole filling studies on Ac-Phe-(Ala)$_3$-(Gly)$_4$-(Ala)$_3$-Lys-H$^+$, a glycine containing peptide, after an IR excitation in the N-H stretch region. The last part of this chapter describes an experiment designed to populate new conformations using a UV-UV pump-cool-probe scheme.

5.2 Infrared Hole-filling spectroscopy in a cold ion trap

As described in detail in *Chapter 3*, we produce biomolecular ions in the gas phase *via* nanoelectrospray, collect them in an RF-only hexapole ion trap, and then transfer an ion packet to a 22-pole cooled ion trap, where the molecule ions have sufficient time to cool via collisions with cold helium. An IR laser pulse, which is tuned to a transition of a single conformer, pumps energy into the molecule. After re-cooling the excited molecules by collisions with remaining helium, the UV laser then interrogates the electronic spectrum and hence monitors the new conformer population, noting in particular the change in intensities of peaks corresponding to different conformers.

5.2.1 Infrared hole-filling spectroscopy of a single amino acid

The protonated form of the amino acid phenylalanine was the test molecule to start performing the population transfer experiments in our laboratory. It is close to the size of molecules studied by the Zwier group, and we had already demonstrated the existence of two stable conformations that differ in the orientation of the backbone with respect to the ring. Comparison of our experiments with calculation suggest that the *gauche* structure is 3.2 kJ/mol higher in energy than the structure *anti* structure, which corresponds to the global minimum [41] (*see Section 4.1.2*). The cool-pump-recool-probe principle of the hole-filling experiment remains the same as that described by Zwier [33]. Shortly after the ions arrive in the trap we pulse an IR pump laser, which is fixed at a specific wavenumber that excites a vibrational band of a single conformation. We then leave the ions enough time to recool to their zero-point energy level *via* collisions with the He buffer gas, before firing a UV probe laser that photodissociates the parent ions. The wavenumber of the UV laser is scanned,

generating an electronic spectrum that reveals the conformational composition of the ions after the heating and reecoling cycle.
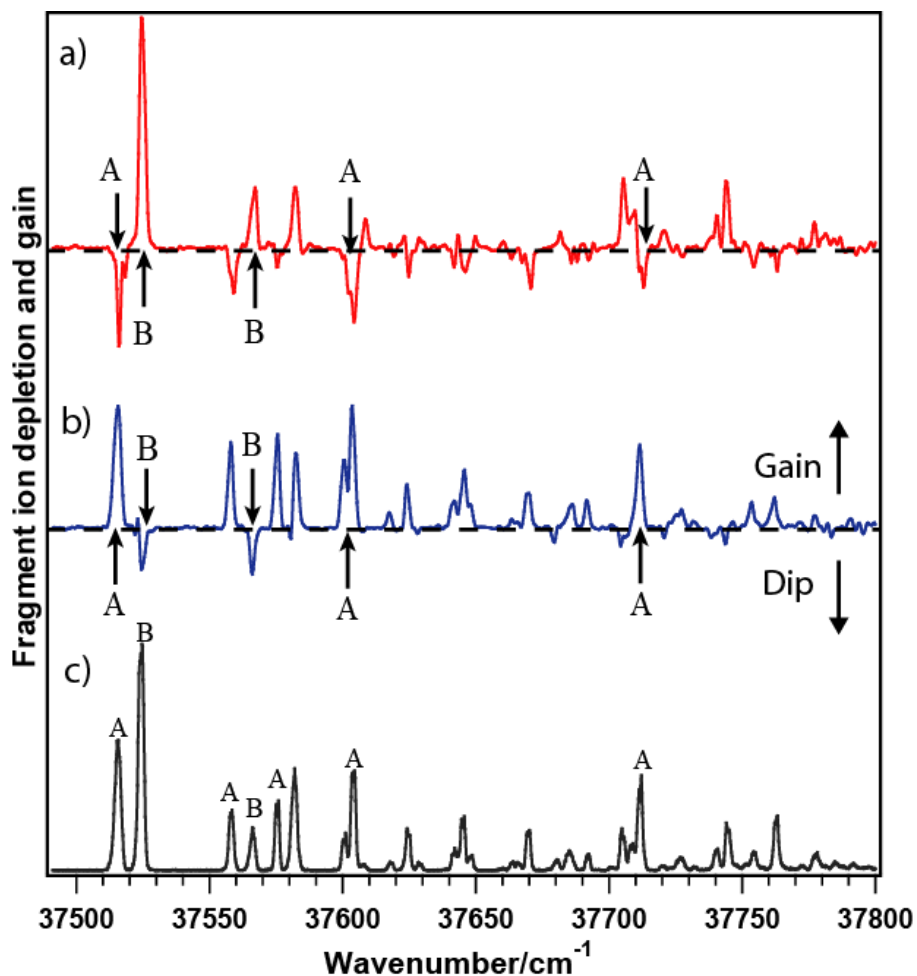
Figure 5.1: Hole-filling spectra of protonated phenylalanine measured with the infrared laser fixed on a) the N-H stretch transition of conformer A at 3122 cm^{-1}, b) the N-H stretch transition of conformer B at 3079 cm^{-1}. The black trace c) corresponds to the ultraviolet photofragmentation spectrum of PheH$^+$.

Figure 5.1 shows the resulting spectra from the difference of photodissociation signal with the IR laser off and on, which we call an IR hole-filling spectrum. The red trace in Figure 5.1a shows the first 260 cm^{-1} of this spectrum with the IR laser fixed at the N-H transition of conformation A at 3122 cm^{-1}. The blue trace in Figure 5.1b represents the first part of the IR hole-filling spectrum while pumping the N-H transition of conformer B at 3079 cm^{-1}. The black trace corresponds to the ultraviolet photofragmentation spectrum of PheH$^+$, showing the major peaks that correspond to the two different conformers. As one can see, IR excitation of conformer A leads to depletion of its population which produces a dips in the photofragmentation signal at the transitions belonging to conformer A. At the same time, this loss in population, of conformer A manifests itself as gains in the photodissociation signal of

the transitions where conformer B absorbs. Likewise, selectively exciting a transition in conformer B drives population out of conformer B into conformer A.

These spectra clearly demonstrate the feasibility of the IR-UV population transfer experiment under our experimental conditions: ions in a cold ion trap and using photofragmentation as a detection method. The population transfer experiment reported by Dian *et al.* was applied to molecules in a molecular beam having significantly higher density and higher helium pressure, and used fluorescence detection [33]. Figure 5.1 shows that an infrared excitation that selectively interacts with a single conformation is able to create a new conformational population distribution in the trap. It is important to note that we create this new distribution among the conformations already having population in them (i.e., those that already appear in the spectrum), but seem not to populate any new conformational minima as no new peaks appear. Finally we can conclude that barrier to isomerization for the protonated phenylalanine is less than the photon energy we used to pump the selected conformation (3122 and 3079 cm^{-1} for respectively conformers A and B).

We tried to predict theoretically the transition state separating the two minima of PheH$^+$, for comparison with our experimental data. We used Gaussian03 [43] to generate a starting structure for a transition state optimization based upon the starting and the final geometries, which represent in our case the two conformational structures of the protonated phenylalanine linked by this transition state. Gaussian employs the method known as STQN [44] (*Synchronous Transit-Guided Quasi-Newton*), which does not require a guess for the transition structure; instead, only the starting and ending conformational structures are taken as input. Re-optimization of the energy of the generated transition state structure and calculation of its harmonic vibrational frequencies were carried out using B3LYP/6-31++G** level of theory. The final predicted energy of this structure, shown in Figure 5.2, is approximately 12.1 kJ/mol, yielding of about 8.9 kJ/mol energy barrier for conformer B to overcome in order to transfer into conformer A, and about 12.1 kJ/mol energy barrier transfer from conformer A into B. This energy difference, in part, corresponds to a displacement in the dihedral angle ($\chi_1 = 118°$) involving the backbone orientation, which is what we would expect for a transition state between these two conformers.
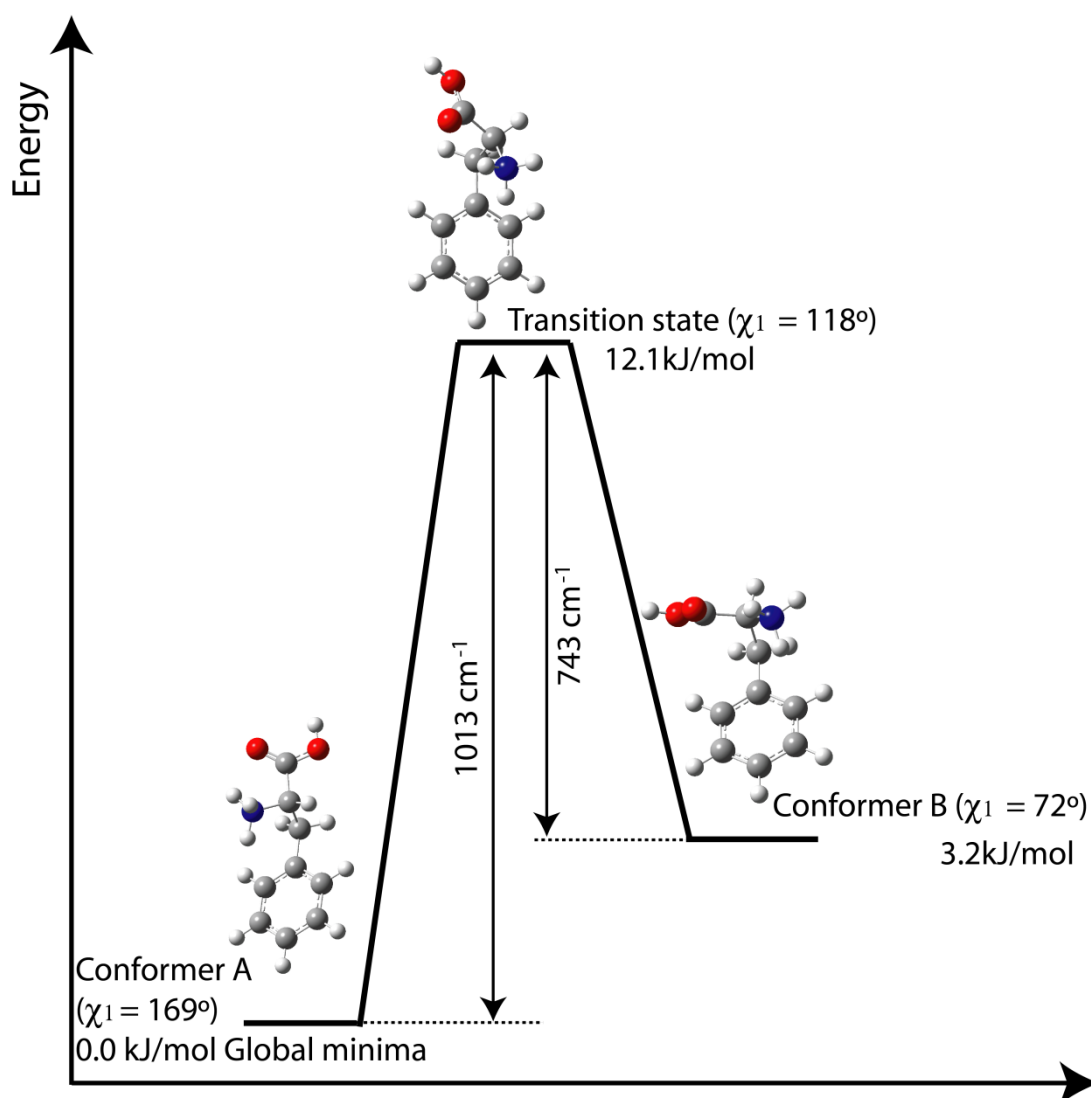
Figure 5.2: A one-dimensional energy level diagram of the protonated phenylalanine, representing the lowest energy conformations and the transition state structure. The transition state calculations were done at the B3LYP/6-31++G** level using the STQN method. The relative energies are zero-point energy corrected.

This simulation confirms our experimental observation that the energy photon used in the N-H stretch region is more than enough to cross the barrier to isomerization. Nevertheless, even with the excess energy available, the excited conformers did not isomerize to region of the conformational spaces that were not populated initially (i.e., in the absence of the IR). This is not particularly surprising, given the relative conformational simplicity of a single amino acid. Recent work by von Helden *et al.* reported simulations to characterize the potential energy surface of the neutral phenylalanine [45]. Most of their transition states are found to be less than 23.9 kJ/mol ($2000cm^{-1}$) above their lowest energy structure. Some of these transition states were also reported by Kaczor *et al.* [46].

Even though our IR excitation energy was significantly above the calculated barrier height for isomerization of protonated phenylalanine, we chose this molecule as a test of our method, since it has simple and well characterized UV and IR spectra. We now go on to apply the same techniques to peptides of considerably greater complexity.

5.2.2 Hole-filling spectroscopy of Ac-Phe-(Ala)$_5$-Lys-H$^+$

After the demonstration of the feasibility of the population transfer experiment in a cold ion trap, we extended these techniques to even larger systems. We reported in *chapter 4.2.2* the identification of four helical conformers of the peptide Ac-Phe-(Ala)$_5$-Lys-H$^+$, and through a combination of conformer specific IR spectroscopy and DFT calculations we sorted them in two families according to the hydrogen-bonding scheme of the peptide backbone [42]. Backbone family II constituted of conformers A and B have a C_{10}-C_{10}-C_{10}-C_{13} hydrogen bonding pattern, while backbone family I consists of conformers C and D which exhibit a C_{10}-C_{10}-C_{13}-C_{13} hydrogen bonding pattern. Within each conformational family the phenylalanine side chain can adopt two different positions by rotation around the C_α-C_β bond. These features make Ac-Phe-(Ala)$_5$-Lys-H$^+$ an interesting candidate to investigate its isomerization dynamics, since transferring population within the same family involves the rotation of the phenyl rings while isomerization between the two families requires breaking and reforming of C_{10} and C_{13} hydrogen bonded structures, which amounts to winding and unwinding of the helical backbone.

We begin the hole-filling experiments on this molecule by fixing the IR laser in the N-H stretch region on a transition associated with a particular conformer while scanning the UV laser over the electronic transition of different conformations. Figure 5.3 shows the hole-filling spectra of family II of Ac-Phe-(Ala)$_5$-Lys-H$^+$ pumping (a) the Phe[1] amide NH of conformation A at 3447 cm^{-1} and (b) the amide NH of Ala[5] and/or Ala[6] of conformation B at 3374 cm^{-1}. In the hole-filling spectrum of conformation A (Figure 5.3a), the UV transitions associated with this conformer appear as a depletion in the photodissociation signal whereas a clear gain signal is observed at the transition of conformer B at 37'560 cm^{-1}. Analogous results are obtained from the hole-filling spectrum of conformer B, Figure 5.3b. Its ground state population is partially depleted, producing dips in the vibronic transition associated with the pumped conformer and gains in the transitions belong to conformer A. These observations demonstrate the efficiency of IR induced population transfer within this same conformational family (backbone II). At the same time, both spectra show an increase of the population of

conformers C and D *via* the transitions at 37'526 and 37'556 cm^{-1} respectively, which signals a helical rearrangement, going from conformational family II to family I.
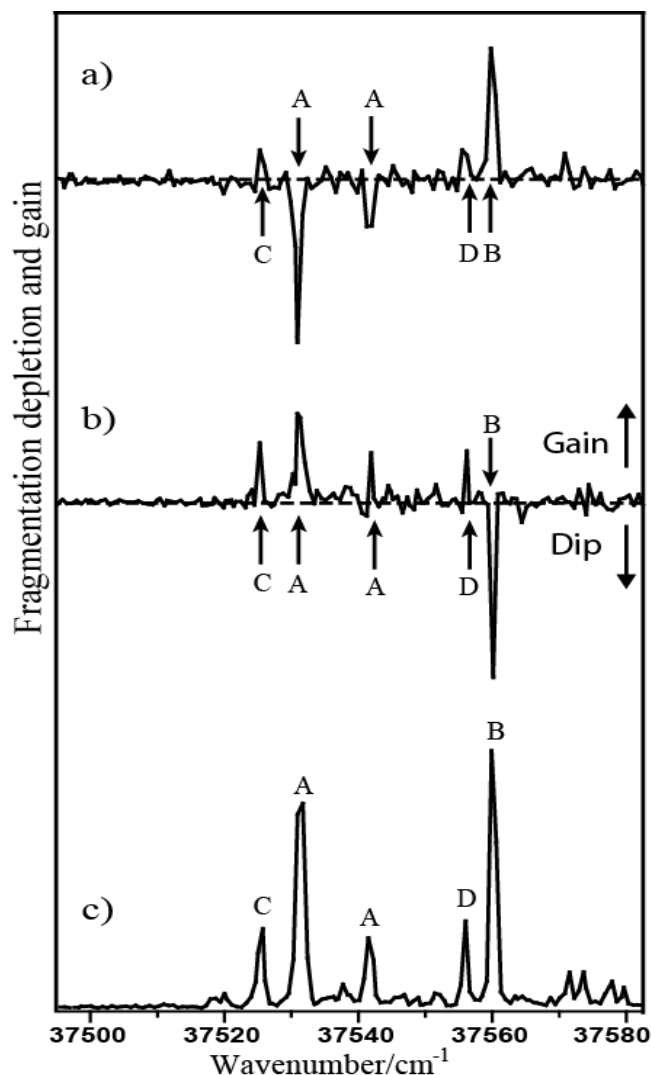
Figure 5.3: Hole-filling spectra for Ac-Phe-(Ala)$_5$-Lys-H$^+$. In (a) the IR laser is fixed to the Phe^1 amide NH stretch of conformer A at 3447 cm^{-1}, (b) the IR laser is fixed to the amide NH of Ala^5 or Ala^6 of conformer B at 3374 cm^{-1}. c) corresponds to the ultraviolet photofragmentation spectrum of Ac-Phe-(Ala)$_5$-Lys-H$^+$.

Figure 5.4 presents the hole-filling spectrum recorded by fixing the IR laser on a transition associated (a) with conformer C at 3444 cm^{-1} and (b) conformer D at 3442 cm^{-1} while scanning the UV laser. The depletion in the photofragmentation signal of the origin transition of conformer C, depicted in Figure 5.4a, is explained by the increase in population of the other conformations A, B and D. It is also obvious from the dip in the hole-filling spectrum of Figure 5.4b that the IR excitation removes population from the ground state of conformer D and, after the relaxation time, populates those of conformer A, B and C reflected by the gains in their photofragmentation signal.
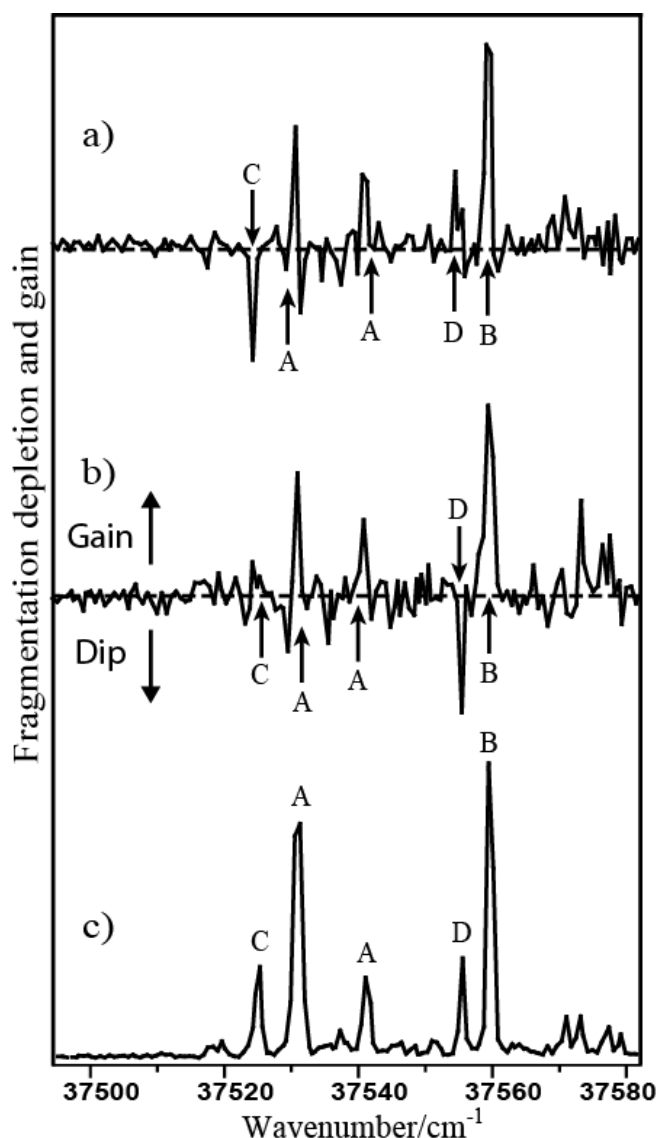
Figure 5.4: Hole-filling spectra for Ac-Phe-(Ala)$_5$-Lys-H$^+$. In (c) the IR laser is fixed to the Phe[1] amide NH stretch of conformer C at 3444 cm^{-1}, (b) the IR laser is fixed to the amide NH of Ala[2] of conformer D at 3442 cm^{-1}. c) corresponds to the ultraviolet photofragmentation spectrum of Ac-Phe-(Ala)$_5$-Lys-H$^+$.

An evident deduction from these four hole-filling spectra is the feasibility of the population transfer on relatively large molecule (i.e., a 7-residue peptide) under the conditions of our trapping experiment, which can open a new dimension to explore intramolecular bonding and isomerization dynamics. From these spectra we can conclude that with the photon energy used (about ~ 41.8 kJ/mol), the molecule can cross the barrier to isomerization and is cooled back to their lowest energy minima. Nevertheless, we did not observe any new transitions in these hole-filling spectra that would result from populating new minima (i.e., reaching stable conformations of the molecule that were not populated during the initial cooling process). The transfer within the same conformer family of Ac-Phe-(Ala)$_5$-Lys-H$^+$

involves the rotation of the phenylalanine side chain around the C_α–C_β bond from the *gauche+* (+60°) to the *gauche-* (-60°) position and conversely. At the same time, Ac-Phe-$(Ala)_5$-Lys-H^+ has two interacting families of conformers separated by an energy barrier lower than the IR excitation in the NH stretch region. The transfer from conformer A and B to C and D, respectively, requires the breaking of the hydrogen bond of the Ala^5 NH that participates in C_{10} interaction and the formation of a hydrogen bond, sharing the same carbonyl with Ala^6, thereby creating a C_{13} ring. Driving the population transfer in the opposite direction means replacing the C_{13} ring in the middle of the helix backbone I by a C_{10} ring. The schematic in Figure 5.5 illustrates the structures of the four conformers of Ac-Phe-$(Ala)_5$-Lys-H^+, with the phenyl ring rotation from *gauche-* (-60°) to *gauche+* (+60°) represented on the x-axis and the helical rearrangement along the y-axis.
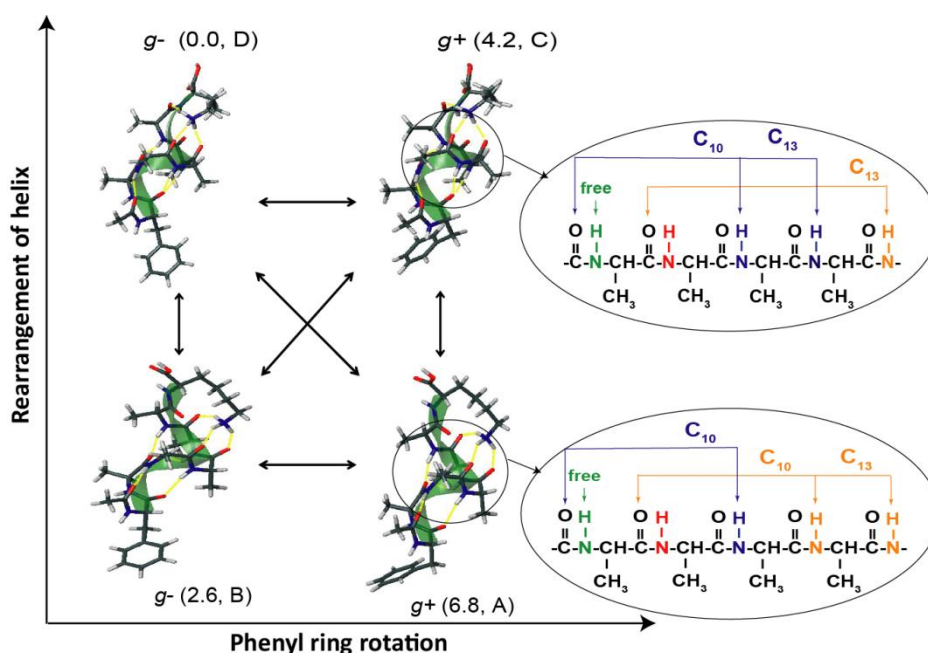
Figure 5.5: Schematic depictions of the structures of the four conformers of Ac-Phe-$(Ala)_5$-Lys-H^+. The x-axis represents the phenyl ring rotation from *gauche-* (-60°) to *gauche+* (+60°). The y-axis corresponds to the rearrangement of the helix. The hydrogen-bonding schemes of the involved region are represented on the right. The conformers are also labeled with their zero-point corrected energy in kJ/mol and their assignment (A, B, C, or D).

The diagonal transfer going form A and B to D and C, respectively, involves a rearrangement of the helix accompanied by phenyl ring rotation, the combination of which is likely to require higher energy to overcome the barrier. We have extended the wavelength range of our laser to cover the Amide I and II regions (1500-2000 cm^{-1}) in order to access a wider range of energies and better bracket our estimate for the barrier to conformational

isomerization. In the case of this 7 residue peptide, pumping the conformation with lower energy may be insufficient to overcome the barrier for a diagonal transfer.

The IR spectra of all four conformers of this molecule in the region of the CO stretch band, reported in *Chapter 4.2.2 and Figure 4.10*, show that the absorption bands are heavily overlapped making it impossible to selectively excite individual conformation in this region. We choose to record infrared spectra of an isotopically substituted Ac-Phe-(Ala)5-Lys-H+, illustrated in Figure 5.6, in which the carbon-12 of the acetyl carbonyl group was replaced by carbon-13.
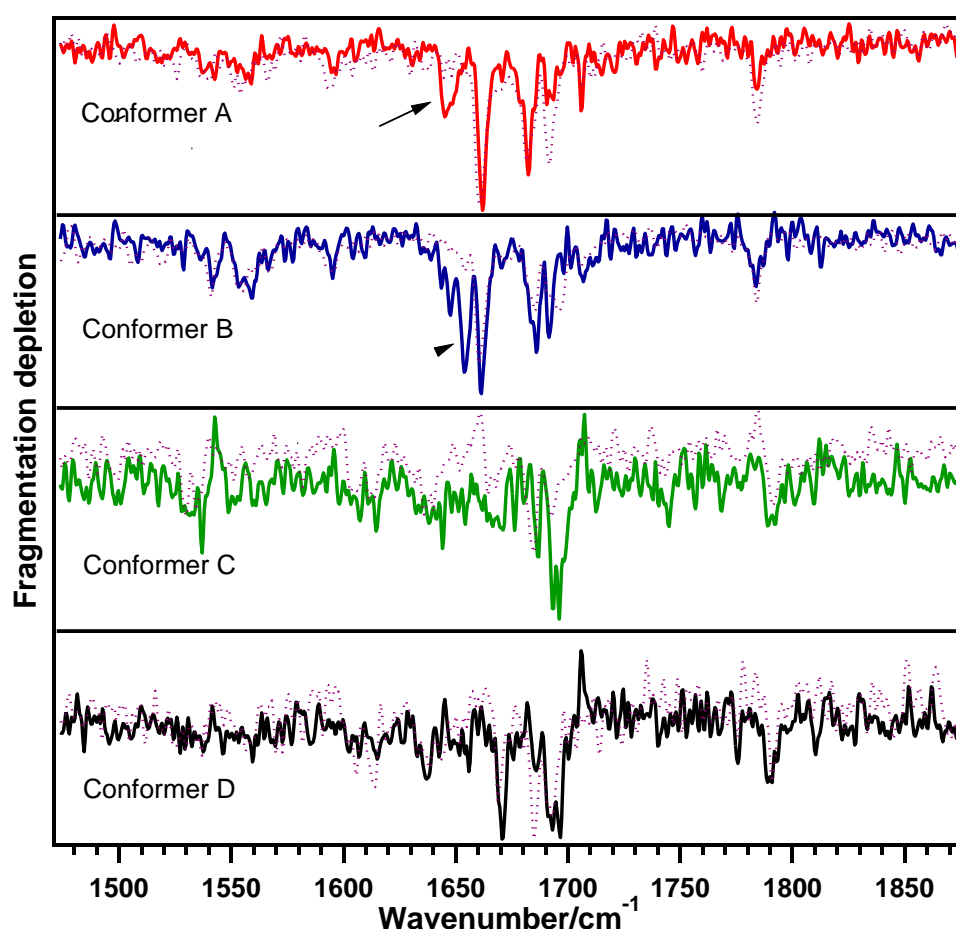
Figure 5.6: IR-UV double resonance spectra in the amide I and II region of Ac-Phe-$(Ala)_5$-Lys-H$^+$, isotopically substituted with C-13 at the carbonyl of the acetyl group, recorded at the UV origin transition of each conformations. The dashed curves correspond to the IR-UV double resonance spectra of unsubstituted Ac-Phe-$(Ala)_5$-Lys-H$^+$, reported here for a direct comparison.

In a simple diatomic model for the CO oscillator, the difference in reduced mass due to the heavier isotope would shift the carbonyl stretch frequency to lower energy by ~37 cm^{-1}. For the most part in each spectrum a single transition is shifted by ~37 cm^{-1}, and in the case of conformer A and B, this transition appears at 1645 and 1654 cm^{-1}, respectively. In the case of

conformer C and D it is not clear where the single shifted transition appears - it is probably overlapping another CO stretch band. Nevertheless, the shift due to carbon-13 substitution isolates a transition at 1654 cm^{-1} where only conformer B absorbs, and this, allows us to selectively excite this conformation. The hole-filling spectrum resulting from pumping conformer B at 1654 cm^{-1} in the infrared and scanning the UV probe beam is shown in Figure 5.7.
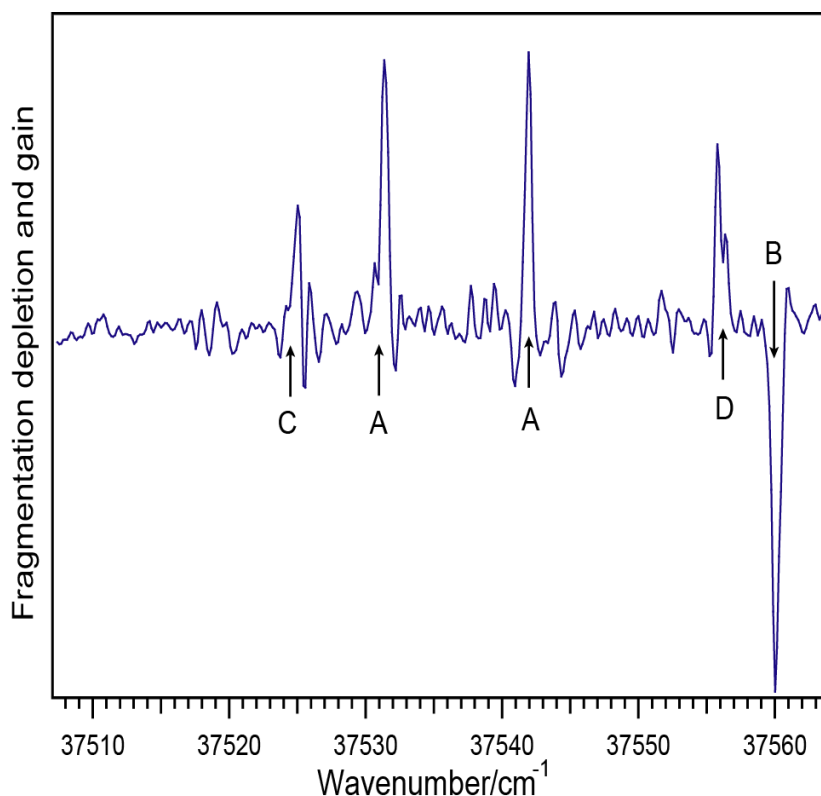
Figure 5.7: Hole-filling spectra of Ac-Phe-(Ala)$_5$-Lys-H$^+$, isotopically substituted C-13 of the acetyl group, measured with the infrared laser fixed on the C-O stretch transition of conformer B at 1654 cm^{-1}.

It is clear that population is driven out of conformation B leading to depletion in the photodissociation signal, whereas clear gains occur in the signal at the transitions of A, C and D (at 37'532, 37'526 and 37'556 cm^{-1} respectively). This gain in the population of the other conformations means that whatever are the pathways between these three conformations and B, the energy needed to cross the barrier to isomerization is less than 19.8 kJ/mol (1654 cm^{-1}). Thus, even by going to low energy, isomerization along the unfolding coordinate of the helix is still possible while going from conformer B to C and D.

5.2.3   Hole-filling spectroscopy of Ac-Phe-(Ala)₃-(Gy)₄-(Ala)₃-Lys-H⁺

The third system investigated in this thesis by hole-filling spectroscopy is the twelve residue peptide Ac-Phe-(Ala)$_3$-(Gly)$_4$-(Ala)$_3$-Lys-H$^+$. Although this molecule was designed to destabilize the helix so that it could adopt both globular and helical forms, the IR spectra reported in *Chapter 4.2.3*, indicates the existence of two conformations having the same hydrogen-bonding scheme of the peptide backbone. The similarity between the IR spectra of this molecule and a twelve amino residue peptide with ten alanines [47], suggest a helical shape for the glycine containing peptide.
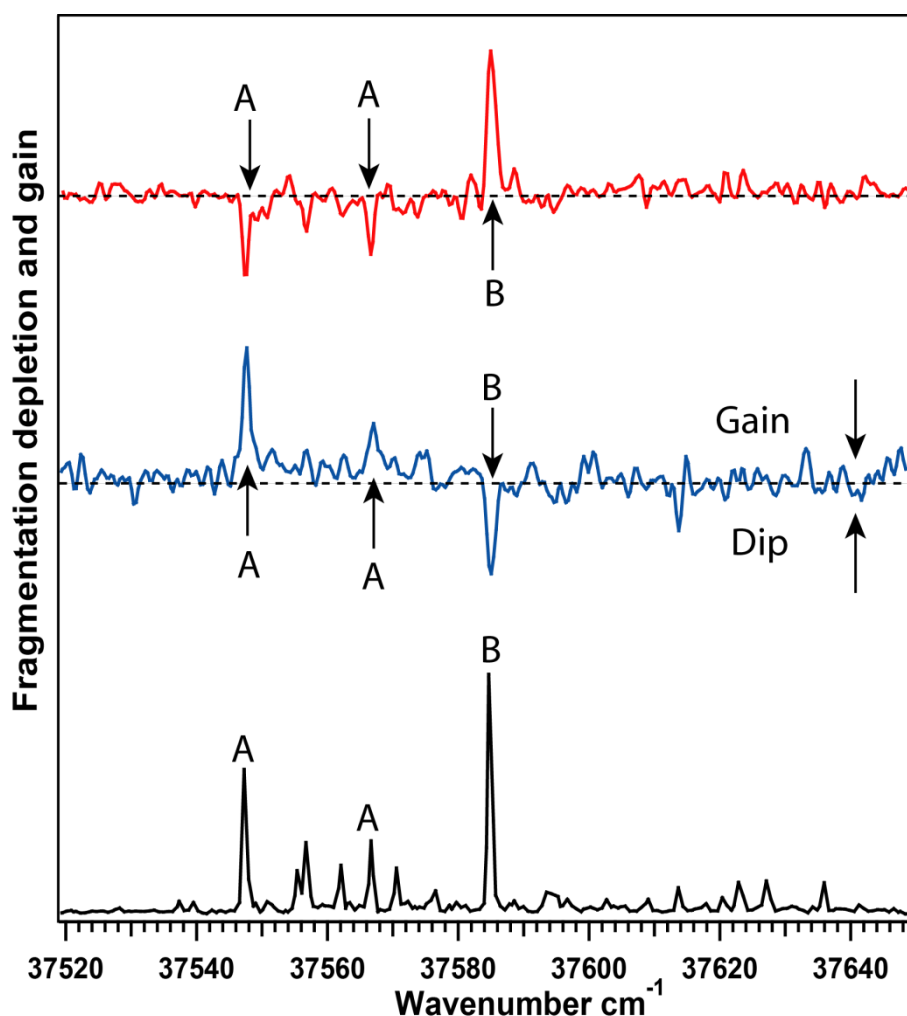
Figure 5.8: Hole-filling spectra of Ac-Phe-(Ala)$_3$-(Gly)$_4$-(Ala)$_3$-Lys-H$^+$, measured with the infrared laser fixed on a) the N-H stretch transition of conformer A at 3412 cm^{-1}, b) the N-H stretch transition of conformer B at 3447 cm^{-1}. The black trace, c), corresponds to the ultraviolet photofragmentation spectrum of Ac-Phe-(Ala)$_3$-(Gly)$_4$-(Ala)$_3$-Lys-H$^+$.

The importance to investigate the isomerization of such a system comes first from the size of the molecule which helps explore the limits of this technique. On the other hand, the

low helix-forming propensity of the glycine residue is supposed to destabilize helical conformations, thereby lowering the barrier to isomerization which could permit the population of new conformational minima after IR excitation and cooling.

We record the hole-filling spectra of Ac-Phe-(Ala)$_3$-(Gly)$_4$-(Ala)$_3$-Lys-H$^+$, presented in Figure 5.8, by fixing the IR laser on a transition associated with a particular conformer in the NH stretch region, while scanning the UV laser and monitoring intensity of the fragment ion signal. In the spectrum of Figure 5.8a, the IR pump laser fixed at 3412 cm^{-1} removes population from the ground state of conformation A. This conformer acquires the amount of energy needed to cross the barrier to isomerization and this manifests as depletion in the photofragment signal when the UV laser probes the transition of conformation A. This depletion explains the gain in the photofragment signal where conformation B absorbs in the UV. The hole-filling spectrum, in Figure 5.8b, depicts the redistribution of the population after the relaxing of the IR excitation, held fixed at 3447 cm^{-1} to pump up the population of conformation B. The decrease of the initial population of conformation B manifests as depletions in the photofragment signal when the UV laser tuned though its transitions, while the photofragment signal due to conformation A show clear gains, indicating that the population lost in conformer B has undergone isomerization to form A.

These spectra illustrate the changes in population induced with the IR laser following selective excitation of a single conformer in the NH stretch region. These excitations were able to move population between the minima that had already population in them. Even for such relatively big molecule, the barrier separating its minima is lower than the energy photon 41 kJ/mol, implying that the isomerization coordinate must be a relatively simple one. While we would have liked to extend our study to the CO stretch region, the absorption bands of the IR spectra of both conformers in this region, reported in *Section 4.2.3*, are heavily overlapped making it impossible to selectively excite individual conformations in this region. It is also important to stress that there is no evidence of the formation of new conformations having a barrier to isomerization lower than the energy photon used.

5.2.4 Discussion and conclusions

The dynamics of conformational isomerization of the three systems studied in this work have been probed using IR-UV hole-filling spectroscopy. This cool-pump-recool-probe approach is able to induce changes in the conformational population of the molecules

following conformation-specific excitation. This method is able to remove population out of a single conformation leading to population gains in the other conformation. As a consequence, it is possible to control the conformational population in our trap.

We estimate the temperature of the ions arriving to the trap to be near room temperature before they are collisonaly cooled to their zero-point level and this energy is removed. In the hole-filling experiments, the cold ions are then excited with an energy corresponding to 3300 cm^{-1} if the IR photon absorb is in the NH stretch region or 1645 cm^{-1} in the case of the amide I region. Because of the difference in complexity of the studied systems, two states of figure have to be taken in consideration. In the case of the single amino acid phenylalanine, the molecule arrives to the trap with an average internal energy estimated to 1852 cm^{-1} which is lower than the energy deposited *via* the infrared excitation, ~ 3100 cm^{-1}. While this later energy will be first concentrated in a specific mode, within the cooling time scale of few milliseconds (Cf. section 3.4.3) this vibrational energy will redistribute among the vibrational modes of the molecules, putting them in states of mixed vibrational character having components that represent population in many low frequency vibrational modes. After IVR the energy dissipation through the isomerization process involves displacement in the dihedral angle (from $\chi_1 = 72°$ to $\chi_1 = 169°$) and the backbone orientation. However the excess of energy was not sufficient to cross high barrier to isomerization and the cooling process did not drive the population to different regions of the potential surface leading to different minima. Besides that, one would argue that even if the absorption of the photon will excite the molecule to region on the potential energy surface where other conformations can occur, the excited molecule are cooled slowly enough to always find the global minimum. But then again we were able to demonstrate the existence of more than one conformer, meaning that at some point the molecules start to be trapped kinetically.

In the case of the two peptides, the average energy of the molecule at room temperature is 10980 cm^{-1} in the case of 7-residue peptide and 15833 cm^{-1} in the case of the 12-residue peptide which is significantly higher than the energy of the excited molecule through one of the NH (3440 cm^{-1}) or CO (1654 cm^{-1}) vibrational transitions. In contrast to the case of phenylalanine, despite the fact that the potential energy surface increased in complexity, the energy deposited in the molecule may be insufficient to overcome the transition states separating other major conformational families and thus limit the region to be mapped out on the potential energy surface. This could explain the fact that no new minima

were populated and we just detect the set of conformations that had population in them upon initial cooling. Although, both molecules showed an efficient transfer between their identified conformations, meaning that the energy acquired by the absorption of the IR photon is above some of the energy barriers to isomerization. The excitation energy, even if initially localized, should be rapidly dispersed among the other vibrational modes through IVR will lead to the mixing of the vibrational states that are conformationally mixed in character. Radiative and nonradiative process will be competing in order to bring the molecule into their lowest energy level. In the case of Ac-Phe-(Ala)$_5$-Lys-H$^+$, we observed isomerization deactivation which leads to the rotation of the phenylalanine side chain around the C$_\alpha$–C$_\beta$ bond from *gauche+* (+60°) to *gauche-* (-60°) position and conversely as well as the helical rearrangement involving the formation/breaking of C$_{10}$ and C$_{13}$ ring. Although the conformational structure for Ac-Phe-(Ala)$_3$-(Gly)$_4$-(Ala)$_3$-Lys-H$^+$ was not assigned, from the similarity in its IR-UV double resonance spectra we suggest a similar hydrogen-boding pattern and thus the isomerization process in this case will probably not involve the helical rearrangement. However the cooling process in both peptides did not form new conformational structures. Such results on large flexible molecules open an avenue to probe their multidimensional potential energy surfaces by identifying the accessible minima and different pathways connecting them.

The technique of buffer-gas cooling used in these experiments differs from cooling in the supersonic expansion used by Zwier and coworkers [33, 35]. Cooling is much faster in their approach, since the helium backing pressure could reach 10 bar and has the possibility of competing with isomerization in molecules which may lead to populating new minima on the potential energy surface, where in our case the rate of isomerization is likely to be fast compared to the slower collisional cooling rate.

On the other hand, our studies did not yield a direct measurement of the barriers to isomerization which might be possible using simulated emission pumping (SEP), a method used in Zwier group for this purpose [37, 40]. Unfortunately, such experiments are much more difficult when photodissociation is used as the detection method, since one must be able to distinguish between the fragment ions induced by each laser.

Another objective of this study was to search for trapping population in new minima on the potential energy surface. In the case of the three studied systems, we did not observe any minima that did not have population in them in the absence of the IR excitation. This

could be due to the fact that the barriers between different conformational families are higher than the IR energy photon used. In the case of the two peptides studied here, the IR excitation energy was less than the initial thermal energy of the molecule. In the following section, we will describe an additional experiment designed with the idea to populate new conformations, using a UV-UV pump-cool-probe approach.

5.3 UV-UV hole-filling spectroscopy in a cold 22-pole ion trap

In the first part of this chapter we reported an approach, to study the conformational isomerization in three different biological molecules, using an infrared laser to selectively excite a single conformation. The energy of the IR photon was well above the lowest barriers to isomerization so we were able to redistribute population in between the minima that already have population in them. However, this excess of energy was not sufficient to cross high barriers and drive the population into new minima. Here, we introduce an UV-UV hole-filling experiment where the IR excitation of the previous approach is replaced with a UV excitation.

5.3.1 Description of the method

In the UV-UV hole-filling spectroscopy, the cool-pump-recool-probe configuration of the previously described experiment, IR-UV hole filling, is maintained while the IR laser excitation is replaced by a UV laser excitation. However the absorption of the UV photon puts an order of magnitude more energy in the molecule than the IR excitation and thus the delay between the lasers corresponding to the relaxation time is increased to provide more collisional cooling to the UV-excited molecules. Experimentally, the ions produced by electrospray are pulsed into the 22-pole trap with a frequency of 20Hz and cooled to about 10 K by collisions with helium, which is injected and thermalized to the temperature of the trap housing 1ms prior the arrival of the ions. Once the ions are cold, a single conformation interacts with a 10 Hz UV laser fixed at a specific transition. After a 20 ms delay the UV probe laser, operating at 20 Hz, is sent through the trap. Figure 5.9 depicts the energy level and timing diagram of the UV-UV hole-filling approach.
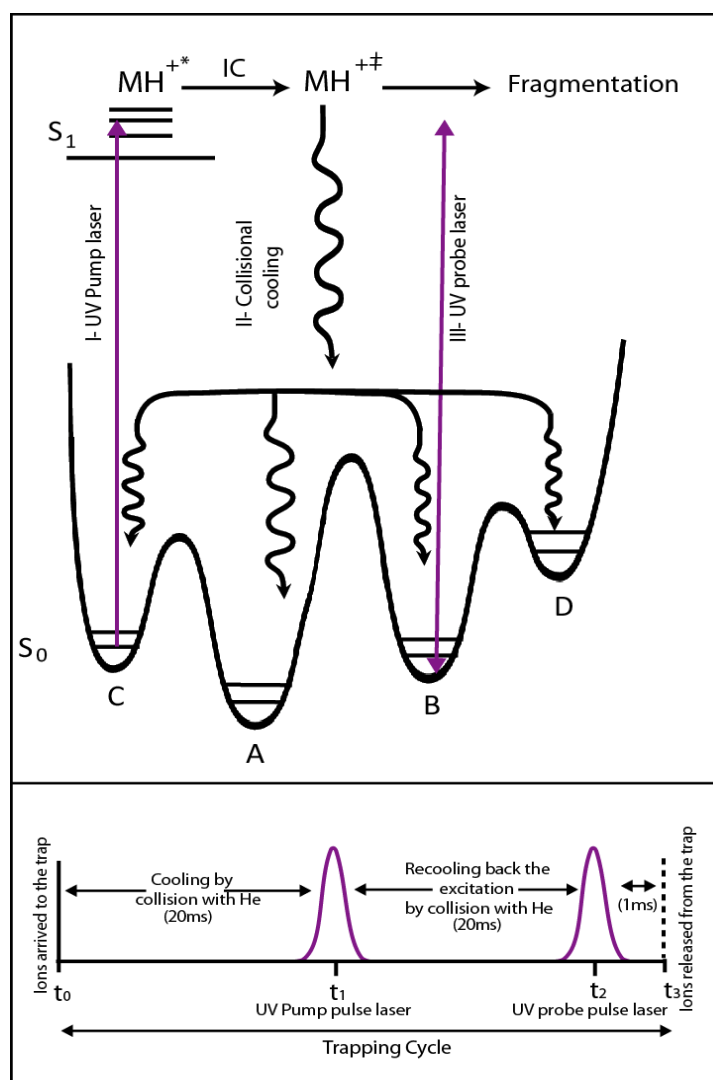
Figure 5.9: Energy level and timing diagram of the UV-UV hole-filling experiment.

The first laser fixed at a specific transition of one conformation will excite some of the ions to the electronic state S_1 and induce photofragmentation. Different mechanisms can lead to fragmentation, subsequent to UV absorption: (i) a direct dissociation if the S_1 state is purely repulsive in the coordinate of a given bond (ii) an indirect dissociation (i.e., predissociation) if the S_1 excited state crosses a repulsive state S_2 through which fragmentation occurs, or (iii) dissociation on the ground potential energy surface after internal conversion from the excited state S_1 back to a highly excited vibrational state of the electronic ground state. Other studies in our laboratory [48] have shown that following UV excitation of the aromatic amino acid chromophores loss of the aromatic side chain occurs via dissociation from an excited electronic state ((i) or (ii) above). However, since only a small fraction of ions dissociate, it is possible that a large fraction undergoes internal conversion to highly vibrationally excited levels of the ground electronic state. If this is the case, the vibrationally excited molecules

would have sufficient energy to explore a much larger portion of the conformational space, and upon collisional cooling this might populated new conformers. If this occurs, the second UV laser will probe the appearance of new absorption bands in the electronic spectrum. The following section presents the UV-UV hole-filling spectra of peptide ions of seven and twelve amino acids.

5.3.2 Results

We applied this technique to Ac-Phe-(Ala)$_5$-Lys-H$^+$ and Ac-Phe-(Ala)$_3$-(Gly)$_4$-(Ala)$_3$-Lys-H$^+$. Figure 5.10 illustrates the outcome of these experiments. The red traces correspond to the UV hole-filling spectra when the UV pump laser is on and the blue traces to the spectra when this laser is off, which correspond to the photofragmentation spectra previously obtain for these molecules. The offset between the laser on/off traces correspond to the fragmentation due to the first UV laser. In Figure 5.10a the UV pump laser excites conformation D of the Ac-Phe-(Ala)$_5$-Lys-H$^+$ at its origin transition at 37'556 cm^{-1}, where the ion internal temperature after UV excitation is estimated to be 588 K. Under the same conditions we record the UV-UV hole-filling spectra (not shown here) of the conformation A, B and C by fixing the UV wavelength of the pump laser on their respective origin transitions. In these spectra, the linewidth of the transitions is about 1.3 cm^{-1}, similar to those in the photofragmentation spectra. This confirms that the time delay between the two lasers and the residual helium in the trap was sufficient to successfully cool the excitation. On the other hand, none of these UV-UV hole-filling spectra of Ac-Phe-(Ala)$_5$-Lys-H$^+$ reveal the appearance of any new transitions.

We extended this approach to the twelve amino acid peptides Ac-Phe-(Ala)$_3$-(Gly)$_4$-(Ala)$_3$-Lys-H$^+$. The resulting UV-UV hole-filling spectrum is shown in Figure 5.10b measured by pumping conformation A at 37'536 cm^{-1}. It shows a high level of noise coming primarily from intensity fluctuations in the pump laser. Because of this uncertainty this spectrum was recorded more than 10 times in order to verify whether any of these small features could be attributed to any new conformations. These different spectra confirm that these fluctuations were just noise and do not belong to new bands that could result from the population of new a conformation. The UV hole-filling spectrum exciting conformation B was also recorded, but it also showed no clear evidence of new transitions.
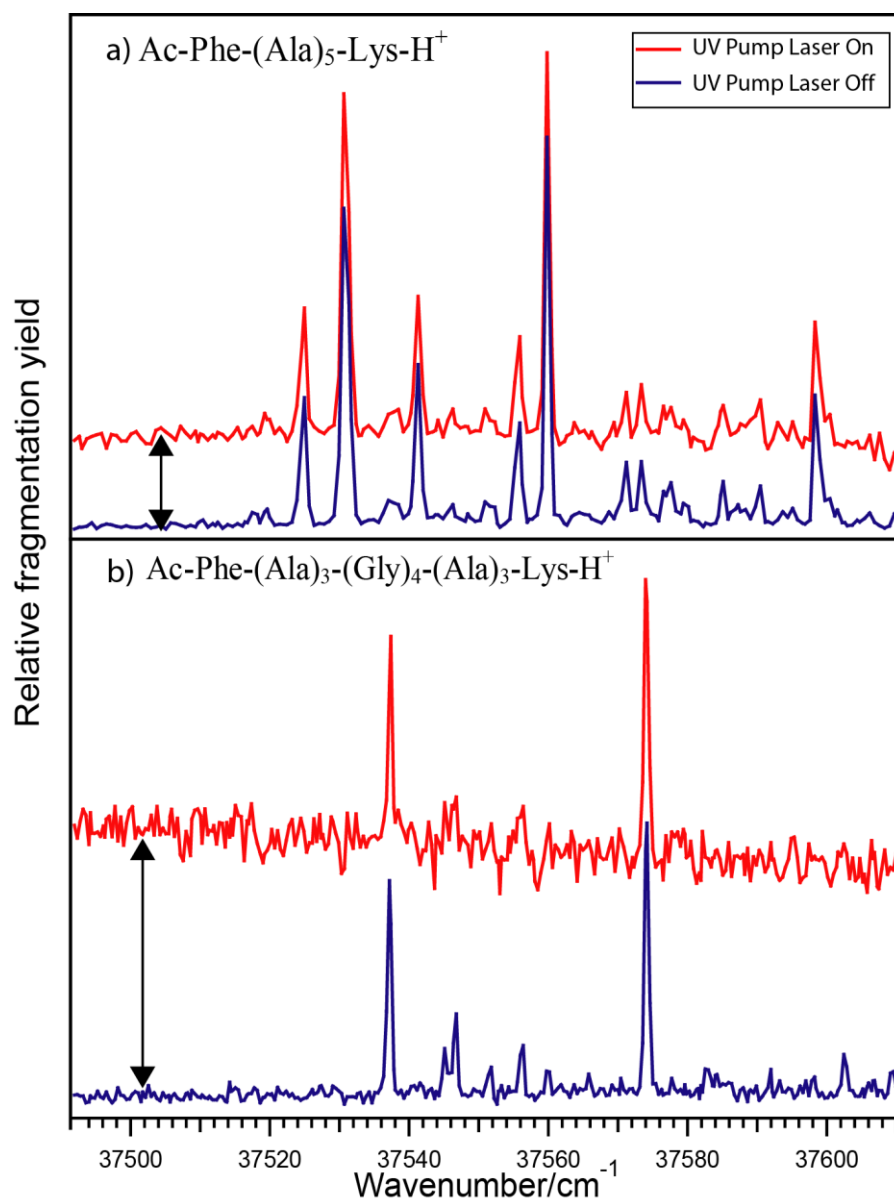
Figure 5.10: UV-UV hole-filling spectra measured by pumping a) conformation D of Ac-Phe-(Ala)$_5$-Lys-H$^+$, at 37'556 cm^{-1} b) conformation A of Ac-Phe-(Ala)$_3$-(Gly)$_4$-(Ala)$_3$-Lys-H$^+$, at 37'536 cm^{-1}

  The fluctuations could be due to the fact that the UV-UV spectrum is recorded by counting the ion fragments induced from both lasers (pump and probe). These ion fragment signals depend on each laser power and the number of the parent molecules in the trap, which we were not able to measure on alternate shots, limited by the number of channels that our data acquisition program can record. In addition, both parent and fragment ions are irradiated with the second laser, and hence the possibility that the daughter ions absorb the UV photon and dissociate could not be exclude, which could reduce the numbers of count of the daughter ions produced by the first laser excitation.

5.3.3 Discussion and conclusions

The UV-UV hole-filling spectra of two peptides of seven and twelve amino acids are recorded by pumping a specific conformation with a UV laser and then probing the new population distribution after a 20 ms delay. These spectra show vibrationally well resolved bands suggesting a complete cooling of the pump excitation. The main goal of these experiments was to populate new minima on the potential energy surface.

In order to explain these observations, one has to consider diverse dissociation mechanisms that could occur after UV excitation. Two different processes happen on distinct time scales, fast dissociation directly from the electronic excited state or dissociation on the ground electronic state after internal conversion this mechanism, which should be slower than the previous. Recent works of Schlag and coworkers proposed the co-occurrence of these two mechanisms during biomolecule fragmentation [49]. Thus, a fraction of the excited molecules may undergo nonstatistical dissociation and produce fragments on a short timescale compared to RRKM estimations. The remaining fraction would go through complete IVR and possibly dissociate, according to a statistical rate constant [50, 51]. Using coincidence and femtosecond pump/probe experiments Grégoire *et al.* demonstrate the existence of both statistical fragmentation following internal conversion from the electronically excited state and direct dissociation from the electronic excited surface in single protonated aromatic amino acid and small peptide ions interacting with UV laser radiation [52-56].

Recent experiments in our group intended to measure the electronic and the vibrational spectra of large, protonated peptides using IRLAPS, a photofragment-based detection scheme [48, 57]. This technique was able to enhance the fragmentation produced by the C_α-C_β bond cleavage attributed to direct dissociation on the excited state surface, suggesting the fast formation of a biradical intermediate species after the electronic excitation. Whatever is the nature of the intermediate species, if considering the fraction of the molecules that undergo electronic excited state photodissociation, the lifetime of the excited molecules compared to competing processes is too short and the pre-excited species will dissociate undergo fast dissociation. The activated molecules that dissociate in a nonstatistical manner have a rate for dissociation faster than the rate for internal conversion and thus the branching ratio for internal conversion may simply be small. In this case the UV probe laser firing with a time delay of 20 ms, will not interact with the parent ions that already saw the UV pump laser.

Indeed, in the UV-UV hole-filling experiment reported here, b-type ion fragments, which are associated with dissociation on the ground electronic state after internal conversion from the excited electronic state [58], are monitored in the case of both peptides. The molecules in the excited state decay following internal conversion to the electronic ground state and undergo vibrational energy redistribution and fragmentation. However, on the time scale of the delay between the two lasers (20 ms), the dissociation process will compete with collisional processes reducing the fraction of molecules that survive to isomerize. Thus, at the S_1 origin perhaps only a fraction of the population that undergoes internal conversion to the ground state, will lead to isomerization.

In this case, the isomerization following internal conversion proceeds on the ground-state surface. During relaxation process molecules in highly excited vibrational levels may overcome the barriers between different conformational families, adopting different energy path and end in new local minima. However, for the studied peptides, because of the absence of any new bands in the UV-UV hole-filling spectra these previous possibilities can be ruled out. It appears that the molecules follow the same cooling path as during the first cooling step to populate the minima already identified in the absence of the UV excitation. During the isomerization process and on the time scale of the recooling step (20 ms), the emission of an IR photon could occur [59] so radiative and collisional relaxation pathways compete together to transfer population to cool the molecule.

One should point out that the use of the photodissociation as detection technique in the UV-UV hole-filling approach makes it difficult, if not impossible, to discuss the relative changes in the population of the different conformations. The disadvantage of this technique under our experimental conditions is that daughter ions produced from both lasers are released together from the trap and so no control over the number of fragmentation induced by each laser.

Finally, we attempted to probe excited-state isomerization dynamics using the UV-UV hole-filling method. The excited molecules could follow nonstatistical and statistical manner in order to dissociate, in this later case internal conversion occur and thus isomerization process could lead to the formation of new conformational structures. The resulting spectra of the studied systems did not show any new transition that could be attributed to new conformational minima.

5.4 Conclusion

In this chapter, we demonstrate the feasibility of population transfer experiments on large ions in a cold 22-pole ion trap using photofragment spectroscopy for detection. First the potential energy surfaces of molecules were explored following an infrared excitation, and after collisional recooling a UV laser probes the new conformational distribution. We have applied this method to three different molecules of increase size, starting with the single amino acid phenylalanine then proceeding to a seven residue helical peptide and to a twelve residue peptide. The three systems show evidence of the transfer between its lowest energy minima after IR excitation; however the isomerization process did not populate regions of the potential surface corresponding to new conformers. A possible way to get benefit of this method is to apply the cool-pump-recool configuration multiple times and therefore pumping out a specific conformer in spite of maximizing other conformations, this will be feasible by extending the trapping cycle to hundreds of ms by simply changing the frequency of the machine.

Secondly we developed a method for probing the isomerization dynamics of the peptides after being promoted to an electronic excited state from their lowest vibrational state on the ground electronic state S_0. The isomerization into new conformational minima was not observed, however due to the complexity of the peptides structure, it is difficult to identify the exact pathways.

References

1. C. M. Dobson, *Philosophical Transactions of the Royal Society of London. Series B: Biological Sciences* **356**, 133 **2001**.
2. J. D. Watson, F. H. C. Crick, *Nature* **171**, 737 **1953**.
3. M. H. F. Wilkins, A. R. a. W. Stokes, H. R., *Nature* **171**, 738 **1953**.
4. R. E. Franklin, R. G. and Gosling, *Nature* **171**, 740 **1953**.
5. F. H. C. Crick, J. D. Watson, *Proc. R. Soc. London, Ser. A* **223**, 80 **1954**.
6. M. F. Perutz, M. G. Rossmann, A. F. Cullis, H. Muirhead, G. Will, A. C. T. North, *Nature* **185**, 416 **1960**.
7. M. P. Williamson, T. F. Havel, K. Wüthrich, *J. Mol. Biol.* **182**, 295 **1985**.
8. K. Wuthrich, *Science* **243**, 45 **1989**.
9. K. Wuethrich, *Acc. Chem. Res.* **22**, 36 **1989**.
10. R. Riek, S. Hornemann, G. Wider, M. Billeter, R. Glockshuber, K. Wuthrich, *Nature* **382**, 180 **1996**.

11.　A. G. Tzakos, C. R. R. Grace, P. J. Lukavsky, R. Riek, *Annu. Rev. Biophys. Biomol. Struct.* **35**, 319 **2006**.

12.　S. Raman, O. F. Lange, P. Rossi, M. Tyka, X. Wang, J. Aramini, G. Liu, T. A. Ramelot, A. Eletsky, T. Szyperski, M. A. Kennedy, J. Prestegard, G. T. Montelione, D. Baker, *Science* **327**, 1014 **2010**.

13.　M. S. Braiman, K. J. Rothschild, *Annu Rev Biophys Biophys Chem* **17**, 541 **1988**.

14.　L. Velluz, M. Legrand, *Angewandte Chemie International Edition in English* **4**, 838 **1965**.

15.　W. B. Gratzer, *Proc. R. Soc. London, Ser. A* **297**, 163 **1967**.

16.　S. Beychok, *Annu. Rev. Biochem* **37**, 437 **1968**.

17.　Y.-X. Wen, E. Chen, J. W. Lewis, D. S. Kliger, *Rev. Sci. Instrum.* **67**, 3010 **1996**.

18.　X. Xie, J. D. Simon, *J. Am. Chem. Soc.* **112**, 7802 **1990**.

19.　L. Stryer, *Annu. Rev. Biochem* **47**, 819 **1978**.

20.　S. Nie, R. N. Zare, *Annu. Rev. Biophys. Biomol. Struct.* **26**, 567 **1997**.

21.　M. R. Eftink, *Biophys. J.* **66**, **1994**.

22.　G. V. Semisotnov, N. A. Rodionova, O. I. Razgulyaev, V. N. Uversky, A. F. Gripas, R. I. Gilmanshin, *Biopolymers* **31**, 119 **1991**.

23.　M. T. Zanni, N.-H. Ge, Y. S. Kim, R. M. Hochstrasser, *Proc. Nat. Acad. Sci. U.S.A.* **98**, 11265 **2001**.

24.　A. M. Woys, Y.-S. Lin, A. S. Reddy, W. Xiong, J. J. de Pablo, J. L. Skinner, M. T. Zanni, *J. Am. Chem. Soc.* **132**, 2832 **2010**.

25.　A. Smith, H. Chung, Z. Ganim, A. Tokmakoff, in *Ultrafast Phenomena XV,* P. Corkum, D. M. Jonas, R. J. D. Miller, A. M. Weiner, Eds. (Springer Berlin Heidelberg, **2007**), vol. 88, pp. 350-352.

26.　J. A. Smith, L. G. Pease, *CRC Crit. Rev. Biochem.* **8**, 314 **1980**.

27.　M. C. Asplund, M. T. Zanni, R. M. Hochstrasser, *Proc. Nat. Acad. Sci. U.S.A.* **97**, 8219 **2000**.

28.　H. Fabian, D. Naumann, *Methods* **34**, 28 **2004**.

29.　R. B. Dyer, F. Gai, W. H. Woodruff, R. Gilmanshin, R. H. Callender, *Acc. Chem. Res.* **31**, 709 **1998**.

30.　M. Gruebele, J. Sabelko, R. Ballew, J. Ervin, *Acc. Chem. Res.* **31**, 699 **1998**.

31.　D. T. Leeson, F. Gai, H. M. Rodriguez, L. M. Gregoret, R. B. Dyer, *Proc. Nat. Acad. Sci. U.S.A.* **97**, 2527 **2000**.

32.　M. Eigen, L. D. Maeyer, *In Technique of Organic Chemistry*. A. Weissberger, Ed.; Interscience: New York,, Ed., (**1963**), pp. p:895-1054.

33.　B. C. Dian, A. Longarte, T. S. Zwier, *Science* **296**, 2369 **2002**.

34.　B. C. Dian, A. Longarte, P. R. Winter, T. S. Zwier, *Phys. Chem. Chem. Phys.* **120**, 133 **2004**.

35.　B. C. Dian, G. M. Florio, J. R. Clarkson, A. Longarte, T. S. Zwier, *Phys. Chem. Chem. Phys.* **120**, 9033 **2004**.

36.　J. R. Clarkson, B. C. Dian, L. Moriggi, A. DeFusco, V. McCarthy, K. D. Jordan, T. S. Zwier, *Phys. Chem. Chem. Phys.* **122**, 214311 **2005**.

37.　J. R. Clarkson, E. Baquero, T. S. Zwier, *Phys. Chem. Chem. Phys.* **122**, 214312 **2005**.

38.　T. A. LeGreve, J. R. Clarkson, T. S. Zwier, *J. Phys. Chem. A* **112**, 3911 **2008**.

39.　N. R. Pillsbury, C. W. Muller, T. S. Zwier, *J. Phys. Chem. A* **113**, 5013 **2009**.

40.　B. C. Dian, J. R. Clarkson, T. S. Zwier, *Science* **303**, 1169 **2004**.

41.　J. A. Stearns, S. Mercier, C. Seaiby, M. Guidi, O. V. Boyarkin, T. R. Rizzo, *J. Am. Chem. Soc.* **129**, 11814 **2007**.

42.　J. A. Stearns, C. Seaiby, O. V. Boyarkin, T. R. Rizzo, *PCCP* **11**, 125 **2009**.

43.	G. W. T. M. J. Frisch, H. B. Schlegel, G. E. Scuseria, M. A. Robb, J. R. Cheeseman, J. J. A. Montgomery, T. Vreven, K. N. Kudin, J. C. Burant, J. M. Millam, S. S. Iyengar, J. Tomasi, V. Barone, B. Mennucci, M. Cossi, G. Scalmani, N. Rega, G. A. Petersson, H. Nakatsuji, M. Hada, M. Ehara, K. Toyota, R. Fukuda, J. Hasegawa, M. Ishida, T. Nakajima, Y. Honda, O. Kitao, H. Nakai, M. Klene, X. Li, J. E. Knox, H. P. Hratchian, J. B. Cross, V. Bakken, C. Adamo, J. Jaramillo, R. Gomperts, R. E. Stratmann, O. Yazyev, A. J. Austin, R. Cammi, C. Pomelli, J. W. Ochterski, P. Y. Ayala, K. Morokuma, G. A. Voth, P. Salvador, J. J. Dannenberg, V. G. Zakrzewski, S. Dapprich, A. D. Daniels, M. C. Strain, O. Farkas, D. K. Malick, A. D. Rabuck, K. Raghavachari, J. B. Foresman, J. V. Ortiz, Q. Cui, A. G. Baboul, S. Clifford, J. Cioslowski, B. B. Stefanov, G. Liu, A. Liashenko, P. Piskorz, I. Komaromi, R. L. Martin, D. J. Fox, T. Keith, M. A. Al-Laham, C. Y. Peng, A. Nanayakkara, M. Challacombe, P. M. W. Gill, B. Johnson, W. Chen, M. W. Wong, C. Gonzalez, and J. A. Pople,. (Gaussian, Inc.: Pittsburgh, PA, 2003).
44.	C. Peng, and H. B. Schlegel, *Israel J. Chem.* **33**, 449 **1994**.
45.	G. v. Helden, I. Compagnon, M. N. Blom, M. Frankowski, U. Erlekam, J. Oomens, B. Brauer, R. B. Gerber, G. Meijer, *PCCP* **10**, 1248 **2008**.
46.	A. Kaczor, I. D. Reva, L. M. Proniewicz, R. Fausto, *J. Phys. Chem. A* **110**, 2360 **2006**.
47.	J. A. Stearns, O. V. Boyarkin, T. R. Rizzo, *J. Am. Chem. Soc.* **129**, 13820 **2007**.
48.	M. Guidi, Ph.D Thesis, EPFL **2010**.
49.	E. W. Schlag, R. D. Levine, *Chem. Phys. Lett.* **163**, 523 **1989**.
50.	Y. Hu, B. Hadas, M. Davidovitz, B. Balta, C. Lifshitz, *J. Phys. Chem. A* **107**, 6507 **2003**.
51.	E. W. Schlag, H. L. Selzle, P. Schanen, R. Weinkauf, R. D. Levine, *J. Phys. Chem. A* **110**, 8497 **2006**.
52.	H. Kang, C. Dedonder-Lardeux, C. Jouvet, S. Martrenchard, G. Gregoire, C. Desfrancois, J. P. Schermann, M. Barat, J. A. Fayeton, *PCCP* **6**, 2628 **2004**.
53.	H. Kang, C. Jouvet, C. Dedonder-Lardeux, S. Martrenchard, C. Charriere, G. Gregoire, C. Desfrancois, J. P. Schermann, M. Barat, J. A. Fayeton, *Phys. Chem. Chem. Phys.* **122**, 084307 **2005**.
54.	G. Gregoire, H. Kang, C. Dedonder-Lardeux, C. Jouvet, C. Desfrancois, D. Onidas, V. Lepere, J. A. Fayeton, *PCCP* **8**, 122 **2006**.
55.	G. Grégoire, C. Jouvet, C. Dedonder, A. L. Sobolewski, *J. Am. Chem. Soc.* **129**, 6223 **2007**.
56.	B. Lucas, M. Barat, J. A. Fayeton, C. Jouvet, P. Çarçabal, G. Grégoire, *Chem. Phys.* **347**, 324 **2008**.
57.	M. Guidi, U. J. Lorenz, G. Papadopoulos, O. V. Boyarkin, T. R. Rizzo, *J. Phys. Chem. A* **113**, 797 **2009**.
58.	B. Paizs, S. Suhai, *Mass Spectrom. Rev.* **24**, 508 **2005**.
59.	R. C. Dunbar, *Int. J. Mass Spectrom. Ion Processes* **54**, 109 **1983**.

Chapter 6

Infrared population transfer spectroscopy

An important objective of this work is to provide information about the abundance of different conformers of molecules in our cold ion trap as well as the quantum yield to isomerization after infrared excitation, both of which will serve as benchmarks for theoretical studies. After having demonstrated the feasibility of the population transfer approach and the redistribution of population between the lowest identified minima, we report here results of our infrared population transfer (IRPT) experiment. These data allow the extraction of the fractional population of the protonated phenylalanine as well as the two peptides studied in this work. In association with IR-UV double resonance spectra, the IRPT spectra give the possibility to obtain the isomerization quantum yields of different NH stretch vibrations of phenylalanine and the twelve-residue peptide Ac-Phe-$(Ala)_3$-$(Gly)_4$-$(Ala)_3$-Lys-H$^+$.

6.1 Introduction

Numerous experimental studies seek to understand the mechanisms and dynamics of conformational isomerization in flexible molecules. Unimolecular reaction studies provide information on the reaction energy barrier, time scales, and pathways on the potential energy surface of small molecules where two conformational minima are connected by a single transition state along a well-defined reaction coordinate [1-7]. On the other side, large molecules have very complex potential energy landscape with an enormous number of conformational minima, and thus the pathways connecting them may involve several transition states. This fact makes it very difficult to define all the stationary points on their potential energy landscape and to probe the conformational dynamics [8].

In recent experiments on methyl-capped dipeptides, Zwier and coworkers showed that conformational change in gas-phase biomolecules can be induced by infrared excitation [9]. The important results of these experiments were values of fractional population of the different conformers and the isomerization quantum yields following excitation of each of the unique amide NH stretch fundamentals of these molecules, where evidence of conformation-specific, and to a lesser degree mode-specific, isomerization was found [9-12]. We have performed similar studies on two protonated peptides of somewhat greater size in addition to the single amino acid phenylalanine. We report here the infrared population transfer spectra of three molecules of different size and flexibility and population abundance. Quantum yields for conformational isomerization are extracted for different NH stretch vibrations of phenylalanine and the twelve residue peptide Ac-Phe-$(Ala)_3$-$(Gly)_4$-$(Ala)_3$-Lys-H^+.

6.2 Infrared population transfer experiment in a cold 22-pole ion trap

This method is based on the work of the Zwier group [9]; details of its adaptation to study cold ions in a 22-pole ion trap can be found in *section 3.4.2*. Here we give only a brief description. Ions are generated in the gas phase *via nano*-electrospray and collected in a hexapole, which generates an ion packet every 50 ms and projects it through a quadrupole mass filter, to select the ions of a particular m/z. The mass-selected ions are then guided to a cold 22-pole ion trap where they are cooled by collisions with helium, which is pulsed into the trap 1 ms prior to the arrival of the packet. Once in the trap, the ions are given 20 ms to cool before being excited with an infrared pump laser. The changes in the conformer population were detected 7 ms later using UV laser-induced fragmentation. In these experiments particular attention is given to the spatial overlap between the lasers and the trapped ion packet. The pump and probe lasers were positioned to maximize the population transfer signal. The IR beam has a slightly large diameter than the UV beam and a maximum pulse energy of 5-6 mJ in order to prevent the saturation of the transitions.

6.2.1 Results

6.2.1.1 IRPT spectroscopy of protonated phenylalanine

Phenylalanine is large enough to have some degree of conformational complexity but small enough such that its spectroscopy is still relatively simple. As one of the near-UV

chromophores of proteins, it has been studied by various groups both experimentally and theoretically. These studies have provided structural information on the different conformations of neutral phenylalanine [13-20], their relative abundances and the transition states separating them [16, 18]. We have used single- and double-resonance photofragment-based laser techniques to record ultraviolet and infrared spectra of protonated phenylalanine, and the comparison of these spectra with DFT calculations allowed us to identify two stable conformers [21]. Here, we present the results of the population transfer experiments on PheH[+] and determine which products are formed, and in what abundance. Figure 6.1 presents the infrared population transfer spectra for conformer A and B of PheH[+]. These spectra are measured by fixing the UV probe laser to the band origin of conformer A (red) and conformer B (blue) while scanning the IR laser over the NH stretch region.

The IRPT spectra reflect a symmetry in which depletions in one spectrum are always compensated by gains in other and thus detect the population changes induced in a single conformation by the absorption of an IR photon. The hole filling spectra of the stable conformers of this molecule reported in the previous chapter did not show any change in the total ion population due to the formation of any new minima (c.f. section *5.2.1*). This leads us to consider that the weighted sum of the population transfer spectra for these two conformations at all infrared wavelengths should be zero:

$$p_A . IRPTS_A + p_B . IRPTS_B = 0 \qquad\qquad Eq.6.1$$

where $IRPTS_X$ corresponds to the intensity of the population transfer spectra at a given frequency and p_X the fractional population of conformer *X*.
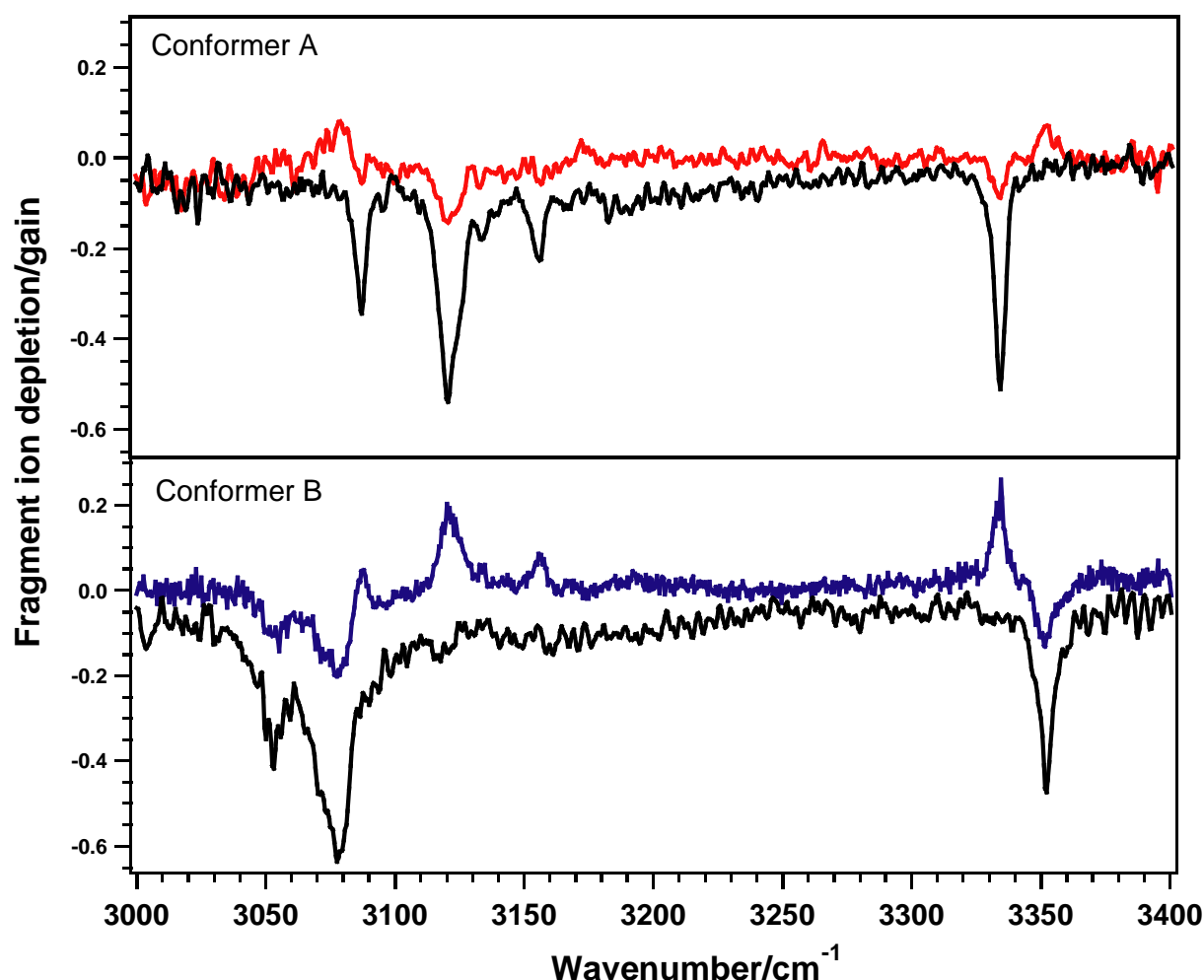
Figure 6.1: Infrared population transfer spectra of conformer A (red) and B (blue) of PheH$^+$. The black traces correspond to the IR-UV double resonance spectra of the respective conformer, taken under the same condition of the population transfer experiment.

The fitted curve represented in black in Figure 6.2, shows clearly that Equation 6.1 was satisfied over the entire wavelength range, confirming the redistribution of IR excited molecules among the two detected conformers. The fractional populations for the conformation of the protonated phenylalanine are p_A= 0.63 and p_B= 0.37 with an error of ±0.02. Based on the simulations presented section *4.1.2*, the structure of conformer B with χ_1 = 72° (*gauche*) is predicted to be 3.2 kJ/mol higher in energy than the global minimum structure, which corresponds to conformer A having χ_1= 169° (*anti*). The higher abundance for conformer A is consistent with it being the lower energy conformer of the two even though the population difference is not related in a simple way to the difference in zero-point energies.

These values for the fractional populations of the conformations of PheH$^+$ are independent of the dissociation quantum yields and oscillator strengths of the vibronic

transitions in the photodissociation spectra. These experiments can thus be considered as a direct method to determine the fractional abundance of the conformers in a cold 22-pole ion trap given the assumption (supported by experiment) that no new conformers are formed subsequent to IR excitation.
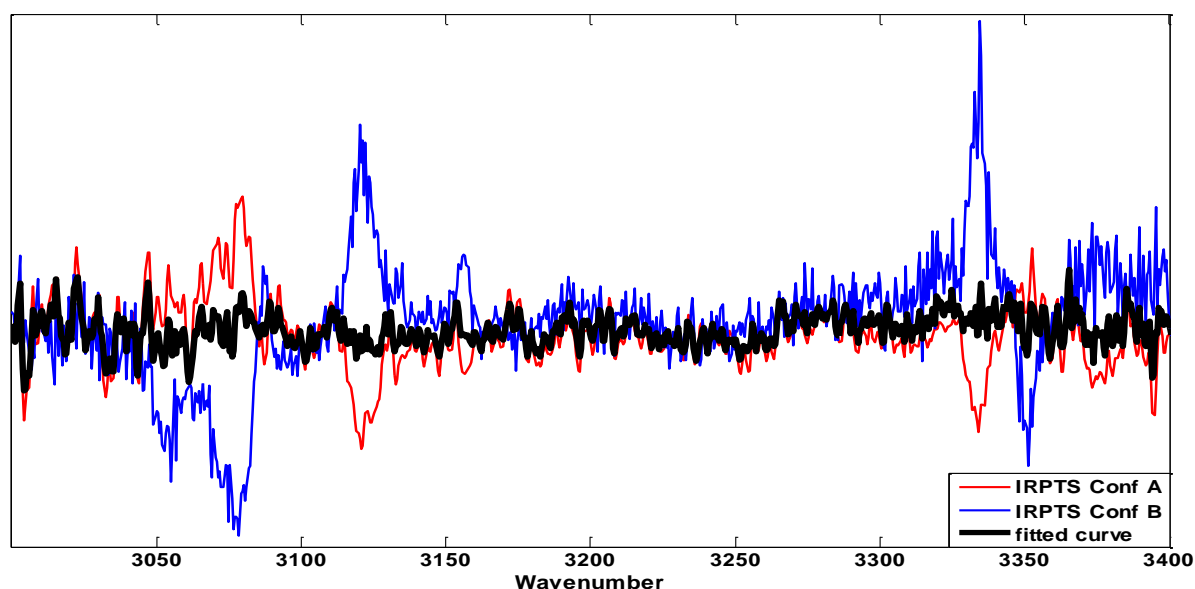
Figure 6.2: The back trace is the weighted sum of the infrared population transfer spectra of conformer A (red) and B (blue) of PheH$^+$.

One important conclusion that jumps out right away from these relative populations is that they are very different from the relative intensities of band origins of the two conformers in the UV spectrum. As shown in Figure 6. 3, the band origin that we attribute to conformer A is roughly half the intensity of that assigned to conformer B. From these relative intensities alone we might be tempted to conclude that conformer B has twice the population of A. However the analysis presented above indicates that the opposite is true: conformer A has twice the population of B. While this discrepancy may seem to arise from a simple mislabeling of conformers, it is not the case. One can see that the relative intensities of the vibronic band of the two conformers at ~540 cm^{-1} to higher frequency is completely different, reflecting more nearly the relative conformer populations. The observed band origin intensities must therefore have oscillator strengths that differ by a factor of four for these two conformers. This emphasizes something that Zwier has already pointed out [22] – the importance of not judging the conformer populations as being simply proportional to the band intensities.
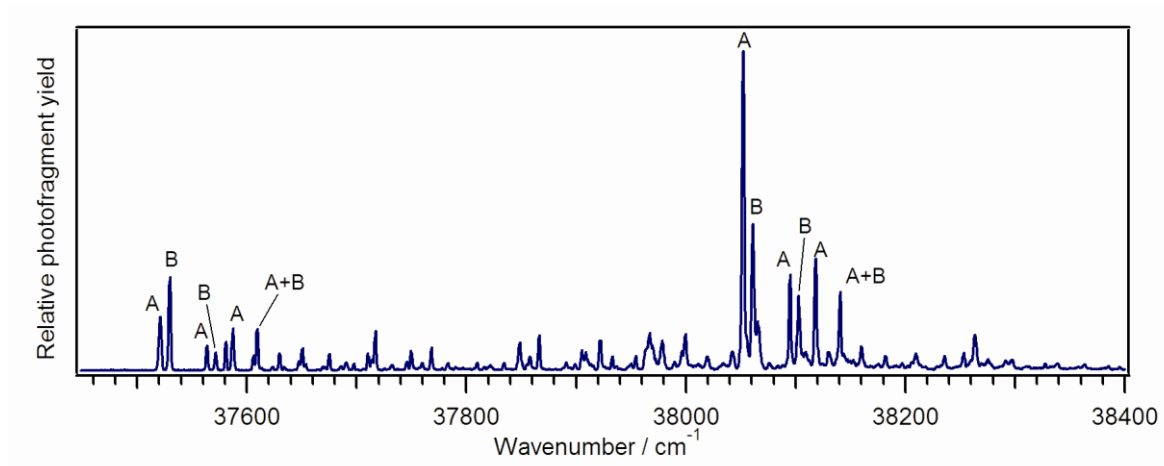
Figure 6. 3: Ultraviolet photofragment excitation spectrum of PheH+ recorded by detecting the m/z 74 fragment. The conformational assignments are based on the infrared and IR-UV hole burning spectra.

In addition to being able to determine the relative conformer populations from the IRPT spectra of Figure 6.1, the difference in the NH stretch frequencies of the two conformations makes it possible to determine the isomerization quantum yields after exciting in the infrared *via* each of these three transitions. In order to do so we need, in addition to the fractional abundance, the intensities of the infrared bands in both the population transfer spectrum and the normal infrared spectrum of each conformer. The later measures the fraction of the population of a specific conformer that absorbs an IR photon after being cooled in the trap for 20 ms. These infrared spectra are presented in Figure 6.1(black).

The equations to extract the quantum yields are developed in detail in Appendix A. Here we give the final result applicable in the case of the two conformers of PheH$^+$ for a specific wave number where both absorb:

$$IRPTS_A = \left(-\frac{p_B}{p_A} \cdot IR_B \cdot \Phi_{BA} + IR_A \cdot (1 - \Phi_{AA}) \right) \cdot \gamma$$

$$IRPTS_B = \left(-\frac{p_A}{p_B} \cdot IR_A \cdot \Phi_{AB} + IR_B \cdot (1 - \Phi_{BB}) \right) \cdot \gamma \qquad Eq.6.2$$

where $\gamma = \dfrac{\max(A_{UV}, A_{IR})}{A_{ion}}$

IRPTS$_X$ and *IR$_X$* are the intensities of the transition in the population transfer and IR-UV double resonance spectra for conformer *X* at a specific frequency and Φ_{XY} is the

112

isomerization quantum yield for going from conformer *X* to conformer *Y* following excitation of a specific IR transition of conformation *X*. The factor γ corresponds to the maximum overlapped area of the two laser beams with the total number of ions. Working under the optimized condition for maximum of overlap between the pump probe lasers and the ions, this factor is assumed to be close to 1.

If the quantum yields are extracted at an NH stretch where just conformer A absorbs, Equation 6.2 will simplify to:

$$IRPTS_A = IR_A.(1-\Phi_{AA})$$

$$IRPTS_B = -\frac{p_A}{p_B} IR_A.\Phi_{AB}$$

Eq.6.3

The same equations in the case of the unique NH stretch of conformer B give:

$$IRPTS_B = IR_B.(1-\Phi_{BB})$$

$$IRPTS_A = -\frac{p_B}{p_A} IR_B.\Phi_{BA}$$

Eq.6.4

In these final equations the only unknowns are the quantum yields Φ_{XY}, since the fractional population p_X has been already extracted from the weighted sums of the population transfer spectra, and the population transfer ($IRPTS_X$) and infrared (IR_X) peak intensities are measured experimentally. In order to get these intensities, all the bands in the spectra were fitted by Gaussians:

$$I(\tilde{v}) = \frac{I_{Int.A}}{\sqrt{2\pi}.\varphi}.\exp\left[-\frac{(\tilde{v}-\tilde{v}_0)^2}{2\varphi^2}\right]$$

Eq.6.5

In the fits of the population transfer spectra, the peak width and the center frequencies are set from the bands in the IR spectra taken under the same conditions. Using these values we calculate for every IR absorption band the isomerization quantum yields, presented in Table 6.1. These quantum yields are determined separately, as independent quantities, however the sum of each set of values has to satisfy the equation $\Phi_{XY} + \Phi_{XX} = 1$ and thus we scale them to be so [9, 10, 22]. In no case are these scale factors more than 25% and in most cases much less.

	Isomerization quantum yields for PheH$^+$						
	PheH$^+$ conformer A				PheH$^+$ conformer B		
Quantum yields	3087 cm^{-1}	3122 cm^{-1}	3156 cm^{-1}	3335 cm^{-1}	3054 cm^{-1}	3079 cm^{-1}	3352 cm^{-1}
Φ_{XA}	0.92±0.04	0.73±0.02	0.69±0.09	0.71±0.03	0.25±0.02	0.10±0.04	0.27±0.05
Φ_{XB}	0.08±0.05	0.26±0.02	0.31±0.05	0.29±0.06	0.75±0.02	0.90±0.05	0.73±0.06

Table 6.1: IR-induced isomerization quantum yields for the protonated phenylalanine. $\Phi_{XA/B}$ is the quantum yield for formation of conformer A/B following IR excitation of conformer X. Quantum yields have been normalized so that their sum equals 1.

The quantum yields are also displayed graphically in Figure 6.4. Under the slow cooling conditions of the experiment (see below) and after energy relaxation, one would expect that most of the population will find its way back to the lowest energy conformation, which is A in this case. Figure 6.4 shows that the excitation of a specific conformation preferentially leads to the reformation of this same conformation. By exciting the global minimum A and after energy dissipation, the conformational distribution is similar to the initial distribution formed during the initial cooling of ions in the trap: 63% of conformation A and 37% of conformation B. However, starting from conformation B the final distribution showed that almost 70% of the excited molecules find its way back to the initially excited conformer. Thus, the repartitioning of the population after vibrational excitation depends on which conformer one starts with.
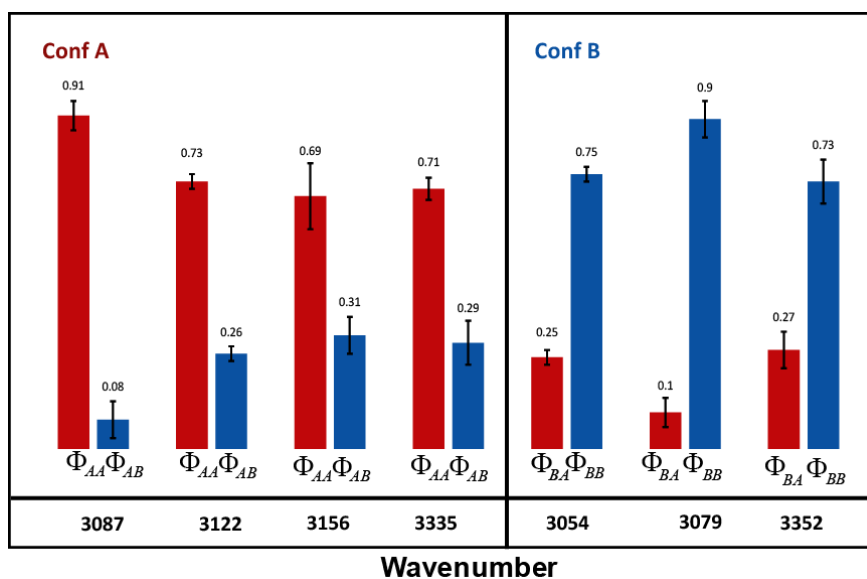
Figure 6.4: Quantum yields for isomerization following IR excitation of the indicated NH stretch of conformation A and B of PheH$^+$. Φ_{xy} is the quantum yield for formation of conformer y following IR excitation of conformer x.

After the absorption of an infrared photon, phenylalanine is promoted to a vibrational level above the barrier to isomerization – we know this because we probe and observe the isomerization product. This means that upon vibrational excitation, intramolecular vibrational redistribution (IVR) must occur and that the vibrationally mixed states include levels that are conformationally mixed in character. The time scale of IVR to such conformationally mixed states, which is essentially an isomerization rate, is difficult to estimate because it depends on coupling matrix elements to states of very different conformational character. If these rates were to be slow enough, collisional cooling might compete with isomerization, and in this case it would direct population back into the initially excited minimum. To see if this might be the case in a molecule the size of protonated phenylalanine, we could compare with the results from Zwier and coworkers [9, 10, 22].

Dian *et al.* reported conformational specificity in the population transfer experiment of N- acetyl tryptophan methyl amide (NATMA) in a supersonic expansion [9, 22]. Simulations carried out by Evans *et al.* to explain the population dynamics of this molecule revealed that at sufficiently high rates of collisional cooling one should indeed observe conformer selectivity, since the cooling process begins to compete with the isomerization rate [11, 23]. In the supersonic molecular beam experiments on NATMA, the time to cool the vibrationally excited molecule back down to the zero point level is estimated to be on the order of 900 ns, and the initial time between collisions is ~100 ps. These timescales are at least 10^4 times shorter than in our experiment.

The initial density of helium ρ_{He} in our trap was calculated by measuring the background pressure of helium inside the vacuum chamber and based on the pumping speed of the turbo-pump, it was found to be on the order of 10^{15} cm^{-3} [24]. The number of collisions per second, Z, is given by the density of the helium atom ρ_{He} times their average velocity $\bar{\upsilon}$ at 10 K (2.10^4 cm/sec) and the molecular diameter, which is estimated to be about 1 nm based on the molecular diameter of the benzene ring:

$$Z = \sqrt{2}.\rho_{He}.\pi.D^2_{ion}.\bar{\upsilon} \qquad\qquad Eq.6.6$$

This gives a frequency of 10^6 sec^{-1} and time between collisions of about 1 μsec. In addition, we have measured the time for vibrationally excited phenylalanine to cool back to its

vibrational zero-point level in our cold ion trap. Figure 6.5 illustrates the gain in the photofragment signal of conformer B of phenylalanine while the IR laser is fixed at a transition belongs to conformer A. The curve shows an increase in the signal after which it stays stable for 7ms. The cooling occurs during the first microseconds, and reaches a maximum after 200 μsec. This clearly puts our population transfer experiment in the cold ion trap under slow cooling conditions as defined by Evans *et al.* [11]. It is thus difficult to imagine the possibility that collisional cooling quenches the vibrational energy fast enough restrict the molecule from crossing the isomerization barrier.
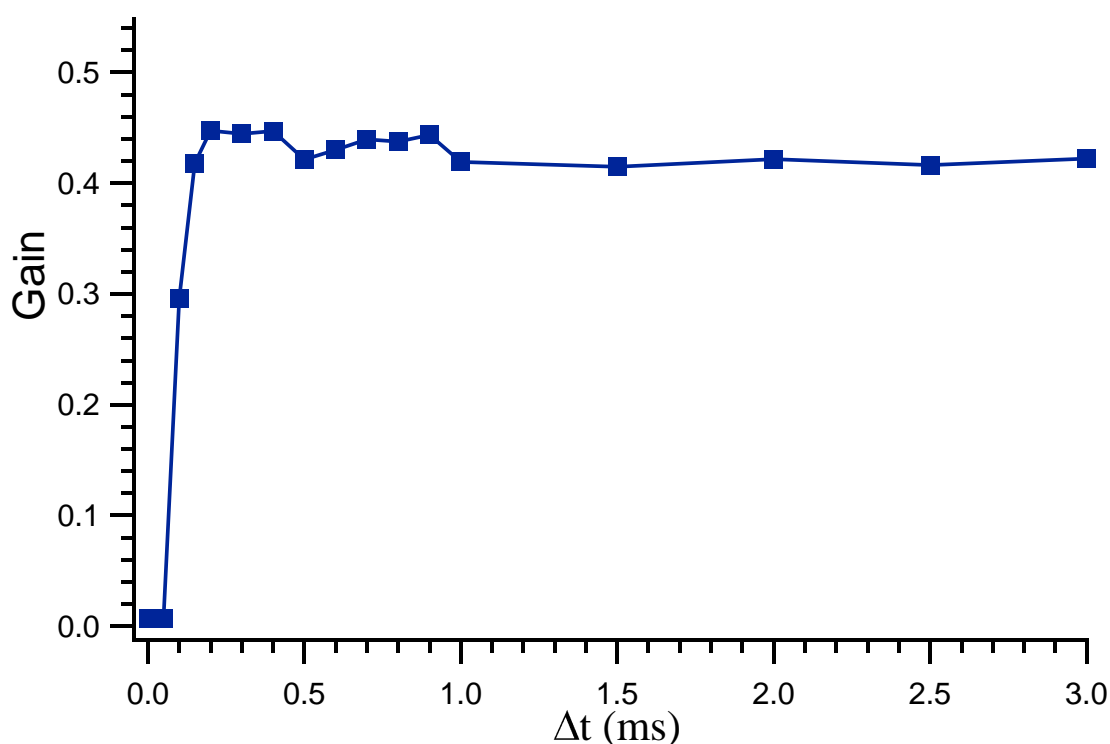
Figure 6.5: The gain in the photofragment signal, of phenylalanine conformer B, detected as a function of time delay between the IR and UV lasers, fixed in wavenumber. The IR laser is set to a vibrational transition of conformer A at 3122 cm^{-1} while the UV laser probes conformer B at 37 529.6 cm^{-1}.

On the other hand, excited PheH$^+$ ions have more internal energy (~ 3100 cm^{-1}) compared to the room temperature molecules that initially arrive at the trap with an internal energy estimated to 1852 cm^{-1}. While this additional energy allows the molecule to explore a wider region of the potential energy surface and in principle could make other deactivation pathways accessible, it is difficult to imagine how this would result in increased population in a conformer (B), which is not the lowest in energy. This fact could be verified if the transitions in the CO stretching region did not overlap. However we did not find any fundamental explanation for this unexpected result. This point will be discussed in more detail in *Section 6.3*.

116

It is interesting to extend this experiment to larger, flexible molecules to probe the isomerization dynamics following the excitation of specific vibration. We will show in the next sections the application of the infrared population transfer spectroscopy on peptides of 7- and 12 amino acid residues.

6.2.1.2 IRPT spectroscopy of Ac-Phe-(Ala)$_5$-Lys-H$^+$

The secondary structures of Ac-Phe-(Ala)$_5$-Lys-H$^+$ and its different intramolecular hydrogen bonding patterns were reported in section *4.2.2*. Spectroscopic studies together with DFT calculations inferred helical structures with α- or 3_{10} helix-like hydrogen bonded rings as the most stable conformers [25, 26], and this was confirmed by isotopic substitution. These studies reveal the existence of four conformers. The lowest energy conformer, D, contains two C_{10} and two C_{13} rings, and together with conformer C constitute backbone family I. The second-lowest-energy hydrogen-bonding pattern (conformer B) has three C_{10} rings and one C_{13} ring, and together with conformer A constitutes backbone family II. Within the same family the backbones are identical but the orientation of the phenylalanine side chain changes by rotation around the C_α-C_β bond. After the lowest energy minima were identified, we applied conformational isomerization spectroscopic techniques, initiating the transfer *via* vibrational excitation of a specific NH or CO stretch transition and detecting, after a delay time to allow collisional relaxation, the resulting distribution with a UV probe laser. The hole-filling spectroscopic studies described *Chapter 5* prove the possibility of the transferring population to conformers within the same family, which involves rotation of the phenylalanine side chain around the C_α-C_β bond, as well as between backbone families, which requires rearrangement of the helical backbone (breaking and forming hydrogen bonds). Here we present the results of infrared population transfer studies of cold Ac-Phe-(Ala)$_5$-Lys-H$^+$. The peptide ions were first irradiated with a scanned infrared laser followed 7 ms later with an UV probe laser fixed at the origin transition of a specific conformer. Figure 6.6 shows the infrared population transfer spectra (black) for all four conformers and their respective IR-UV spectra (red).
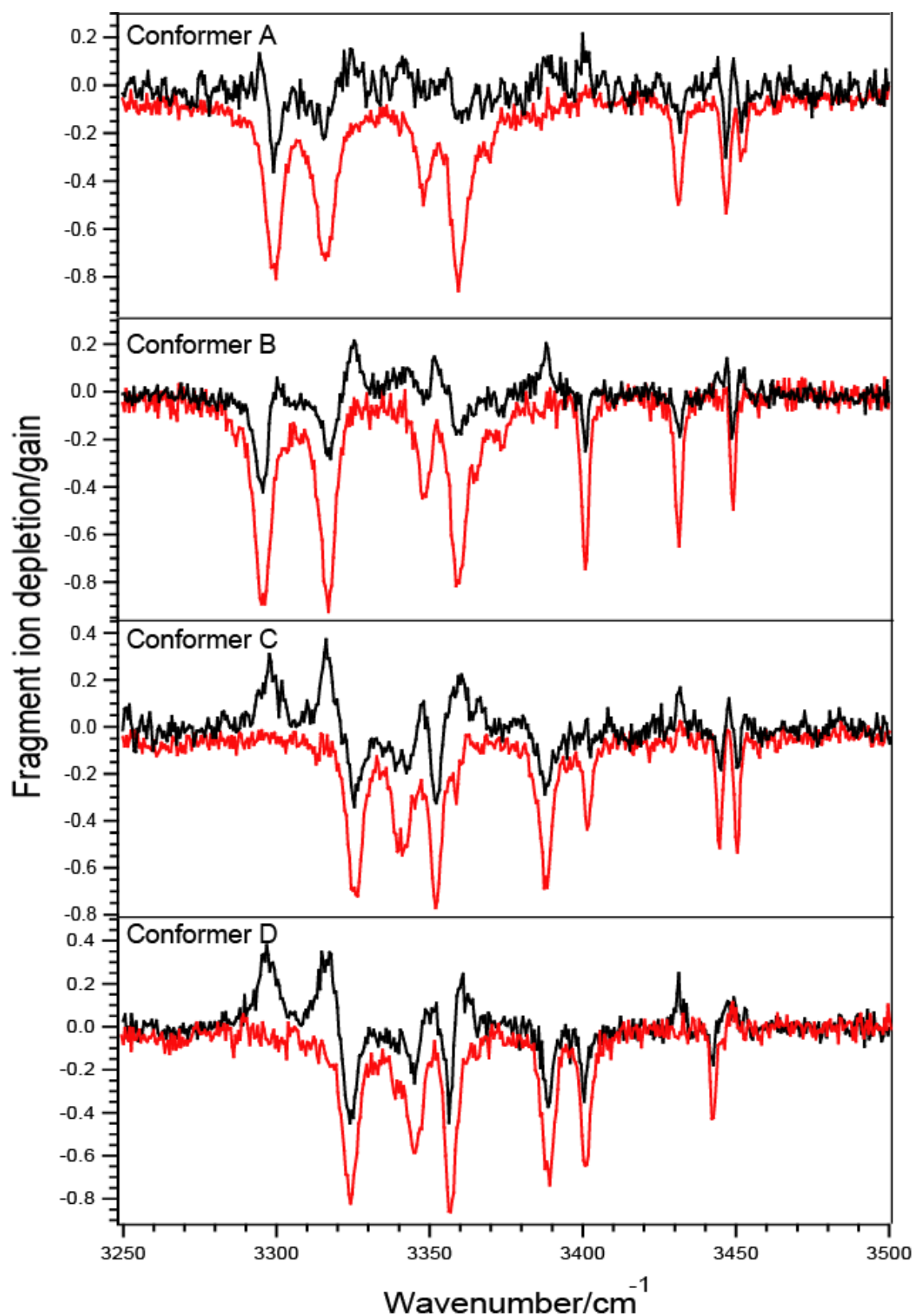
Figure 6.6: The black traces correspond to the infrared population transfer spectra of conformer A-D of Ac-Phe-(Ala)$_5$-Lys-H$^+$. The red traces are the IR-UV double resonance spectra of the respective conformers, taken under the same condition of the population transfer experiment.

The outcome of these population transfer experiments shows how the excited population redistributes itself for each IR absorption band. Gain signals in the spectra measure the additional population that the probed conformer gains from the relaxation of the excitation of another conformer (i.e., the one corresponding to each vibrational band). In the absence of overlapping IR bands, the depletion signals represent the amount population that is transferred from the probed conformer to the others. If there are overlapping bands in the IR spectrum, gains from the transfer in to the probed conformer may compensate the transfer of population out of this conformer, and the depletion will be less pronounced. The IR-UV spectra show that almost all the vibrational absorption bands are at least partially overlapped, due to the structural similarity between each pair of conformers (i.e. conformers within a given family). While we were able to find specific infrared wavenumbers to selectively excite individual conformers in this region for hole-filling spectroscopy (conformation A at 3447 cm^{-1}, conformation B at 3374 cm^{-1}, conformer C at 3444 cm^{-1} and conformer D at 3442 cm^{-1}), it is impossible to extract isomerization quantum yields using these partially overlapped transitions. In order to extract the quantum yields we need experimental determination of the intensities of the bands in each of the four infrared population transfer spectra, and in the partially overlapped transition every single value will include contributions from different conformers.

Even if these spectra do not allow us to extract the isomerization quantum yields, they are still of a great importance as they contain information on the fractional abundance of the four conformations in the 22-pole ion trap. The previously measured IR-UV hole-filling spectra demonstrate that the excited population is relaxed back to fill the zero energy levels of conformers A, B, C and D and hence show no evidence for the formation of new conformations. As a consequence, at all IR wavelengths the changes in population in the four conformers must sum to zero, satisfying the following equation: (c.f. annex A)

$$p_A.IRPTS_A + p_B.IRPTS_B + p_C.IRPTS_C + p_D.IRPTS_D = 0 \qquad Eq.6.7$$

where *IRPTS$_X$* represents to the intensity of the population transfer spectra at a given frequency and p_X the fractional population of conformer *X*. This equation is used to find the abundance of the four conformers in the absence of the infrared excitation. As shown in Figure 6.7, the black trace representing the weighted sum of infrared population transfer spectra is almost zero and thus Equation 6.6 is satisfied with the fractional population of conformers A-D:

$$p_A = 0.31 \pm 0.02$$

$$p_B = 0.34 \pm 0.02$$

$$p_C = 0.18 \pm 0.02$$

$$p_D = 0.17 \pm 0.02$$

with an error bars of ± 0.02. These fractional populations of different conformations are completely independent of the dissociation quantum yields or the electronic oscillator strengths of vibronic transitions in the photodissociation spectra of the conformers and thus represent a direct measurement of the conformational abundance of this peptide in the trap.
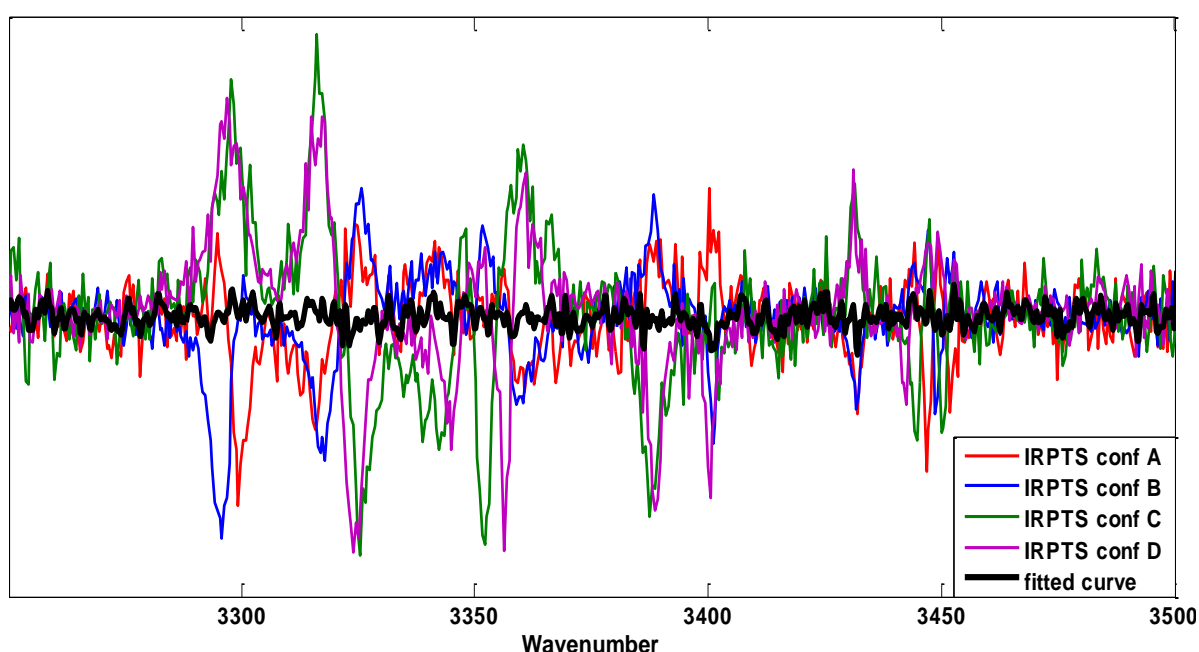
Figure 6.7: The back trace is the weighted sum of the infrared population transfer spectra of conformer A (red), B (blue) C (Green) and D (violet) of Ac-Phe-(Ala)$_5$-Lys-H$^+$.

The conformer assignments of the bands in the electronic spectrum of this molecule were made by comparing the corresponding conformer-specific infared spectra taken by IR-UV spectroscopy with calculated spectra [25, 26]. This procedure suggests conformation D to be the lowest in energy followed by conformers B, C and A with respective energies of 2.6, 4.2 and 6.8 kJ/mol higher than the global minimum. The conformational search was done using AMBER force field [27] in Macromodel [28] that gives an initial collection of over 1000 structures under 50 kJ/mol in energy, nearly all of which are helical. The choice of the force field was not driven by a particular reason, although it performed rather favorably in previous calculations on protonated amino acids and dipeptides [21, 29]. In calculations of

protonated amino acids, AMBER tends to overestimate the stabilizing effect of an NH … OH C_5 interaction at the C-terminus by about 15 kJ/mol, so all structures that had this type of interaction were eliminated from further consideration, retaining instead those with the more favorable NH … O=C C_5 structure. Single-point energies were calculated using B3LYP/6-31G** in Gaussian03 [30] for the remaining structures and a full geometry optimization and harmonic frequency analysis were performed on a subset that included all major degrees of flexibility of the backbone, the phenylalanine side-chain, and other flexible coordinates. In all, 45 structures were optimized, and vibrational frequencies were calculated for the 21 most stable of these. The energies we report are corrected for zero-point energies using the unscaled harmonic frequencies, while the hydride stretch frequencies are scaled by a factor of 0.952 for comparison to the measured infrared spectra. The theoretical and experimental spectra are in a good agreement, and to help test the accuracy of theoretical predictions, isotopic substitution experiments were performed [26]. However, the predicted relative conformational energies D<B<C<A are different from the experimental results described above, which proposes B-A<C-D. In conclusion, this energy difference may vary strongly between different force fields and DFT [31], and thus the results presented here provide an additional reference point that can be used to critically assess, compare, and improve the choice and parameterization of both methodologies, empirical force fields and DFT, used in biomolecular simulations.

Because of the overlapping of different bands in the IR spectra we were not able to extract the quantum yields to isomerization and thus we could not investigate the possibility of mode- or conformer-specific isomerization. In order to overcome this limitation one might think of investigating more flexible molecules, in which the lowest energy conformations may have very different structure and hence spectra. The next section presents infrared population transfer results of a twelve residue peptide that was designed with the objective of destabilizing the helical structure of the Ac-Phe-$(Ala)_n$-Lys-H$^+$ peptides [25, 26, 32] by the addition of four glycine residues.

6.2.1.3 IRPT spectroscopy of Ac-Phe-$(Ala)_3$-$(Gly)_4$-$(Ala)_3$-Lys-H$^+$

Using ion mobility spectrometry, Jarrold *et al.* reported a study of the formation of helical secondary structure from the solution phase *in vacuo* for a series of charged polyalanine peptides Ac- Ala_n-Lys-H$^+$ (*n*=5-20) [33]. Further studies followed to establish the nature of the helix by coupling ion-mobility cross-sections to molecular dynamics results [34-

38]. On the other hand, the combination of spectroscopic measurements with DFT and MP2 calculations has led to the identification of the helical structure exhibited by the alanine-based peptides [25, 26, 39, 40]. The key element for disturbing the helical shape of these alanine-based peptides is the addition of glycine, it is well known that this amino acid has a low helix-forming propensity [38, 41]. We thus substituted four alanines by four glycines in the 12-residue helical peptide Ac-Phe-(Ala)$_{10}$-Lys-H$^+$ [26] to tune the stability of the helical structure to the point where helical and non-helical conformers might have similar stability. On the theory side, we employ the AMBER force field to generate the initial conformational searches on the designed molecule, Ac-Phe-(Ala)$_3$-(Gly)$_4$-(Ala)$_3$-Lys-H$^+$, which gives an initial collection of both folded and unfolded conformers with similar energies under 50 kJ/mol. On the experimental side, however, the conformational-specific IR-UV spectra reveal no significant structural differences between the lowest energy minima of the glycine-containing peptide (c.f. *section 4.2.3*). Based on the common transitions in the amide II and amide A regions between these spectra and those of conformers C and D of Ac-Phe-(Ala)$_5$-Lys-H$^+$, we suggested that this molecule adopts a helical shape. While the substitution of four alanines by glycines does not seem to destabilize the helical structure, it is still interesting to investigate the dynamics of this molecule following selectively vibrational excitation. The hole-filling spectra show that the photon energy of the infrared excitation is able to move population between the minima that had already population in them. The nonappearance of any new minima means that there is no net change in the population of the two conformers, and thereby one can extract their fractional populations by measuring infrared population transfer spectra.

Figure 6.8 presents the population transfer spectra of Ac-Phe-(Ala)$_3$-(Gly)$_4$-(Ala)$_3$-Lys-H$^+$. The red and blue curves were recorded by fixing the UV probe laser wavenumber at the origin transition of conformer A and B respectively and scanning the IR, with a time delay of 7 ms between the lasers. The black curves underneath are the corresponding IR-UV double resonance spectra recorded by firing both lasers after 20 ms of the arrival of the ions into the trap, with a delay of 200 ns.
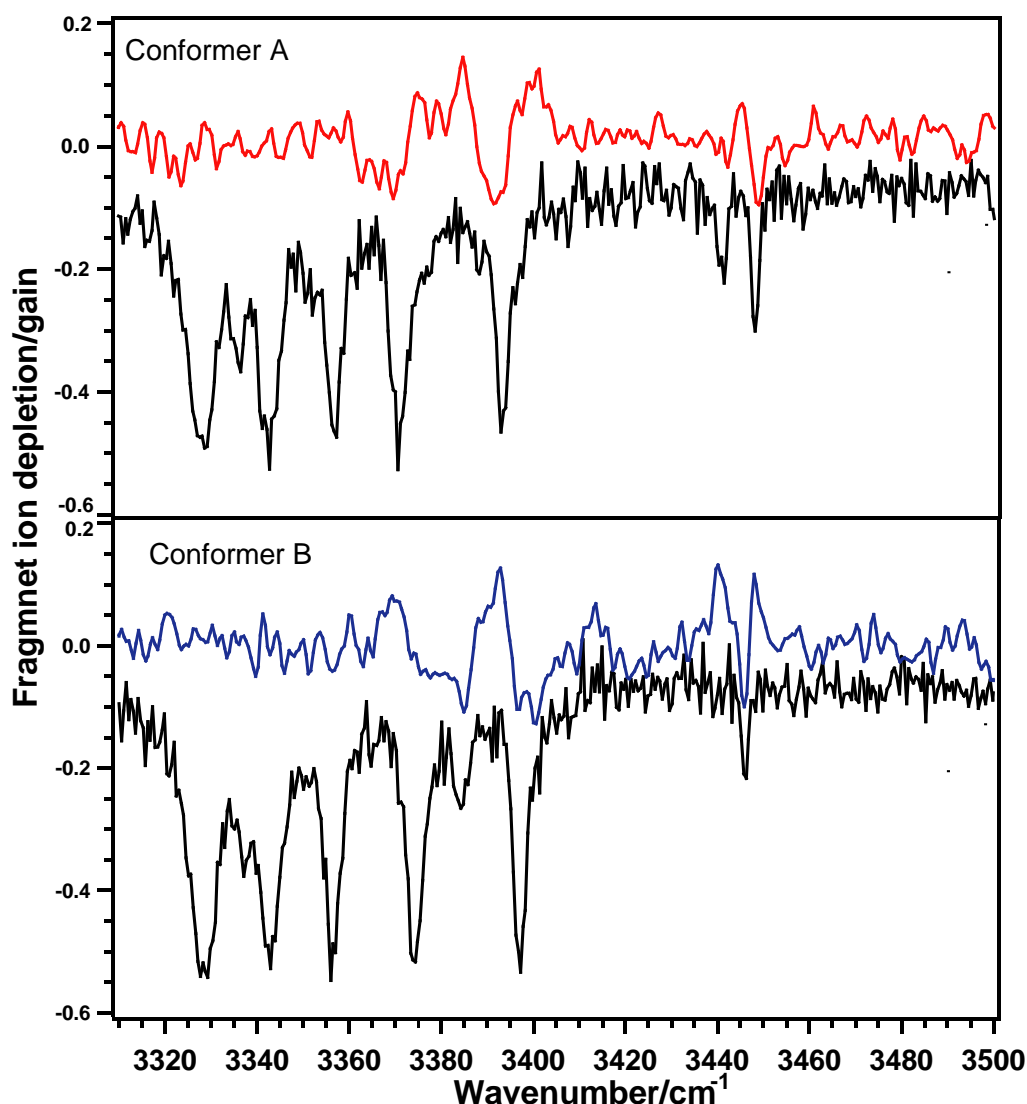
Figure 6.8: Infrared population transfer spectra of conformer A (red) and B (blue) of Ac-Phe-(Ala)$_3$-(Gly)$_4$-(Ala)$_3$-Lys-H$^+$. The black traces correspond to the IR-UV double resonance spectra of the respective conformers, taken under the same condition of the population transfer experiment.

The black trace in Figure 6.9 is the weighted sum of the population transfer spectra of the two conformations A and B, satisfying equation 6.1 over the entire wavelength range:

$$p_A.IRPTS_A + p_B.IRPTS_B = 0$$

with $IRPTS_X$ the intensity of the population transfer spectra at a given frequency and p_X the fractional population of conformer X. The fractional populations for conformation of A and B are $p_A = 0.51$ and $p_B = 0.49$, respectively, with an error of ±0.03. This additional information on the conformational abundance could be useful for the theoretical simulations since the conformational structure should be, in addition to the similarity of the helical backbone, very close in energy. This was also observed in the case of the previous molecule

Ac-Phe-(Ala)$_5$-Lys-H$^+$, where conformers within the same family having identical backbones had nearly equal fractional populations.
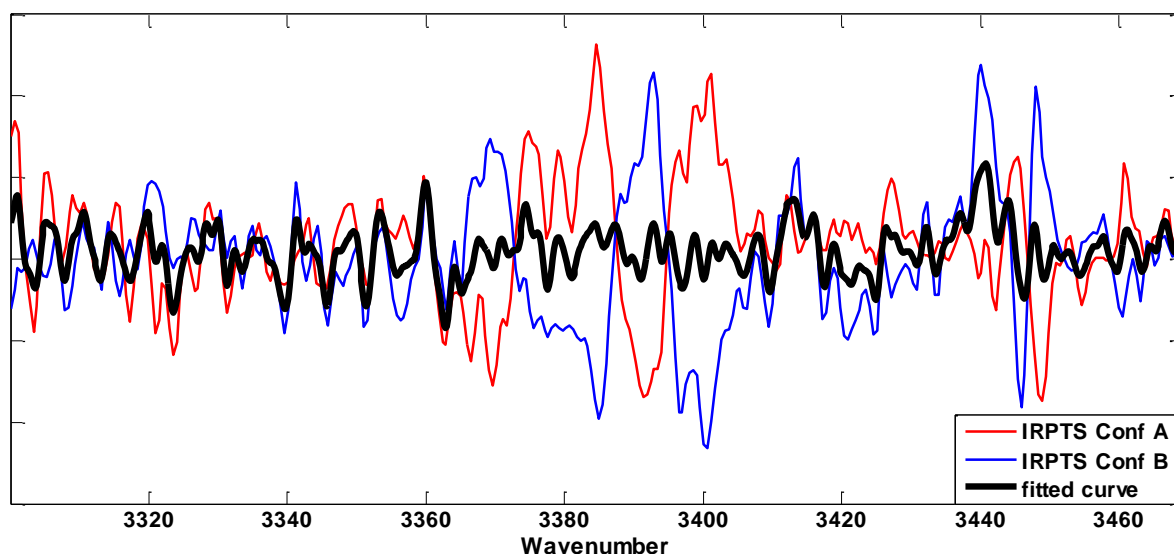
Figure 6.9: The back trace is the weighted sum of the infrared population transfer spectra of conformer A (red) and B (blue) of Ac-Phe-(Ala)$_3$-(Gly)$_4$-(Ala)$_3$-Lys-H$^+$.

In the region below 3380 cm^{-1} corresponding to strongly hydrogen bonded NH groups, the transitions in both spectra severely overlap, and due to this fact, no net gains or depletions are clearly observed in the IR-population transfer spectra. If both NH stretches of conformation A and B are pumped simultaneously, it is evident that after relaxation the excited populations refilled equally the lowest minima. In order to induce a large population change one has to selectively pump vibrations. At the highest energy, we could isolate vibrations specific for a particular conformation: A at 3448 cm^{-1} and B at 3384 and 3054 cm^{-1}, and thus extract the quantum yields to isomerization making use of the set of equations developed in Annex A and reported in the first part of this chapter (equations 6.3 and 6.4). Table 6.2 and Figure 6.10 present the quantum yields for conformer A and B of Ac-Phe-(Ala)$_3$-(Gly)$_4$-(Ala)$_3$-Lys-H$^+$. The values are quite similar to one another within the error bars, which are somewhat large due to the low fragmentation yields of this molecule. At the same time these values are close to the fractional populations of the conformers in the absence of infrared excitation. This resemblance mainly means that the energy deposited in the NH stretching mode of a particular structure is rapidly redistributed among all the modes *via* intramolecular vibrational relaxation (IVR) and the isomerization process guides the population to the equilibrium distribution. As mentioned previously, the conformers should have similar energy, and since they receive almost equal amounts of energy by vibrational

124

excitation, it is not surprising that all transitions in both conformers would distribute their excited population in an identical way under the low density of buffer gas (i.e., slow cooling conditions) in the 22-pole ion trap. Contrary to the case of the protonated phenylalanine, this molecule did not show any evidence for conformation selectivity. We cannot provide specific information on the pathway of the energy relaxation in this large molecule, but it is likely that energy dissipation and isomerization process adopt the same pathways in dictating the population redistribution as for cooling the room temperature molecule.

	Isomerization quantum yields for Ac-Phe-$(Ala)_3$-$(Gly)_4$-$(Ala)_3$-Lys-H$^+$		
	Conformer A	Conformer B	
Quantum yields	**3448 cm^{-1}**	**3384 cm^{-1}**	**3446 cm^{-1}**
Φ_{XA}	0.58±0.15	0.52±0.14	0.52±0.16
Φ_{XB}	0.42±0.16	0.48±0.15	0.48±0.14

Table 6.2: IR-induced isomerization quantum yields for Ac-Phe-(Ala)3-(Gly)4-(Ala)3-Lys-H+. $\Phi_{XA/B}$ is the quantum yield for formation of conformer A/B following IR excitation of conformer X. Quantum yields have been normalized so that their sum equals 1.
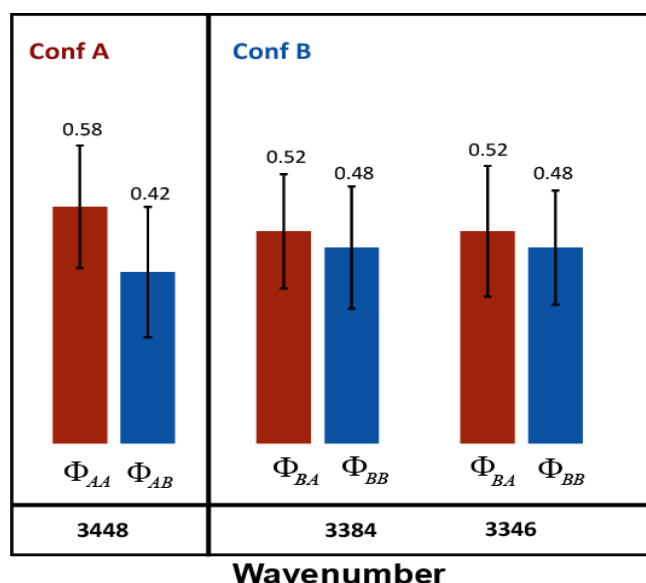
Figure 6.10: Quantum yields for isomerization following IR excitation of the indicated NH stretch of conformation A and B Ac-Phe-(Ala)3-(Gly)4-(Ala)3-Lys-H+. Φ_{xy} is the quantum yield for formation of conformer y following IR excitation of conformer x.

6.3 Comparison between the isomerization quantum yields

The isomerization dynamics of molecules of different size were studied through infrared population transfer techniques. The isomerization process after the absorption of an infrared photon showed quite different behavior in the single amino acid phenylalanine and the 12-residue peptide Ac-Phe-$(Ala)_3$-$(Gly)_4$-$(Ala)_3$-Lys-H$^+$. In the case of PheH$^+$, the quantum yields extracted seem to indicate evidence of conformational selectivity. The excited molecules out of conformer A are redistributed in such a way as to form mostly the lowest energy conformation (which is conformer A), and the final population distribution is almost the same as in the absence of IR excitation. Upon exciting different NH stretches of conformer B, however, the energy dissipation and isomerization process drives 70% of the excited molecules back to form conformer B instead of reaching the "equilibrium" distribution (that is, the distribution formed in the initial cooling process of room temperature molecules). For the larger molecule, Ac-Phe-$(Ala)_3$-$(Gly)_4$-$(Ala)_3$-Lys-H$^+$, the quantum yields after IR excitation are such that they produce the same population distribution as in the initial cooling process (i.e., in the absence of infrared), with no conformational selectivity.

Conformational specificity in the quantum yields would only be possible if on the time it takes for the molecule to be recooled collisionally, IVR would be complete within a given conformational well but not fully complete between wells of other minima. In other words, coupling to states that have character of other conformational isomers would have to be slow on the timescale of collisional cooling. In this case the cooling will capture the isomerization process in different ways if the isomerization is initiated through conformation specific vibrational excitation from different conformational wells. This appears to be what we observe in the quantum yields of PheH$^+$. Nevertheless, given the long time scale of collisional cooling in our experiment, which is in order of tens of µs, it is difficult to imagine that energy could be trapped in a particular conformer for that long. It is not clear why with such a slow cooling rate we detect conformational specificity in the case of phenylalanine. To help us rule out any systematic error in our determination of the isomerization yields, we compare the overall behavior of protonated phenylalanine with that of Ac-Phe-$(Ala)_3$-$(Gly)_4$-$(Ala)_3$-Lys-H$^+$. The absence of such behavior in the case of the glycine containing peptide, even though its quantum yields were extracted using the same equations as in the case of the single amino acids, suggests that the treatment of the data is correct. Perhaps our assumption of $\gamma=1$ (the overlap factor) is incorrect – could this distort the quantum yield results for protonated

phenylalanine? From the experimental spectra we could put a lower limit on this factor of 0.7, and while within this limit γ will have an impact on the value of the quantum yields, it does not affect the overall picture and thus could not be the cause the mode specificity seen in PheH$^+$. Moreover, the experimental procedure followed to maximize the laser overlap was identical for the set of population transfer experiments of different molecules studied in this thesis. These also reduce the possibility of any experimental manipulation leading to the conformational specificity in case of phenylalanine.

Even though the number of internal modes and the complexity of the two systems are not comparable, we should point out that the difference in excitation energy relative to the initial thermal energy is largely different in case of both molecules. The energy gained by the protonated phenylalanine from the excitation of the NH stretches is about the double of what it has at room temperature when it first arrives at the cold ion trap, while the energy put into Ac-Phe-(Ala)$_3$-(Gly)$_4$-(Ala)$_3$-Lys-H$^+$ *via* excitation at 3400 cm^{-1} is about five times lower than the internal energy of the room temperature molecule (16'000 cm^{-1}). Conclusions regarding the unusual result in protonated phenylalanine may have to await both more extensive calculations as well as additional test experiments.

6.4 Conclusion

Having already demonstrated the feasibility of the population transfer experiments in the 22-pole ion trap and its application on large protonated molecules in *Chapter 5*, we presented here in *Chapter 6* the results or products of conformational isomerization induced by infrared excitation. From these experimental data we first extracted the fractional population of different conformations of the investigated molecules. This piece of information is of great importance for the theoretical work, as it furnishes additional critical information that would be extremely useful to compare and improve the parameterization of empirical force fields and the accuracy of DFT functionals, both of which are used in simulating biomolecular structures. The combination of force field and DFT basis set in the case of phenylalanine predicts the structural conformation with the right energetic order; the global minimum determined theoretically (conformer A) had the highest abundance extracted experimentally. For the helical seven residue peptide, the fractional abundances determined by the IRPT spectra indicate a similar abundance for conformations within the same backbone

family. From the extracted values we can conclude that backbone family II has higher fractional population than backbone family I, and, if the molecules are fully annealed, should be of lower energy. This suggested order of conformational stability based on the fractional populations differs from that proposed by our theoretical simulations, meaning that this later was good enough in assigning the structure but not in predicting their energy order. The third system reported here is the twelve residue peptide, whose extracted fractional populations suggest an equal partitioning between its two stable conformations that should have barely similar structures.

In addition to allowing us to extract absolute conformer populations, the infrared population transfer spectra enable us to probe the dynamics of isomerization following the excitation of single vibrational modes of specific conformation. In association with IR spectra taken under the same conditions, the IRPT spectra allow the extraction of the isomerization quantum yields subsequent to excitation of different NH stretches in PheH$^+$ and Ac-Phe-(Ala)$_3$-(Gly)$_4$-(Ala)$_3$-Lys-H$^+$. Depending on which conformation was excited, protonated phenylalanine showed distinguishable isomerization patterns revealing a conformational specificity. This may suggest the existence of different pathways on its energy landscape that could be accessible at different internal energies. Theoretical studies on the accessible pathways between the minima on the potential energy surface at different excitation energies would help in drawing better picture of the dynamics in this molecule. In the case of Ac-Phe-(Ala)$_3$-(Gly)$_4$-(Ala)$_3$-Lys-H$^+$, the conformational distribution produced after the IR excitation is the same as in the initial cooling step from room temperature.

References

1.   G. Gershinsky, E. Pollak, *Phys. Chem. Chem. Phys.* **107**, 812 **1997**.
2.   F. F. Crim, *Annu. Rev. Phys. Chem.* **35**, 657 **1984**.
3.   J. S. Baskin, L. Banares, S. Pedersen, A. H. Zewail, *J. Phys. Chem.* **100**, 11920 **1996**.
4.   D. Green, S. Hammond, J. Keske, B. H. Pate, *Phys. Chem. Chem. Phys.* **110**, 1979 **1999**.
5.   D. A. McWhorter, E. Hudspeth, B. H. Pate, *Phys. Chem. Chem. Phys.* **110**, 2000 **1999**.
6.   M. Gruebele, P. G. Wolynes, *Acc. Chem. Res.* **37**, 261 **2004**.
7.   T. Ebata, K. Kouyama, N. Mikami, *Phys. Chem. Chem. Phys.* **119**, 2947 **2003**.
8.   P. N. Mortenson, D. J. Wales, *Phys. Chem. Chem. Phys.* **114**, 6443 **2001**.
9.   B. C. Dian, A. Longarte, T. S. Zwier, *Science* **296**, 2369 **2002**.
10. B. C. Dian, G. M. Florio, J. R. Clarkson, A. Longarte, T. S. Zwier, *Phys. Chem. Chem. Phys.* **120**, 9033 **2004**.

11. D. A. Evans, D. J. Wales, B. C. Dian, T. S. Zwier, *Phys. Chem. Chem. Phys.* **120**, 148 **2004**.
12. T. S. Zwier, *J. Phys. Chem. A* **110**, 4133 **2006**.
13. S. J. Martinez, J. C. Alfano, D. H. Levy, *J. Mol. Spectrosc.* **156**, 421 **1992**.
14. L. C. Snoek, E. G. Robertson, R. T. Kroemer, J. P. Simons, *Chem. Phys. Lett.* **321**, 49 **2000**.
15. Y. Lee, J. Jung, B. Kim, P. Butz, L. C. Snoek, R. T. Kroemer, J. P. Simons, *J. Phys. Chem. A* **108**, 69 **2004**.
16. A. Kaczor, I. D. Reva, L. M. Proniewicz, R. Fausto, *J. Phys. Chem. A* **110**, 2360 **2006**.
17. Z. Huang, W. Yu, Z. Lin, *Journal of Molecular Structure: THEOCHEM* **758**, 195 **2006**.
18. G. v. Helden, I. Compagnon, M. N. Blom, M. Frankowski, U. Erlekam, J. Oomens, B. Brauer, R. B. Gerber, G. Meijer, *PCCP* **10**, 1248 **2008**.
19. Y. Lee, J. Jung, B. Kim, P. Butz, L. C. Snoek, R. T. Kroemer, J. P. Simons, *J. Phys. Chem. A* **108**, 69 **2003**.
20. T. Hashimoto, Y. Takasu, Y. Yamada, T. Ebata, *Chem. Phys. Lett.* **421**, 227 **2006**.
21. J. A. Stearns, S. Mercier, C. Seaiby, M. Guidi, O. V. Boyarkin, T. R. Rizzo, *J. Am. Chem. Soc.* **129**, 11814 **2007**.
22. B. C. Dian, A. Longarte, P. R. Winter, T. S. Zwier, *Phys. Chem. Chem. Phys.* **120**, 133 **2004**.
23. J. K. Agbo, D. M. Leitner, D. A. Evans, D. J. Wales, *Phys. Chem. Chem. Phys.* **123**, 124304 **2005**.
24. S. Mercier, Ph.D Thesis, EPFL **2008**.
25. J. A. Stearns, O. V. Boyarkin, T. R. Rizzo, *J. Am. Chem. Soc.* **129**, 13820 **2007**.
26. J. A. Stearns, C. Seaiby, O. V. Boyarkin, T. R. Rizzo, *PCCP* **11**, 125 **2009**.
27. W. D. Cornell, P. Cieplak, C. I. Bayly, I. R. Gould, n. Jr, D. M. Ferguson, D. C. Spellmeyer, T. Fox, J. W. Caldwell, P. A. Kollman, *J. Am. Chem. Soc.* **117**, 5179 **1995**.
28. . (vesion 9.1; Schrödinger LLC:New York 2005).
29. J. A. Stearns, M. Guidi, O. V. Boyarkin, T. R. Rizzo, *Phys. Chem. Chem. Phys.* **127**, 154322 **2007**.
30. G. W. T. M. J. Frisch, H. B. Schlegel, G. E. Scuseria, M. A. Robb, J. R. Cheeseman, J. J. A. Montgomery, T. Vreven, K. N. Kudin, J. C. Burant, J. M. Millam, S. S. Iyengar, J. Tomasi, V. Barone, B. Mennucci, M. Cossi, G. Scalmani, N. Rega, G. A. Petersson, H. Nakatsuji, M. Hada, M. Ehara, K. Toyota, R. Fukuda, J. Hasegawa, M. Ishida, T. Nakajima, Y. Honda, O. Kitao, H. Nakai, M. Klene, X. Li, J. E. Knox, H. P. Hratchian, J. B. Cross, V. Bakken, C. Adamo, J. Jaramillo, R. Gomperts, R. E. Stratmann, O. Yazyev, A. J. Austin, R. Cammi, C. Pomelli, J. W. Ochterski, P. Y. Ayala, K. Morokuma, G. A. Voth, P. Salvador, J. J. Dannenberg, V. G. Zakrzewski, S. Dapprich, A. D. Daniels, M. C. Strain, O. Farkas, D. K. Malick, A. D. Rabuck, K. Raghavachari, J. B. Foresman, J. V. Ortiz, Q. Cui, A. G. Baboul, S. Clifford, J. Cioslowski, B. B. Stefanov, G. Liu, A. Liashenko, P. Piskorz, I. Komaromi, R. L. Martin, D. J. Fox, T. Keith, M. A. Al-Laham, C. Y. Peng, A. Nanayakkara, M. Challacombe, P. M. W. Gill, B. Johnson, W. Chen, M. W. Wong, C. Gonzalez, and J. A. Pople,. (Gaussian, Inc.: Pittsburgh, PA, 2003).
31. E. Penev, J. Ireta, J.-E. Shea, *The Journal of Physical Chemistry B* **112**, 6872 **2008**.
32. J. A. Stearns, O. V. Boyarkin, T. R. Rizzo, *CHIMIA* **62**, 240 **2008**.
33. R. R. Hudgins, M. A. Ratner, M. F. Jarrold, *J. Am. Chem. Soc.* **120**, 12974 **1998**.
34. R. R. Hudgins, M. F. Jarrold, *J. Am. Chem. Soc.* **121**, 3494 **1999**.
35. M. Kohtani, M. F. Jarrold, *J. Am. Chem. Soc.* **126**, 8454 **2004**.

36. M. Kohtani, T. C. Jones, J. E. Schneider, M. F. Jarrold, *J. Am. Chem. Soc.* **126**, 7420 **2004**.
37. M. Kohtani, B. S. Kinnear, M. F. Jarrold, *J. Am. Chem. Soc.* **122**, 12377 **2000**.
38. M. F. Jarrold, *PCCP* **9**, 1659 **2007**.
39. T. D. Vaden, T. S. J. A. de Boer, J. P. Simons, L. C. Snoek, S. n. Suhai, B. l. Paizs, *J. Phys. Chem. A* **112**, 4608 **2008**.
40. A. Cimas, T. D. Vaden, T. S. J. A. de Boer, L. C. Snoek, M. P. Gaigeot, *J. Chem. Theory Comput.* **5**, 1068 **2009**.
41. C. Nick Pace, J. Martin Scholtz, *Biophys. J.* **75**, 422 **1998**.

Chapter 7

Conclusions and perspectives

This thesis investigated the energy landscapes and conformational dynamics of biological molecules in a cold ion trap using a variety of photofragmentation-based double-resonance techniques. In the first part, spectroscopic studies in the Amide A, I and II stretch region provided information about local minima on the potential energy surfaces of the different systems studied, starting from the single amino acid phenylalanine and moving to molecules of increasing size: the 7-residue peptide Ac-Phe-$(Ala)_5$-LysH$^+$ and the 12-residue peptide Ac-Phe-$(Ala)_3$-$(Gly)_4$-$(Ala)_3$-LysH$^+$. The second part focuses on the conformational isomerization of these molecules, implementing infrared and ultraviolet hole-filling spectroscopy. In the last chapter, the fractional conformer populations and the isomerization quantum yields are determined through infrared-induced population transfer spectroscopy.

The study of the phenylalanine infrared spectra, in combination with DFT calculations, allowed the identification of two stable conformations that differ in the orientation of the backbone with respect to the ring by a rotation of the angle χ_1 [1]. In the case of the lysine-capped polyalanine peptide, the lowest energy conformer adopts a helical three-dimensional structure, and thus the presence of the phenylalanine chromophore does not change the helical shape predicted by the ion mobility studies [2, 3]. The measured infrared spectra, in comparison with theoretical simulations and isotopic substitution experiments, allowed the identification of four helical conformers that are sorted out in two families according to the hydrogen-bonding scheme of their peptide backbone [4, 5]. The NH, CO and OH stretch vibrations have proven to be sensitive probes of hydrogen bonding (or the lack thereof) and thus of the folding of the peptide backbone in these structures. These fingerprints

are used to suggest a helical shape for the most stable conformer of the glycine containing peptide, which is too large for us to compare with theory. The spectroscopic evidence thus suggests that the addition of four glycines was not enough to disturb the helical structure of a lysine-capped polyalanine helix. Also the number of detected conformers decreased from four to two, which may indicate an increased tendency to relax to the global minimum -- behavior that was also reported by Bakker et al. using IR-UV double-resonance spectra of jet-cooled Trp, Trp-Gly and Trp-Gly-Gly [6].

In the second part of this thesis we demonstrated the feasibility of infrared hole-filling spectroscopy in the 22-pole ion trap. This method was initially developed in the Zwier group to probe the isomerization of neutral biomolecules cooled in a supersonic expansion [7]. For the systems investigated here, an infrared excitation that selectively interacts with a single conformation was able to create a new population distribution among the conformations initially having population in them (i.e., in the absence of the IR). Vibrational relaxation to the buffer gas cannot compete with the early stages of isomerization (i.e., IVR), but it is likely that towards the end of the sequence such a competition may occur and the molecule gets trapped kinetically, and this is proven by the detection of population in several stable minima. Nevertheless, the relaxation process after IR excitation did not lead to the formation of any new conformational minima, even though in the case of the single amino acid the excited molecule had double the amount of internal energy of the room temperature molecule initially arriving in the trap. Such a result is perhaps not surprising for the two larger peptides, since the amount of internal energy gained *via* the infrared excitation is approximately 3 times less than that of room temperature molecules. After infrared excitation, it appears that the recooling process follows a similar path as the initial cooling of the room temperature molecules. We also attempted to use infrared hole-filling spectroscopy to probe the height of the isomerization barrier in Ac-Phe-(Ala)$_5$-LysH$^+$. In order to define a tighter upper limit to this barrier, we went to the mid-infrared region and selectively pumped the CO vibrational transition of conformation B of this molecule. The fact that we were still able to induce conformational isomerization means that the barrier for this process is less than 1654 cm^{-1}.

We attempted to probe the excited-state isomerization dynamics of the peptides using a UV-UV hole-filling method. The activated molecule could dissociate on the electronic excited state or undergo internal conversion and dissociate on the electronic ground state. We attempted to observe whether subsequent to UV excitation and recooling some molecules might form new conformations as internal conversion would allow the exploration of a much

wider part of the potential energy surface. Since no new conformational minima were observed, we could not tell whether this means that the fraction of excited molecules that dissociate following internal conversion to the ground state is small or whether even with this large amount of internal energy the cooling process results in the same conformational distribution. A further elaboration of this work might be the study of molecules that act as photo-switches, in particular these peptides can switch conformation in solution either by changing pH or by irradiation with light [8]. In the case of the UV switch peptide, a bulky side chain is broken, and this might make a large conformation change that could easily be detected. This type of molecules is used to investigate biological dynamics and get insight about the mechanism of folding and aggregation that occurs in living cells [8, 9].

We extracted fractional populations of different conformations of the three molecules we studied in a cold 22-pole ion trap. These quantities are independent of the dissociation quantum yields or oscillator strengths of the vibronic transitions in the photodissociation spectra of the different conformers, and thus correspond to the fractional abundance of the conformers. The combination of different force fields, DFT functionals and basis sets may be sufficient to help assign the infrared spectra, but they seem not to be particularly accurate for predicting the relative conformer energies. These fractional population values thus provide valuable information that could help improve the theoretical modeling of peptides. In the case of protonated phenylalanine, the level of theory used was good enough to assign the structures and predict their relative energy ordering, but in the case of the seven-residue peptide the theoretical studies need to be improved in this respect.

Finally, in this work we presented quantitative data concerning isomerization quantum yields that reflect the dynamics of conformational isomerization following the excitation of single vibrational modes of a specific conformation. Surprising results on protonated phenylalanine show evidence of conformational selectivity. The excited molecules out of a specific conformer are redistributed in a way to form mostly the same conformer. Although it might be that the additional amount of energy deposited in the excited molecule opens different pathways on the potential energy surface than those adopted by the room temperature molecule and hence drives the population into the well of the excited conformer. The overlapping of the transitions in the CO stretching region did not allow us to selectively excite a single conformer in order to confirm this speculation. However the extracted quantum yields of Ac-Phe-$(Ala)_3$-$(Gly)_4$-$(Ala)_3$-LysH$^+$ reflect an equilibrium distribution independent of which conformation is excited. In this case, energy dissipation and isomerization results in

133

the same conformational distribution as the initial cooling process from room temperature, perhaps implying that the excited molecules follow the same pathways after IR excitation as they do initially.

One of the limitations in applying these techniques is the overlapping of the vibrational bands in the spectra of different conformations. It would therefore be useful to separate the conformers prior to their entrance in the mass spectrometer. We expected to achieve this type of separation by coupling a Field Asymmetric Ion Mobility Spectrometer (FAIMS) [10] to our tandem mass spectrometer. If then we allow the transmission of only a single conformer through FAIMS, the hole filling experiment will be conducted on a zero background, and this will make the detection of the new conformational distribution much more sensitive. In addition, this zero background will provide the possibility to selectively excite out of what would otherwise be overlapped transitions, which will greatly increase the applicability of this technique to larger molecules.

On the other hand, adding FAIMS to our machine might give insight into the processes that the ions undergo during their separation in this device, since we are able to give structural details by double resonance techniques, and hence better understand the mechanism of ion separation in FAIMS. However, one must address the possibility of interconversions of the conformer-selected ions after being selected by FAIMS. This drawback is currently being addressed in our group.

References

1. J. A. Stearns, S. Mercier, C. Seaiby, M. Guidi, O. V. Boyarkin, T. R. Rizzo, *J. Am. Chem. Soc.* **129**, 11814 **2007**.
2. R. R. Hudgins, M. F. Jarrold, *J. Am. Chem. Soc.* **121**, 3494 **1999**.
3. M. F. Jarrold, *PCCP* **9**, 1659 **2007**.
4. J. A. Stearns, O. V. Boyarkin, T. R. Rizzo, *J. Am. Chem. Soc.* **129**, 13820 **2007**.
5. J. A. Stearns, C. Seaiby, O. V. Boyarkin, T. R. Rizzo, *PCCP* **11**, 125 **2009**.
6. J. M. Bakker, C. Plützer, I. Hünig, T. Häber, I. Compagnon, G. v. Helden, G. Meijer, K. Kleinermanns, *ChemPhysChem* **6**, 120 **2005**.
7. B. C. Dian, A. Longarte, T. S. Zwier, *Science* **296**, 2369 **2002**.
8. A. Taniguchi, Y. Sohma, M. Kimura, T. Okada, K. Ikeda, Y. Hayashi, T. Kimura, S. Hirota, K. Matsuzaki, Y. Kiso, *J. Am. Chem. Soc.* **128**, 696 **2005**.
9. S. Dos Santos, A. Chandravarkar, B. Mandal, R. Mimna, K. Murat, L. Saucède, P. Tella, G. Tuchscherer, M. Mutter, *J. Am. Chem. Soc.* **127**, 11888 **2005**.
10. R. W. Purves, R. Guevremont, *Anal. Chem.* **71**, 2346 **1999**.

Appendix A

This appendix contains the development of the equations used to extract the fractional population and the quantum yields to isomerization.

1.   Extracting the fractional population

The IR-population transfer spectrum detects the population changes induced in a single conformation by the absorption of an IR photon. Consider the case of a molecule with population in three stable conformations in the ion trap, labeled A, B and C. If the hole-filling spectra of all the stable conformers of a given molecule do not show evidence of any new minima, this will mean that there is no change in the total ion population and the following equation will be satisfied:

$$\Phi_{XA} + \Phi_{XB} + \Phi_{XC} = 1 \qquad\qquad Eq.1$$

where Φ_{XY} is the isomerization quantum yield going from conformer X to conformer Y.

The peak intensity of an IR-population transfer spectrum is given by subtracting the IR laser-on signal and IR laser-off signal and dividing it by the IR off signal acquired almost simultaneously. If the IR pulse is fixed at a wavenumber at which all three conformers absorb, the UV pulse is tuned to conformer A, and there is enough time for the absorbed IR energy to be completely dissipated and the ions to be redistributed in the trap, the IR-population transfer peak intensity will be given by:

$$IRPTS_A = \frac{F_{A:UV,IR} - F_{A:UV}}{F_{A:UV}} \qquad\qquad Eq.2$$

where,

$F_{A:UV}$ is the total number of fragment ions from conformer A; and

135

$F_{A:UV,IR}$ is the total number of fragment ions from conformer A after cooling the IR excitation.

Assuming that N ions are trapped and the UV is tuned to a transition of conformer A, the rate equation for the fragmentation of this conformation is obtained by integrating in cylindrical coordinates over the rate equation for spatial conformation density in the trap (in this case conformation A):

$$\frac{dF_{A:UV}}{dt} = \varepsilon_A \cdot \int \sigma_{A,UV} \cdot \Omega_{UV} \cdot N_A \, r dr d\phi dz \qquad \text{Eq.3}$$

where ε_A and N_A is the fragmentation quantum yield of ions in conformation A and the number of ions in conformation A, which could be expressed by $N_A = N.p_A$, with p_A the fractional population of ions in conformation A. $\sigma_{A,UV}$ is the absorption cross section at the utilized laser wavelength. Ω_{UV} is the photon flux density of the UV laser that is considered to be constant along the laser beam parallel to the z axis and is given by

$$\Omega_{UV} = \frac{E_{UV}}{A_{UV}.\tau_{UV}.\hbar\omega} \qquad \text{Eq.4}$$

Where,

τ_{UV} is UV the laser pulse duration.

A_{UV} is the area of the UV laser beam.

E_{UV} is the pulse energy of the UV laser pulse.

If we consider the cylindrical symmetry for the trapping potential, Figure 1, the ion density becomes independent of the angle ϕ. Assuming further a dilute ion cloud with negligible ion-ion interaction the integration of the density over the z axis lead to the integration over the ion column density ρ, with $\rho = \frac{1}{A_{ion}}$, $\int \rho dA = 1$
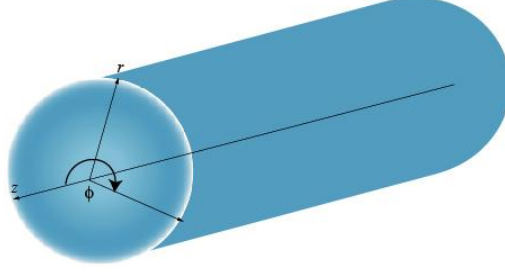
Figure 1: Illustration of the cylindrical ion cloud in the trap.

In this case Equation *3* is given by:

$$\frac{dF_{A:UV}}{dt} = \varepsilon_A \cdot \sigma_{A,UV} \cdot p_A \cdot N \cdot \frac{E_{UV}}{A_{ion} \cdot \hbar\omega_{UV} \cdot \tau_{UV}} \qquad Eq.5$$

The total number of fragments will be the integral of the fragmentation rate over the laser pulse time and is obtained by the following expression:

$$F_{A:UV} = \frac{dF_{A:UV}}{dt} \cdot \tau_{UV} = \varepsilon_A \cdot \sigma_{A,UV} \cdot p_A \cdot N \cdot \frac{E_{UV}}{A_{ion} \cdot \hbar\omega_{UV}} \qquad Eq.6$$

Following the same assumptions, the number of fragments, after the IR absorption is dissipated, will be given by:

$$F_{A:UV,IR} = \varepsilon_A \cdot \sigma_{A,UV} \cdot N_A \cdot \frac{E_{UV}}{A_{ion} \cdot \hbar\omega_{UV}} \qquad Eq.7$$

In this case N_A is the total number of ions that still populate conformation A after the IR pulse and this can be expressed by the sum of the initial total number of ions in conformation A and those transferred into A from B and C after IR absorption and recooling, minus the number of ions that transferred out of A:

$$N_A = N \cdot p_A$$
$$+ \sigma_{B,IR} \cdot p_B \cdot N \cdot \frac{E_{IR}}{A_{ion} \cdot \hbar\omega_{IR}} \cdot \Phi_{BA}$$
$$+ \sigma_{C,IR} \cdot p_C \cdot N \cdot \frac{E_{IR}}{A_{ion} \cdot \hbar\omega_{IR}} \cdot \Phi_{CA}$$
$$- \sigma_{A,IR} \cdot p_A \cdot N \cdot \frac{E_{IR}}{A_{ion} \cdot \hbar\omega_{IR}} \cdot (1 - \Phi_{AA})$$

$$N_A = N \cdot \left(p_A + \frac{E_{IR}}{A_{ion} \cdot \hbar\omega_{IR}} \cdot \left[\sum_{X \neq A} p_X \cdot \sigma_{X,IR} \cdot \Phi_{XA} - p_A \cdot \sigma_{A,IR} \cdot (1 - \Phi_{AA}) \right] \right) \qquad Eq.8$$

Replacing N_A in by its value in the Equation *7* gives the following expression:

$$F_{A:UVIR} = \varepsilon_A . \sigma_{A,UV} . \frac{E_{UV}}{A_{ion}.\hbar\omega_{UV}} \ .$$

$$N.\left(p_A + \frac{E_{IR}}{A_{ion}.\hbar\omega_{IR}} \ .\left[\sum_{X \neq A} p_X . \ \sigma_{X,IR} \ .\Phi_{XA} - p_A.\sigma_{A,IR} \ .(1-\Phi_{AA}) \right] \right)$$

The peak intensity of an IR-population transfer spectrum given by Equation *2* could then be expressed by:

$$IRPTS_A = \frac{F_{A:UV,IR} - F_{A:UV}}{F_{A:UV}}$$

$$IRPTS_A = \frac{\varepsilon_A.\sigma_{A,UV}.N.\dfrac{E_{UV}}{A_{ion}.\hbar\omega_{UV}} \ .\dfrac{E_{IR}}{A_{ion}.\hbar\omega_{IR}} \ .\left[\sum_{X \neq A} p_X . \ \sigma_{X,IR} \ .\Phi_{XA} - p_A.\sigma_{A,IR} \ .(1-\Phi_{AA}) \right]}{\varepsilon_A.\sigma_{A,UV}.p_A.N.\dfrac{E_{UV}}{A_{ion}.\hbar\omega_{UV}}}$$

$$IRPTS_A = \frac{\left[\sum_{X \neq A} p_X . \ \sigma_{X,IR} \ .\Phi_{XA} - p_A.\sigma_{A,IR} \ .(1-\Phi_{AA}) \right].E_{IR}}{p_A.A_{ion}.\hbar\omega_{IR}}$$

The weighted sum of the population transfer spectra for the three conformation at all infrared wavelengths is given by:

$$p_A.IRPTS_A + p_B.IRPTS_B + p_C.IRPTS_C = \qquad\qquad Eq.9$$

$$\left(\sum_{X \neq A} p_X . \ \sigma_{X,IR,} \ .\Phi_{XA} - p_A.\sigma_{A,IR} \ .(1-\Phi_{AA}) \right).\frac{E_{IR}}{A_{ion}.\hbar\omega_{IR}}$$

$$+\left(\sum_{X \neq B} p_X . \ \sigma_{X,IR,} \ .\Phi_{XB} - p_B.\sigma_{B,IR} \ .(1-\Phi_{BB}) \right).\frac{E_{IR}}{A_{ion}.\hbar\omega_{IR}}$$

$$+\left(\sum_{X \neq C} p_X . \ \sigma_{X,IR,} \ .\Phi_{XC} - p_C.\sigma_{C,IR} \ .(1-\Phi_{CC}) \right).\frac{E_{IR}}{A_{ion}.\hbar\omega_{IR}}$$

$$= \frac{E_{IR}}{A_{ion}.\hbar\omega_{IR}}.\left(\begin{array}{l} p_A.\sigma_{A,IR}. (\Phi_{AB} + \ \Phi_{AC} - \ (1-\Phi_{AA})) \\ + p_B.\sigma_{B,IR}. (\Phi_{BA} + \ \Phi_{BC} - \ (1-\Phi_{BB})) \\ + p_C.\sigma_{C,IR}. (\Phi_{CA} + \ \Phi_{CB} - \ (1-\Phi_{CC})) \end{array} \right)$$

Since equation *3.2* holds for all conformers, then:

$$\Phi_{AB} + \ \Phi_{AC} - \ (1-\Phi_{AA}) =$$
$$\Phi_{BA} + \ \Phi_{BC} - \ (1-\Phi_{BB}) =$$
$$\Phi_{CA} + \ \Phi_{CB} - \ (1-\Phi_{CC}) = 1-1 = 0$$

and therefore,

$$p_A.IRPTS_A + p_B.IRPTS_B + p_C.IRPTS_C = 0$$

This equation demonstrates that all the infrared excited population is redistributed among the existing conformers. In the meantime the fractional population of the molecule sum to 1:

$$\sum p_X = p_A + p_B + p_C = 1 \qquad\qquad Eq.10$$

The $IRPTS_X$ are obtained experimentally and thus from the weighted-sum of the infrared population transfer spectra and Equation *10* we can extract the fractional populations of the conformation of the molecule under the trap conditions.

2.   Extracting the quantum yields to isomerization

To extract the quantum yield to isomerization from the IRPT spectra, we need information about the amount of molecules that are infrared excited. This piece of information could be extracted from an IR dip spectrum taking under the same condition of the IR population transfer spectrum. This is done by moving the UV laser pulse in time and so it will fire, early in the trapping cycle, 200ns after the IR laser. The IR spectrum peak intensity is given by:

$$IR_A = \frac{F_{A:UV,IR} - F_{A:UV}}{F_{A:UV}} \qquad\qquad Eq.11$$

The number of fragments from UV only can be expressed as demonstrated earlier by Equation 3.4. Under the assumption that the ions do not move between the arrivals of the two laser pulses, the number of fragments from the UV laser when the IR is fired first will be given by:

$$F_{A:UVIR} = \varepsilon_A.\sigma_{A,UV} \cdot p_A.N \cdot \frac{E_{UV}}{A_{ion}.\hbar\omega_{UV}}$$

$$= \varepsilon_A \cdot \tau_{UV}\cdot N \cdot \int \sigma_{A,UV}.\Omega_{UV} \cdot \varrho_A.rdrd\phi$$

$$F_{A:UVIR} = \varepsilon_A \cdot N \cdot \sigma_{A,UV} \cdot p_A \cdot \frac{E_{UV}}{A_{ion}.\hbar\omega_{UV}} \cdot \left(1 - \sigma_{A,IR} \cdot \frac{E_{IR}}{\max(A_{UV}, A_{IR}).\hbar\omega_{IR}}\right) \qquad Eq.12$$

The expression for the IR spectrum is then:

$$IR_A = \frac{F_{A:UV,IR} - F_{A:UV}}{F_{A:UV}} = -\sigma_{A,IR} \cdot \frac{E_{IR}}{\max(A_{UV},A_{IR}).\hbar\omega_{IR}} \qquad Eq.13$$

Substituting $\sigma_{A,IR}$ into the IRPTS expression:

$$IRPTS_A = \frac{\left[\sum_{X \neq A} p_X. \sigma_{X,IR} .\Phi_{XA} - p_A.\sigma_{A,IR} .(1-\Phi_{AA})\right].E_{IR}}{p_A.A_{ion}.\hbar\omega_{IR}}$$

$$= \frac{\left[\sum_{X \neq A} p_X. (-IR_X.\max(A_{UV},A_{IR})) .\Phi_{XA} - p_A. (-IR_X.\max(A_{UV},A_{IR})) .(1-\Phi_{AA})\right]}{p_A.A_{ion}}$$

$$= \frac{-\max(A_{UV},A_{IR})}{p_A.A_{ion}}.\left(\sum_{X \neq A} p_X. IR_X.\Phi_{XA} - p_A.IR_A.(1-\Phi_{AA})\right)$$

If we consider $\gamma = \dfrac{\max(A_{UV},A_{IR})}{A_{ion}}$

This will lead to a final set of IRPTS equations for the three conformers A, B and C:

$$IRPTS_A = \left(-\frac{p_B}{p_A}. IR_B.\Phi_{BA} - \frac{p_C}{p_A}. IR_C.\Phi_{CA} + IR_A.(1-\Phi_{AA})\right).\gamma \qquad Eq.14$$

$$IRPTS_B = \left(-\frac{p_A}{p_B}. IR_A.\Phi_{AB} - \frac{p_C}{p_B}. IR_C.\Phi_{CB} + IR_B.(1-\Phi_{BB})\right).\gamma \qquad Eq.15$$

$$IRPTS_C = \left(-\frac{p_A}{p_C}. IR_A.\Phi_{AC} - \frac{p_B}{p_C}. IR_B.\Phi_{BC} + IR_C.(1-\Phi_{CC})\right).\gamma \qquad Eq.16$$

However if the quantum yields are extracted at transition where just conformer A absorbs, this set of equation will give:

$$IRPTS_A = IR_A.(1-\Phi_{AA}).\gamma$$

$$IRPTS_B = -\frac{p_A}{p_B} IR_A.\Phi_{AB}.\gamma$$

$$IRPTS_C = -\frac{p_A}{p_C} IR_C.\Phi_{AC}.\gamma$$

In the case of the unique absorption band of conformer B:

$$IRPTS_B = IR_B.(1 - \Phi_{BB}).\gamma$$

$$IRPTS_A = -\frac{p_B}{p_A} IR_B.\Phi_{BA}.\gamma$$

$$IRPTS_C = -\frac{p_B}{p_C} IR_C.\Phi_{BC}.\gamma$$

In the case of the unique vibration band of conformer C, give

$$IRPTS_C = IR_C.(1 - \Phi_{CC}).\gamma$$

$$IRPTS_A = -\frac{p_C}{p_A} IR_C.\Phi_{CA}.\gamma$$

$$IRPTS_B = -\frac{p_C}{p_B} IR_B.\Phi_{CB}.\gamma$$

The only unknown quantities in these equations are the quantum yields since the peak intensities of the infrared population transfer and infrared spectra are measured experimentally and the fractional population could be extracted from the weighted sums of the population transfer spectra us demonstrated in the previous paragraph. We assume to be working under optimized conditions for a maximum of overlapping between the lasers and the ions and thus γ is assumed to be close to 1.

List of figures

List of tables

Acknowledgments

152

Curriculum vitae

Caroline Seaiby
Born on 24 May 1982 in Ram, Lebanon
Lebanese nationality

EDUCATION

2005-2010: Ph.D. thesis in Physical Chemistry at the École Polytechnique Fédérale de Lausanne (EPFL), Switzerland, in the group of Prof. Thomas Rizzo *Spectroscopic probes of conformational isomerization of biological molecules in a cold ion trap*

2004-2005: D.E.A (Master of Science) in Analytical and Material Chemistry at University Louis Pasteur Strasbourg I, France.
Diploma work at the Ecole européenne de Chimie, Polymères et Matériaux (ECPM), France.

2000-2004: "Maîtrise de Chimie" at the Lebanese University, Fanar, Lebanon

PUBLICATIONS

Conformation-Specific Spectroscopy and Photodissociation of Cold, Protonated Tyrosine and Phenylalanine, J. A. Stearns, S. Mercier, C. Seaiby, M. Guidi, O. V. Boyarkin, and T. R. Rizzo, **2007**, *J. Am. Chem. Soc.* 129 (38), 11814-11820.

Spectroscopy and Conformational Preferences of Gas-Phase Helices, J. A. Stearns, C. Seaiby, O. V. Boyarkin, and T. R. Rizzo, **2009**, *Phys. Chem. Chem. Phys.*11, 125-132.

LANGUAGES

Arabic (mother tongue), English (fluent), French (fluent)